An airlift loop redux cycle reactor for alcohol oxidations : hydrodynamics, mass transfer and reactor design

An airlift loop redox cycle reactor for alcohol oxidations: Hydrodynamics, mass transfer and reactor design

PROEFSCHRIFT

ter verkrijging van de graad van doctor aan de
Technische Universiteit Eindhoven, op gezag van de
Rector Magnificus, prof.dr. R.A. van Santen, voor een
commissie aangewezen door het College voor
Promoties in het openbaar te verdedigen
op woensdag 19 maart 2003 om 16.00 uur

door

Jeroen Hendrik Jacob Kluytmans

geboren te Berkel-Enschot

Dit proefschrift is goedgekeurd door de promotoren:

prof.dr.ir. J.C. Schouten
en
prof.dr.ir. A.A.H. Drinkenburg

Copromotor:
dr.ir. B.F.M. Kuster

CIP-DATA LIBRARY TECHNISCHE UNIVERSITEIT EINDHOVEN

Kluytmans, Jeroen H.J.

An airlift loop redox cycle reactor for alcohol oxidations : hydrodynamics, mass transfer and reactor design / by Jeroen H.J. Kluytmans. - Eindhoven : Technische Universiteit Eindhoven, 2003

Proefschrift. - ISBN 90-386-2854-4
NUR 913

Trefwoorden: chemische reactoren ; airliftreactoren / heterogene katalyse ; platina / katalytische oxidatie ; alcoholen / bellenkollomen / beeldverwerking / fysische transportverschijnselen ; stofoverdracht

Subject headings: chemical reactors ; airlift reactors / heterogeneous catalysis ; platinum / catalytic oxidation ; alcohols / imaging / bubble columns / physical transport phenomena ; mass transfer

Printed by Eindhoven University Press
Cover design: Seña Ontwerpers, Eindhoven, www.senaontwerpers.nl

Summary

The aim of this thesis is the design of an airlift loop reactor for the catalytic selective oxidation of alcohols, towards valuable intermediates for fine chemistry and pharmaceutical applications. The selective oxidation of alcohols seems a promising reaction pathway for fine chemistry applications, because the products made from starting materials like sucrose, glucose, cellulose, and starch can possibly replace products and intermediates made out of fossil resources, in the near future. Moreover, the selective oxidation reactions are performed at relative mild process conditions. However, before these processes can be applied on industrial scale, some major problems still have to be overcome. One of the most challenging problems to solve, is the fast deactivation of the platinum on carbon (Pt/C) catalyst, due to overoxidation of the platinum surface, in an oxidizing environment. The Pt/C looses activity of a factor of 10 within hours. Regeneration of the catalyst to its initial activity is possible by contacting the catalyst with a reducing environment. This alternating contact of the catalyst with a reducing and an oxidizing environment can be achieved by alternating the gas feed between an oxygen rich gas-feed and a gas-feed stream without oxygen. However, a more elegant alternative would be the design of a specific reactor in which the alternating contacting takes place inside the reactor, while operating at a constant gas-feed stream. This can be achieved with an airlift loop redox cycle (ALRC) reactor. To show the feasibility of such an airlift loop reactor for this specific purpose, quantitative data is required about the hydrodynamic and mass transfer properties of this reactor. Furthermore, the effect of the presence of catalyst particles and electrolytic products on these properties should be known in detail. This thesis describes the investigation of the hydrodynamics and mass transfer properties of an airlift loop reactor, and of the changes in these properties upon addition of catalyst particles and electrolytes. This quantitative information is then used as an input for the design of an industrial size ALRC reactor, for the selective oxidation of alcohols, while maintaining a high catalyst activity.

The airlift loop redox cycle reactor consists of a central part, the riser, in which the oxidation reaction takes place, and an internal or an external draft tube, the downcomer, in which the catalyst is recirculated and regenerated. The design of the airlift loop reactor is mainly determined by the hydrodynamic and mass transfer properties of the riser. These properties are investigated in a sparged gas-liquid reactor, without an internal or external loop. This is justified as the hydrodynamic and mass transfer phenomena in a bubble column closely resemble those in the riser of an airlift loop reactor. For this specific study, a 2D gas-liquid bubble column (width*height*depth 0.3*2.0*0.015 m) was built in which the gas hold-up and mass transfer was studied.

A high speed video camera is used to provide quantitative input for gas hold-up and mass transfer studies, like bubble size distribution, small and large bubble volumes, specific gas-liquid surface area etc. Images are captured at a frequency of 955

Hz. The obtained images are analyzed with specific image processing software to determine volume and surface area for each observed bubble. Furthermore, specific image processing software is developed to track bubbles throughout image sequences, to obtain accurate data about for example the bubble size distribution and the bubble rise velocities as a function of the superficial gas velocity in the bubble column. The image processing is also used to study the coalescence behavior of large bubbles under flow conditions. It is shown that the coalescence behavior is difficult to study in low viscous systems, because the way bubbles near each other, before they collide determines to a large extent the rate of bubble coalescence. It is shown that imaging is a powerful method to quantify parameters which determine the coalescence behavior of bubbles as well as parameters which determine the gas hold-up and mass transfer in bubble columns.

The gas hold-up in a bubble column, and the influence of carbon particles (0.1 - 20 g l^{-1}, d_p = 30 μm) and of electrolyte (0.05 - 2.0 M, Sodium gluconate), is investigated in a 2D bubble column. The overall gas hold-up is monitored using a float, which follows the movement of the liquid at the top of the liquid column, while the local gas hold-up is measured with pressure sensors which are connected at several heights in the column. The regime transition point, which denotes the transition from the homogeneous to the heterogeneous flow regime, is calculated from the dynamics of the pressure signal, by calculating the average cycle frequency. Two gas spargers are used to study the effect of the initial bubble size on the gas hold-up for distilled water, carbon slurry, and electrolyte systems. This study shows that both electrolyte and carbon particles increase the gas hold-up with increasing concentration. However, it is found that the increase in gas hold-up is due to multiple mechanisms. Carbon particles increase the gas hold-up because the rise velocity of the small bubbles in the homogeneous regime is affected, and because of a decreased rate of bubble coalescence. The increased gas hold-up in the electrolyte solutions is also caused by two effects: a decreased average size of the small bubbles due to a change in the surface tension of the liquid, and a decreased rate of bubble coalescence.

For the correct interpretation of the gas hold-up data obtained in a 2D bubble column with relation to 3D systems, the effect of the column scale on parameters like bubble rise velocity, transition gas hold-up, transition superficial gas velocity, bubble-wall interactions and bubble-bubble interactions, should be known. A 3D gas hold-up model was used as starting point for this investigation. It is shown that by adapting the rise velocity of the large bubbles, in the heterogeneous regime, and by applying the correct transition parameters, the gas hold-up in distilled water, carbon slurries, and electrolyte solutions, obtained in a 2D bubble column, are well described. Furthermore, the derived 2D model predicts nearly the same gas hold-up in the heterogeneous regime as the gas hold-up predicted by the 3D gas hold-up model at higher superficial gas velocities. This shows that under specific circumstances, 2D gas hold-up data can be used in scale-up studies.

It is generally accepted that addition of carbon particles and electrolyte to stirred and sparged systems can lead to an increase in the rate of gas-liquid mass transfer. The mechanism leading to this increased rate of mass transfer is still subject of discussion. The mass transfer properties of the 2D bubble column, a stirred reactor with gas inducing impeller, and a stirred reactor with flat gas-liquid interface are investigated. In each reactor, experiments are performed with distilled water, carbon particle slurries, and electrolyte solutions. Besides mass transfer measurements, high speed video imaging is used to obtain information about the specific gas-liquid interfacial area of the gas bubbles. This allows to show that the increased rate of gas-liquid mass transfer in the 2D bubble column and in the stirred tank reactor with gas inducing impeller is caused only because of an increased specific surface area of the bubbles. It is furthermore concluded that the increased rate of mass transfer in the stirred tank reactor with flat interfacial area is caused by hydrodynamic effects. No evidence was found for the well known shuttle effect.

The information obtained in the gas hold-up, mass transfer, and 2D-3D comparison studies, together with a kinetic model for the selective oxidation of methyl-α-D-glucopyranoside towards 1-O-methyl-α-D-glucuronate, is used for the design of an industrial scale airlift loop reactor, in which a high catalyst activity is maintained. The airlift loop redox cycle (ALRC) reactor is modelled assuming a perfectly mixed oxidation zone and a catalyst regeneration cycle in which the liquid and catalyst are in plug flow. The designed reactor has a volume of approx. 9 m^3 and a yearly production capacity of 2854 metric tons of 1-O-methyl-α-D-glucuronate. The designed airlift loop redox cycle reactor is compared with the alternative option for maintaining a high catalyst activity; a stirred tank reactor with alternating gas feeds. Because the catalyst activity in the ALRC reactor is more than twice the value of the catalyst activity in the stirred tank process, the reactor volume is half. Furthermore, the ALRC reactor can be operated with air as gas feed stream in stead of alternating oxygen rich and oxygen deficient gas feed stream. Therefore, the operating costs favor the ALRC reactor design above the stirred tank alternative.

Samenvatting

Het doel van het werk beschreven in dit proefschrift is het ontwerpen van een airlift loop reactor voor de katalytische omzetting van alcoholen in waardevolle tussenproducten voor de fijnchemie en de farmaceutische industrie. De selectieve oxidatie van alcoholen lijkt veelbelovend, omdat de producten gemaakt uit materialen als glucose, sucrose en zetmeel in de nabije toekomst producten en intermediaren gemaakt uit fossiele brandstoffen mogelijk kunnen vervangen. Tevens worden selectieve oxidatieprocessen vaak uitgevoerd onder milde procescondities. Echter, voordat deze processen kunnen worden toegepast op industriële schaal moeten er nog een aantal problemen worden opgelost. Eén van de grootste uitdagingen is het voorkomen van de snelle deactivering van de platina katalysator op koolstofdrager (Pt/C) in een oxiderende omgeving. De Pt/C katalysator verliest zijn activiteit met een factor 10 binnen enkele uren. De katalysator kan echter volledig worden hersteld, wanneer deze in een reducerende, zuurstofvrije omgeving wordt gebracht. Het afwisselend in contact brengen van de katalysator met een oxiderende en een reducerende omgeving kan worden bereikt door de gasvoeding te schakelen van een zuurstofrijke gasstroom naar een gasstroom, die geen zuurstof bevat. Een meer elegante oplossing is echter het ontwerpen van een reactor, waarin de katalysator in de reactor afwisselend in contact komt met een reducerende en een oxiderende omgeving, terwijl er een constante gasstroom wordt gevoed aan de reactor. Deze optie kan worden gerealiseerd in een airlift loop redox cycle (ALRC) reactor. Om de geschiktheid van deze reactor voor bovengenoemde oxidatieprocessen aan te tonen, is er kwantitatieve data nodig omtrent de hydrodynamische en stoftransporteigenschappen van dit type reactor. Tevens is het belangrijk te weten wat de invloed van de katalysatordeeltjes en van elektrolytische producten op deze eigenschappen is. Dit proefschrift beschrijft het onderzoek dat is verricht naar de hydrodynamische en stoftransporteigenschappen van een airlift loop reactor en de invloed die de katalysatordeeltjes en de elektrolytische producten op deze eigenschappen hebben. De kwantitatieve data zijn tenslotte gebruikt om een industriële ALRC reactor te ontwerpen voor de selectieve oxidatie van alcoholen met een hoge katalysatoractiviteit.

De airlift loop redox cycle reactor omvat een centraal deel, de riser, waar de oxidatiereactie plaatsvindt, en een externe of interne recirculatiebuis, de downcomer, waar de katalysator wordt gerecirculeerd en geregenereerd. Het ontwerp van een airlift loop reactor wordt voornamelijk bepaald door de hydrodynamica en de stofoverdrachteigenschappen van de riser. Deze eigenschappen zijn onderzocht in een met gas doorstroomde gas-vloeistof reactor zonder een interne of externe recirculatie. Deze aanpak is gerechtvaardigd omdat de hydrodynamica en de stofoverdrachteigenschappen van dit soort bellenkolommen sterk lijken op de eigenschappen in een airlift loop reactor. In deze studie is gebruik gemaakt van een 2D gas-vloeistof bellenkolom (breedte*hoogte*diepte: 0.3*2.0*0.015 m), waarin de hydrodynamica en stofoverdracht zijn bestudeerd.

Een hoge-snelheid videocamera is gebruikt om kwantitatieve data te verkrijgen, die gebruikt kunnen worden in gasfractie en stofoverdrachtstudies, zoals de belgrootteverdeling, het volume van de grote en kleine bellen, het specifiek gas-vloeistofoppervlak, etc. Met deze camera kunnen videobeelden worden opgenomen met een snelheid van 955 Hz. De verkregen beelden worden geanalyseerd met beeldverwerkingsprogrammatuur om zo het volume en het specifiek oppervlak van alle bellen te kunnen bepalen. Daarnaast is er specifieke beeldverwerkingsprogrammatuur geschreven om bellen te volgen in verschillende opeenvolgende beelden, om zo nauwkeurige informatie te verkrijgen over bijvoorbeeld de belgrootteverdeling en de stijgsnelheid van de bellen als functie van de superficiële gassnelheid in de bellenkolom. De beeldverwerkingstechniek is tevens gebruikt om het coalescentiegedrag van grote bellen te bestuderen onder stromingscondities. Op deze manier kon worden aangetoond, dat het moeilijk is om het coalescentiegedrag van grote bellen in laag viskeuze systemen te bepalen, omdat de wijze waarop de bellen elkaar benaderen, voordat ze met elkaar botsen, van grote invloed is op de snelheid van coalescentie. Echter, het kon worden aangetoond dat de beeldverwerkingstechniek een waardevolle methode is om de parameters te kwantificeren welke de gasfractie en de stofoverdracht in bellenkolommen beïnvloeden.

De gasfractie in een bellenkolom en de invloed die koolstofdeeltjes (0.1 - 20 g l^{-1}, d_p = 30 μm) en elektrolyt (Natrium gluconaat, 0.05-2.0 M) daarop hebben, is onderzocht in een 2D bellenkolom. De totale gasfractie is gemeten met een vlotter, die de beweging van de vloeistof aan de bovenzijde van het vloeistofbed registreert. De lokale gasfractie in delen van de bellenkolom is gemeten met druksensoren welke op verschillende hoogtes in de kolom zijn aangebracht. De overgang van het homogene regiem naar het heterogene regiem, gekenmerkt door het transitiepunt, kan worden bepaald uit de dynamica van de druksignalen. Twee gasverdelers zijn gebruikt om het effect van de initiële belgrootte op de gasfractie te bestuderen in gedestilleerd water, koolstof slurries en elektrolytoplossingen. Deze studie laat zien dat zowel elektrolyt als koolstofdeeltjes de gasfractie verhogen bij toenemende concentratie. Deze toename is het gevolg van meerdere mechanismen. De toegepaste koolstofdeeltjes verhogen de gasfractie, omdat de stijgsnelheid van de kleine bellen in het homogene regiem wordt verlaagd en omdat de koolstofdeeltjes de snelheid van coalescentie verminderen. De verhoogde gasfractie in elektrolytoplossingen wordt tevens veroorzaakt door twee mechanismen: een verminderde snelheid van coalescentie en een verandering van de gemiddelde belgrootte onder invloed van een verlaagde oppervlaktespanning van de elektrolytoplossingen.

Voor een juiste interpretatie van de gasfractie gegevens verkregen in een 2D kolom, in relatie met 3D systemen, moet het effect bekend zijn van de afmetingen van de kolom op verschillende parameters, zoals de stijgsnelheid van de bellen, de transitie gasfractie, de transitie superficiële gassnelheid, de bel-bel interacties en de bel-wand interacties. Een 3D gasfractie model is gebruikt als beginpunt voor deze studie. Op

deze manier kon worden aangetoond, dat door aanpassing van de stijgsnelheid van de bellen in het heterogene regiem en door het toepassen van de juiste transitieparameters de gasfractie in gedestilleerd water, koolstof slurries en elektrolyt oplossingen, in een 2D kolom goed kan worden beschreven. Tevens is de met het 2D model voorspelde gasfractie nagenoeg gelijk aan de gasfractie zoals voorspeld met het 3D gasfractie model bij hogere gassnelheden in het heterogene regiem. Dit laat zien dat het mogelijk is om 2D gasfractie data te gebruiken bij het opschalen van bellenkolommen.

Het is bekend dat het toevoegen van koolstofdeeltjes of elektrolyt aan geroerde of doorstroomde systemen leidt tot een versnelling van de snelheid van stofoverdracht tussen de gasfase en de vloeistoffase. Er bestaat echter nog steeds discussie over de mechanismen die een rol spelen in deze versnelling. De stoftransporteigenschappen van een 2D bellenkolom, van een geroerde reactor met een gasaanzuigende roerder, en van een geroerde reactor met een vlak gas-vloeistofoppervlak zijn onderzocht. In elke reactor werden experimenten uitgevoerd met gedestilleerd water, koolstofdeeltjes slurries, en elektrolyt oplossingen. Naast de stofoverdrachtsmetingen werden er ook videoopnamen gemaakt om informatie te verkrijgen over het specifieke gas-vloeistofoppervlak van de gasbellen. Op deze manier kunnen we laten zien dat de versnelling van stofoverdracht in een 2D bellenkolom en in een geroerde reactor met gasaanzuigende roerder, volledig valt toe te schrijven aan een vergroting van dit specifieke gas-vloeistofoppervlak. Tevens kon de conclusie getrokken worden, dat de versnelling van stofoverdracht in de geroerde reactor met een vlak gas-vloeistofoppervlak wordt veroorzaakt door hydrodynamische effecten. Er werd geen bewijs gevonden voor de aanwezigheid van het zogenaamde shuttle effect.

De informatie verkregen uit gasfractie en stofoverdrachtsmetingen en de studie naar het vergelijken van 2D-3D kolommen is samen met kinetische informatie over de selectieve oxidatie van methyl-α-D-glucopyranoside naar 1-O-methyl-α-D-glucoraat, gebruikt voor het ontwerp van een industriële airlift loop redox cycle reactor, waarin de activiteit van de katalysator kan worden behouden. De airlift loop redox cycle reactor (ALRC) reactor is gemodelleerd onder aanname, dat de vloeistof in de oxidatieve zone ideaal gemengd is terwijl in de regeneratielus de katalysator en de vloeistof in propstroom worden verondersteld. De ontworpen reactor heeft een volume van ongeveer 9 m^3 en een jaarlijkse productiecapaciteit van 2854 metrische tonnen 1-O-methyl-α-D-glucoraat. De ALRC reactor is vergeleken met een alternatieve mogelijkheid om de katalysatoractiviteit hoog te houden: een geroerde reactor met wisselende gasstromen. Omdat de katalysatoractiviteit in de ALRC reactor ongeveer twee keer zo hoog is als in het proces met de geroerde reactor, is het reactorvolume van de ALRC reactor slechts de helft van het volume van de geroerde reactor. Tevens kan de ALRC reactor worden bedreven met een constante gasstroom in plaats van het wisselen tussen zuurstofrijke en zuurstofarme gasstromen. Daardoor zijn de kosten voor het bedrijven van het ALRC proces aanzienlijk minder dan de kosten

voor het bedrijven van de geroerde tank reactor. De ALRC reactor vormt daarom een realistische mogelijkheid voor het uitvoeren van deze selectieve oxidatiereactie.

Contents

1

Introduction

1.1 Platinum catalyzed alcohol oxidation

The aqueous noble metal catalyzed alcohol oxidation, resulting in ketonic, aldehydic, and carboxylic acid groups, is a very useful reaction for carbohydrate conversion and seems a promising reaction pathway for fine chemistry applications. The products made from starting materials like sucrose, glucose, cellulose and starch can possibly replace products and intermediates made out of fossil resources in the near future. This type of reaction has been reviewed in 1994 by Mallat and Baiker [1]. Within our laboratory the reaction has been subject of kinetic studies since 1967, when van der Baan and de Wilt started exploring catalytic conversion of sugars as renewable, chemical raw materials. The platinum catalysed oxidation of glucose to gluconic acid was the first reaction studied [2, 3], followed by its further oxidation to glucaric acid [4–7]. Using lead promoted platinum, the selectivity for further oxidation of sugars changed from aldaric to 2-keto carboxylic acids [8, 9]. Developing new routes for vitamin C synthesis and applications of carbohydrates in detergents, the platinum catalyzed oxidation of glucosides was undertaken [10–12]. Ethanol was used as model reactant for in depth kinetic studies with in-situ catalyst characterisa-

tion [7, 13–16]. Bismuth promoted palladium was used for lactose oxidation [17] and bismuth, lead and tin promoted platinum for propylene glycol oxidation [18]. Finally, the platinum catalyzed oxidation also has been explored for wastewater treatment up to 200 °C [19–21]. Although the diversity of these studies shows the value of the selective oxidation of alcohols to be applied for fine chemistry applications, some major problems still have to be overcome. One of the most challenging problems for almost all selective alcohol oxidation reactions with palladium or platinum catalysts is the fast catalyst deactivation.

1.2 Catalyst deactivation

Both in the review of Mallat and Baiker [1] and in the work from our laboratory [22], it is shown that four types of catalyst deactivation can be distinguished: Crystallite agglomeration, inhibition (poisoning, coking, product inhibition), crystallite leaching, and over-oxidation (corrosion). It was found that under the mild process conditions (323 K, ambient pressure) under which most selective oxidation reactions are performed, the over-oxidation is mainly responsible for the fast catalyst deactivation. The catalyst looses its activity with a factor of 10 within hours due to this over-oxidation. However, from intrinsic kinetic experiments in continuous stirred tank reactors [23, 24], it appeared that a sufficient catalyst activity can be maintained by a regular interruption of the oxygen flow, as is shown in Figure 1.1. This cyclic operation between aerobic and anaerobic periods is known as the redox cycle. The behavior of the catalyst during this redox cycle was modelled by Markusse et al. [24], who developed a kinetic model for the oxidation of methyl-α-D-glucopyranoside (MGP) towards 1-O-methyl-α-D-glucuronic acid (NaMG). Figure 1.1 shows that the model describes the experiments quite well. This model allows us to predict the optimal time scales for the exposure of the catalyst to the oxidative and the reductive environments, to maintain a high catalyst activity.

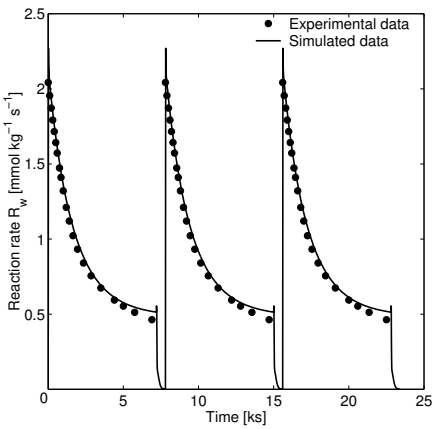

Figure 1.1: Weight specific reaction rate for continuous methyl-α-D-glucopyranoside oxidation over a 3.3% Pt on graphite catalyst as a function of time on stream, with interruption of the oxygen flow [24].

The oxygen flow interruption, as used to maintain a high catalyst activity as shown in Figure 1.1, might not be the most efficient way for catalyst reactivation on a larger scale. It can be envisaged that it would be more practical to cycle the slurry catalyst through aerobic and anaerobic zones inside one reactor. Such operation could be realized using interconnected, stirred reactors, an aerobic one and a small anaerobic one, through which the reaction mixture is slowly circulated. Another possibility would be to use slurry bubble columns with internal or external loops. These reactors are known as airlift loop reactors. This thesis explores the feasibility of the airlift loop reactor to be applied for the selective oxidation of alcohols, whilst maintaining a high catalyst activity.

1.3 Airlift loop reactors

Airlift loop reactors are a collection of reactors which consist of a riser and a downcomer. The liquid and/or solid phases in the riser are transported through the reactor, due to a gas stream entering at the bottom of the column, while in the downcomer the liquid and/or solid phases are recirculated due to the difference in density between the phases in the riser and the downcomer. An example of an internal airlift loop reactor is shown in Figure 6.1. Airlift reactors are found in many different designs, like external or internal airlift reactors [25, 26], agitated airlift reactors [27], or more advanced airlift reactors like the biofilm airlift suspension reactor [28]. The benefits of the airlift reactor are obvious: the airlift loop reactor is extremely suitable for slow reactions, because the airlift loop reactor allows a large recycle stream in an internal or external loop, resulting in larger residence time of the liquid, with little reactor volume, compared to traditional slurry bubble columns, which do not offer the possibility of a recycle stream. Furthermore, the airlift loop reactor is suitable to create different hydrodynamic and/or kinetic regimes in the riser and downcomer, within one reactor. During recent years, much research has been devoted to the application of the airlift loop reactor in many processes. Modelling and experimental studies [29–33] show that the application of the airlift loop reactor in chemical processes is very diverse.

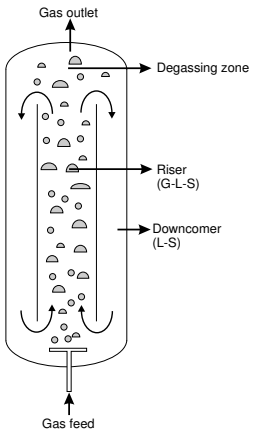

Figure 1.2: Scheme of a three phase airlift loop reactor. The riser is a three phase system, the gas leaves the column at the degassing zone, the liquid and solids are recirculated via the downcomer.

It is clear that the airlift loop reactor can be very useful for the creation of oxidative and reductive zones within one reactor. As mentioned, creation of these zones is beneficial to maintain a high catalyst activity during the selective oxidation of alco-

hols. This type of airlift loop reactor will be addressed as the airlift loop redox cycle (ALRC) reactor.

1.4 Scope and outline of this thesis

This thesis aims to design an ALRC reactor, for the oxidation of methyl-α-D-glucopyranoside (MGP) towards 1-O-methyl-α-D-glucuronic acid (MG). The kinetic model of Markusse et al. [24] is used to describe the kinetics of this alcohol oxidation and to predict the behavior of the catalyst in the reactor. However, to come to a proper design of the ALRC reactor for the selective oxidation of alcohols, the hydrodynamic and mass transfer properties of the ALRC should be known in detail. Furthermore, information is required about the changes in the hydrodynamic and the mass transfer properties upon addition of catalyst particles and the electrolytic products, which are formed during the selective alcohol oxidation. Therefore, the main part of this thesis focusses on the investigation of the gas hold-up and the mass transfer in an ALRC reactor, and the mechanisms underlying the changes in these properties, when catalyst particles or electrolytes are added to the reactor.

The hydrodynamic and mass transfer properties of an ALRC reactor are investigated in a 2D bubble column reactor (width*height*depth 0.3*2.0*0.015 m), without an internal or external draft tube. It was chosen to study the hydrodynamic and mass transfer properties of such a bubble column, because it closely resembles the behavior of the riser of an airlift loop reactor [34]. Moreover, the performance of the riser mainly determines the performance of the ALRC reactor, and is thus the most crucial part in the reactor design.

In Chapter 2 the imaging technique is introduced that is used to obtain quantitative information about bubble size distributions, specific gas-liquid interfacial area, bubble rise velocities, and the coalescence behavior of bubble pairs. This chapter provides a general introduction on the imaging technique developed and gives a brief overview of its applications. The information obtained with the imaging technique is used in the studies on gas hold-up and mass transfer as described in Chapters 3 till 5.

The influence of the carbon catalyst particles and electrolyte on the gas hold-up in the bubble column is shown in Chapter 3. Gas hold-up and transition point measurements are used to investigate which mechanisms are responsible for changes in the gas hold-up in a bubble column, upon addition of small catalyst particles and electrolyte. The changes in gas hold-up are measured with different techniques, like image analysis, pressure signal analysis, and ultrasonic height measurements.

The comparison of the gas hold-up data in the 2D slurry bubble column with 3D bubble column data is treated in Chapter 4. The 3D gas hold-up model of Krishna et al. [35] is adapted in order to describe the gas hold-up phenomena in a 2D slurry

bubble column reactor. It is shown that with slight adaptations to the 3D model, the gas hold-up data in a 2D column is well described. Furthermore, the thus obtained 2D model also gives a good prediction of the gas hold-up in 3D columns, at higher superficial gas velocities.

The mass transfer properties of the bubble column are investigated in Chapter 5. It is investigated which mechanisms are responsible for the increased rate of gas-liquid mass transfer upon addition of electrolyte and carbon particles. This investigation is achieved by exploring the gas-liquid mass transfer in a bubble column and in two stirred reactors. Combining the results obtained in these three reactors, the mechanism responsible for the increased gas-liquid mass transfer upon addition of particles and electrolyte is clarified.

Finally, in Chapter 6, an industrial size airlift loop redox cycle (ALRC) reactor is designed. For this design, information obtained in the previous chapters, about the mass transfer and the gas hold-up properties, is used. The kinetic model of Markusse et al. [24] is used to describe the kinetics of the alcohol oxidation together with the kinetics of the catalyst deactivation and reactivation. Model simulations and a sensitivity study are performed to find the most critical parameters in the reactor design, and these parameters are used in the optimization study of the reactor. The thus designed, industrial scale ALRC reactor, is compared with the stirred tank process as described by Markusse et al. [24] to show the economic feasibility of this reactor for the selective oxidation of MGP.

Chapter 7 summarizes the main conclusions of this thesis on the imaging technique, the gas hold-up and the mass transfer properties of a 2D bubble column, the comparison of 2D and 3D gas hold-up data, and on the design of the ALRC reactor. Furthermore, the possible application of the ALRC reactor for other processes is shortly evaluated.

Bibliography

[1] Mallat, T. and Baiker, A., Oxidation of alcohols with molecular oxygen on platinum metal catalysts in aqueous solutions. *Cat. Today*, 19(2), 247-283, 1994.

[2] Wilt, H.G.J. de, Part I. Oxidation of glucose to gluconic acid: Survey of techniques. *Ind. Eng. Chem. Prod. Res. Develop*, 11(4), 370-373, 1972.

[3] Wilt, H.G.J. de, and Baan, H.S. van der, Part II. Oxidation of glucose to k-gluconate. Platinum-catalyzed oxidation with oxygen in aqueous alkaline solutions. *Ind. Eng. Chem. Prod. Res. Develop*, 11(4), 374-378, 1972.

[4] Dirkx, J.M.H. and Baan, H.S. van der, The oxidation of gluconic acid with platinum on carbon as catalyst. *J. Catal.*, 67(1), 14-20, 1981.

[5] Dirkx, J.M.H., Baan, H.S. van der, and Broek, J.M.A.J. van den The preparation of d-glucaric acid by the oxidation of d-gluconic acid catalyzed by platinum on carbon. *Carbohydr. Res.*, 59(1), 63-72, 1977.

[6] Dijkgraaf, P.J.M., Rijk, M.J.M., Meuldijk, J., and Wiele, K. van der, Deactivation of platinum catalysts by oxygen. 1. Kinetics of the catalyst deactivation. *J. Catal.*, 112(2), 329-336, 1988.

[7] Jelemensky, L., Kuster, B.F.M., and Marin, G.B., Relaxation processes during the selective oxidation of aqueous ethanol with oxygen on a platinum catalyst. *Ind. Eng. Chem. Res.*, 36(8), 3065-3074, 1997.

[8] Smits, P.C.C., Kuster, B.F.M., Wiele, K. van der, Baan, H.S. van der, The selective oxidation of aldoses and aldonic acids to 2-ketoaldonic acids with lead-modified platinum-on-carbon catalysts. *Carbohydr. Res.*, 153, 227-235, 1986.

[9] Smits, P.C.C., Kuster, B.F.M., Wiele, K. van der, Baan, H.S. van der, Lead modified platinum on carbon catalysts for the selective oxidation of 2-hydrocarbonyc acids, and especially polyhydroxycarbonic acids to their 2-keto derivates. *Appl. Catal.*, 33, 83-96, 1987.

[10] Schuurman, Y., Kuster, B.F.M., Wiele, K. van der, and Marin, G.B., The selective oxidation of methyl-α-D-glucoside on a carbon supported platinum catalyst. *Stud. Surf. Sci. Catal.*, 72, 43-55, 1992.

[11] Schuurman, Y., Kuster, B.F.M., Wiele, K. van der, and Marin, G.B., Selective oxidation of methyl-α-D-glucoside on carbon supported platinum. *Appl. Catal. A*, 89(1), 31-46, 1992.

[12] Vleeming, J.H., Kuster, B.F.M., and Marin, G.B., Oxidation of methyl and n-octyl-α-D-glucopyranoside over graphite-supported platinum catalysts, effect of the alkyl substituent on activity and selectivity. *Carbohydr. Res.*, 303(2), 175-183, 1997.

[13] Tillaart, J.A.A. van den, Kuster, B.F.M., and Marin, G.B., Oxidative dehydrogenation of aqueous ethanol on a carbon supported platinum catalyst. *Appl. Catal. A*, 120(1), 127-145, 1994.

[14] Tillaart, J.A.A. van den, Kuster, B.F.M., and Marin, G.B., Platinum particle size effect on the oxidative dehydrogenation of aqueous ethanol. *Catal. Lett.*, 36(1,2), 31-36, 1995.

[15] Jelemensky, L., Kuster, B.F.M., and Marin, G.B., Multiple steady states for the oxidation of aqueous ethanol with oxygen on a carbon-supported platinum catalyst. *Catal. Lett.*, 30(1-4), 269-277, 1995.

[16] Jelemensky, L., Kuster, B.F.M., and Marin, G.B., Kinetic modeling of multiple steady-states for the oxidation of aqueous ethanol with oxygen on a carbon supported platinum catalyst. *Chem. Eng. Sci.*, 51(10), 1767-1776, 1996.

[17] Hendriks, H.E., Kuster, B.F.M., and Marin, G.B., The effect of bismuth on the selective oxidation of lactose on supported palladium catalysts. *Carbohydr. Res.*, 204, 121-129, 1990.

[18] Pinxt, H.H.C.M., Kuster, B.F.M., and Marin, G.B., Promoter effects in the Pt-catalyzed oxidation of propylene glycol. *Appl. Catal. A*, 191(1,2), 45-54, 2000.

[19] Harmsen, J.M.A., Jelemensky, L., Andel-Scheffer, P.J.M., Kuster, B.F.M., and Marin, G.B., Kinetic modeling for wet air oxidation of formic acid on a carbon supported platinum catalyst. *Appl. Catal. A*, 165(1-2), 499-509, 1997.

[20] Ukropec, R., Kuster, B.F.M., Schouten, J.C., and Santen, R.A., Low temperature oxidation of ammonia to nitrogen in liquid phase. *Appl. Catal. B*, 23(1), 45-57, 1999.

[21] Masende, Z.P., Kuster, B.F.M., Ptasinski, K.J., Katima, J.H.Y., and Schouten, J.C. Platinum catalysed wet oxidation of phenol in a stirred slurry reactor: A practical operation window. *Appl. Catal. A*, In press, 2002.

[22] Markusse, A.P., Kuster, B.F.M., and Schouten, J.C., Catalyst deactivation and reactivation during aqueous alcohol oxidation in a redox-cycle reactor. *Stud. Surf. Sci. Catal.*, 129, 273, 1999.

[23] Vleeming, J.H., Kuster, B.F.M., and Marin, G.B., Selective oxidation of methyl-α-D-glucopyranoside with oxygen over supported platinum: Kinetic modeling in the presence of deactivation by overoxidation of the catalyst. *Ind. Eng. Chem. Res.*, 36(9), 3541-3553, 1997.

[24] Markusse, A.P., Kuster, B.F.M., and Schouten, J.C., Catalyst deactivation and reactivation during aqueous alcohol oxidation in a redox-cycle reactor. *Stud. Surf. Sci. Catal.*, 126, 273-280, 1999.

[25] Masry W.A.Al, and Abasaeed, A.E., On the scale-up of external loop airlift reactors: Newtonian systems. *Chem. Eng. Sci.*, 53(24), 4085-4094, 1998.

[26] Heijnen, J.J., Hols, J., Lans, R.G.J.M. van der, Leeuwen, H.L.J.M. van Mulder, A., and Weltevrede. R., A simple hydrodynamic model for the liquid circulation velocity in a full-scale 2-phase and 3-phase internal airlift reactor operating in the gas recirculation regime. *Chem. Eng. Sci.*, 52(15), 2527-2540, 1997.

[27] Chisti, Y., and Jauregui-Haza, U.J., Oxygen transfer and mixing in mechanically agitated airlift bioreactors. *Biochem. Eng. J.*, 10(2), 143-153, 2002.

[28] Benthum, W.A.J. van, Hoogen, J.H.A. van den, Lans, R.G.J.M. van der, Loosdrecht, M.C.M., and Heijnen, J.J., The biofilm airlift suspension extension reactor. part I: design and two-phase hydrodynamics. *Chem. Eng. Sci.*, 54(12), 1909-1924, 1999.

[29] Oey, R.S., Mudde, R.F., Portela, L.M., and Akker, H.E.A. van den, Simulation of a slurry airlift using a two-fluid model. *Chem. Eng. Sci.*, 56(2), 673-681, 2001.

[30] Abashar, M.E., Narsingh, U., Rouillard, A.E., and Judd, R., Hydrodynamic flow regimes, gas holdup, and liquid circulation in airlift reactors. *Ind. Eng. Chem. Res.*, Vol 37(Iss 4), 1251-1259, 1998.

[31] Camarasa, E., Meleiro, L.A.C., Carvalho, E., Domingues, A., Maciel Filho, R., Wild, G., Poncin, S., Midoux, N., and Bouillard, J., A complete model for oxidation airlift reactors. *Comput. Chem. Eng.*, 25(4-6), 577-584, 2001.

[32] Vial, C., Poncin, S., Wild, G., and Midoux, N., A simple method for regime identification and flow characterisation in bubble columns and airlift reactors. *Chem. Eng. Process.*, 40(2), 135-151, 2001.

[33] Rubio, F.C., Garcia, J.L., Molina, E., and Chisti, Y., Steady-state axial profiles of dissolved-oxygen in tall bubble- column bioreactors. *Chem. Eng. Sci.*, 54(11), 1711-1723, 1999.

[34] Mudde, R.F., and Saito, T., Hydrodynamical similarities between bubble column and bubbly pipe flow. *J. Fluid. Mech.*, 437, 203-228, 2001.

[35] Krishna, R., Urseanu, M.I., Baten, J.M. van, and Ellenberger, J., Influence of scale on the hydrodynamics of bubble columns operating in the churn-turbulent regime: experiments vs. eulerian simulations. *Chem. Eng. Sci.*, 54(21), 4903-4911, 1999.

2

Image analysis to quantify sizes, velocities, interfacial areas, and coalescence behavior of gas bubbles in a 2D bubble column

This chapter is submitted for publication as:
Kluytmans, J.H.J., Wachem, B.G.M. van, Kuster, B.F.M., Schouten, J.C., Image analysis to quantify sizes, velocities, interfacial areas, and coalescence behavior of gas bubbles in a 2D bubble column, *Meas. Sci. Tech.*, 2002.

Abstract

This chapter treats the main features of the imaging technique for analysis of the hydrodynamics of 2D bubble column reactors. The described technique consists of the recording and the analysis of captured images of the bubbly flow of the gas in a 2D bubble column reactor. A detailed explanation on the image recording and the

image processing is given. Finally, five examples, viz. determination of the bubble gas hold-up, bubble size distribution, bubble rise velocity, gas-liquid interfacial area, and the coalescence of bubbles in a bubble column, are presented to show the diversity and the capabilities of the imaging technique.

2.1 Introduction

Two-phase and three-phase bubble columns have been subject of research in chemical engineering for many years. The complexity of bubble column hydrodynamics accounts for the long history and the ongoing interest in multiphase flow. Besides the complexity of the flow pattern itself, major problems are encountered in measuring the characteristics of the flow. In the last two decades, many techniques were developed to measure flow and bubble characteristics, which were recently summarized in a comprehensive review [1]. From this review it is clear that measurement techniques, like pressure sensing, hot wire anemometry, and conductivity measurements, have considerably increased the insight in two-phase and three-phase flows. However, these techniques are known to influence the gas-liquid flow pattern to a certain extent. Non-intrusive techniques, like tomography [2], laser-sheeting [3], and radioactive particle tracking [4, 5], which were mainly developed in the last two decades, do not disturb the flow pattern and are therefore considered to be more suitable. However, these techniques are usually quite expensive and require a large amount of expertise in both executing the measurements and in interpreting the results, in obtaining reliable data. A much cheaper technique for flow pattern visualization is the imaging technique. Besides the disadvantage that the imaging can only be applied on two-dimensional (2D) systems, it offers a lot of possibilities to characterize the flow behavior of two-phase and three-phase systems, because it maps the actual situation without having to reconstruct the image from measured data. Imaging exists in many forms and has already been applied in many studies [6–8]. However, in many of these studies the image analysis is restricted to a limited amount of data [6, 9, 10]. Therefore, not all opportunities of imaging are utilized. Furthermore, the image analysis is always performed in 2D bubble columns, to allow a good visibility of the flow patterns and bubble hydrodynamics. It is sometimes questioned whether the data obtained in a 2D bubble column, can be applied in 3D modelling and 3D reactor design studies. This point was addressed and published in a recent study [11] performed in our group. This study clearly showed that hydrodynamic data obtained in 2D bubble columns can be used well for 3D design and modelling studies. The present chapter shows the possibilities which image processing can provide to calculate bubble size distributions, bubble rise velocities, specific gas-liquid interfaces, volume of small and large bubbles etc., which can be applied in mass transfer and gas hold-up studies. All the software, developed for the image analysis, is available at our website[1] and may be used under reference to this chapter.

[1] http://www.chem.tue.nl/scr

2.2 Experimental setup

The image analysis as described in the present study is specifically developed to obtain quantitative data about sizes, rise velocities, and specific gas-liquid surface areas of gas bubbles in a 2D bubble column. To demonstrate the technique, imaging studies were done in a 2D bubble column that consists of two perspex plates with a height of 2 m and a width of 0.3 m. The perspex plates are placed 1.5 cm apart from each other. Gas is fed at the bottom of the column through a gas sparger, while the liquid remains inside the column. Experiments are carried out with distilled water, suspensions containing small amounts of carbon particles (0.1 - 20.0 g l^{-1}, $\overline{d}_p$ = 30 μm), electrolyte solutions (0.05 - 2.0 M sodium gluconate), and combinations of carbon particles and electrolyte solutions.

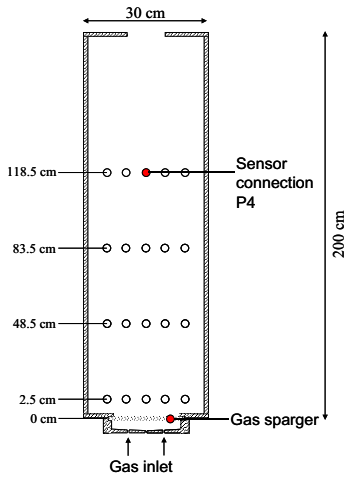

Figure 2.1: 2D perspex bubble column d·w·h 0.015·0.30·2.00 m, with 20 sensor connections located at 2.5, 48.5, 83.5, and 118.5 cm above the gas sparger. If the sensor connections were not used, they were closed flush with the wall.

The video images are captured from the front side of the column, in between the sensor connection rows shown in Figure 2.1. Unless mentioned differently, all images captured in this study cover the complete width of the 2D column and have a size of 30 cm square.

2.2.1 High-speed video recording

The video images are recorded with a high-speed Dalsa CA-D6 camera (Tech5, the Netherlands) at a rate of 955 images per second. During the recording time, the images are stored in the memory of a regular PC, until the memory is full. The working memory size of 1 GB limits the recording time to approximately 14 seconds. However, as will be shown, this recording time is sufficient to capture the hydrodynamics of the moving gas bubbles with enough accuracy. Extension of the recording time can be accomplished by extending the memory of the PC. The data is stored from the memory to the hard disk of the PC, where the images are analyzed off line with

image processing software. Because of the high capturing speed and thus the fast shutter speed of the camera, enough light should be provided to capture the images with sufficient contrast. The light is provided by 10 halogen lights of 500 W each, which enlighten the column via indirect lighting on a white screen behind the 2D bubble column. The power of the lights is transformed from alternating to direct current to prevent fluctuations in the light intensity (standard 50 Hz) which would appear in the captured images when using alternating current. The light intensity can be varied from 0-100% of the total capacity of the light, and is adjusted to provide a good contrast between the gas bubbles and the liquid suspension, depending on the composition of the medium in the column.

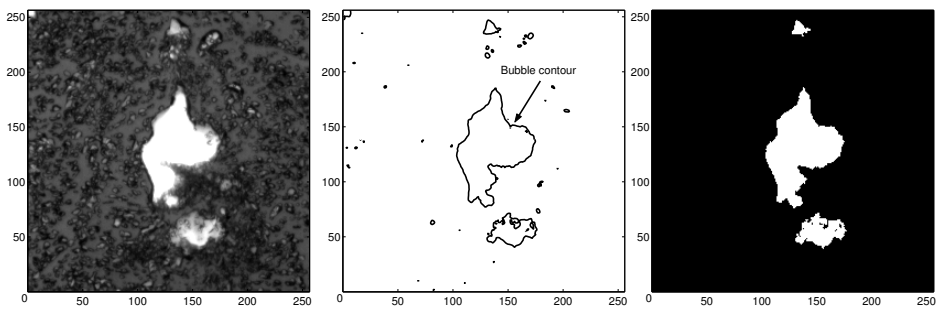

(a) Captured image (b) Bubble contours (c) Bubble areas

Figure 2.2: A recorded image of 256x256 pixels, and two examples of image manipulation. Determination of the bubble contours (b), and of the bubble areas (c). The image was recorded at a superficial gas velocity of 0.15 m s^{-1} in a 0.5 g l^{-1} carbon particle slurry.

2.2.2 Definitions

For better understanding of the image analysis and the method of image recording, some technique related and image analysis related definitions are given below:

Technique related:

Image capturing frequency The speed at which the images are recorded, given as the number of images per unit of time.

Image size The number of pixels in horizontal direction times the number of pixels in vertical direction. Usually the number of horizontal and vertical pixels are equal. In this study the image size is 256x256 pixels.

Measurement location The height above the gas sparger, in between two sensor rows as shown in Figure 2.1, at which the images are captured.

Movie/Image sequence Sequence of captured images.

Number of images The number of images in one movie.

Image analysis related:

Binary image Image in which the gray value of each pixel is replaced by a value of 1, if the gray value is above the threshold value (gas phase), and with a value of 0 as the gray value of the pixel is below the threshold value (liquid phase).

Bubble area (cm^2) The number of pixels occupied by a bubble when looking from the front side to the image (Figure 2.2c), multiplied by the pixel area.

Bubble contour (cm) The one-dimensional contour of a bubble taken from the front side of the image (Figure 2.2b).

Bubble mass middle point The mass middle point of a bubble based on the number of pixels of which the bubble consists, each pixel is considered to have the same mass.

Bubble volume (cm^3) The bubble area multiplied by the depth of the column (1.5 cm).

Equivalent bubble diameter (cm) The diameter of a flat circular bubble, covering the same number of pixels as the particular bubble that is considered.

Filtering Removal of small objects from a binary image, which are considered to be noise or objects belonging to the small bubble population. The pixels of these small objects are given the value of "0", which is the same value as for the liquid phase. These objects are thus not seen as gas bubbles anymore.

Gray value color map Color map which is used for the reconstruction of the image, in which the vales of the pixels are related to gray values, ranging from black (gray value 0) to white (gray value 255).

Image processing strategy The strategy that is followed to analyze the properties of both the large bubbles and the small bubbles in the images (Figure 2.3).

Image width (cm) The actual width covered by the image, generally equal to the width of the 2D column, 30 cm.

Large bubbles Bubbles with an average size larger than 2 cm, which touch both walls of the 2D column.

Pixel area (cm^2) Actual surface area of a pixel, $(\text{width}/256)^2 = (30\ \text{cm}/256)^2 = 0.013\ cm^2$.

Pixel size (cm) The actual size of a pixel, image width/number of pixels = 30 cm/256 = 0.12 cm.

Reconstructed image An image drawn according to the specific image data as stored in the data file on the hard disk of the PC.

Small bubbles Bubbles with an average size smaller than 2 cm, which do not touch both walls of the 2D column, of which the properties are estimated by assuming that these bubbles have an average size of 8 mm.

Specific gas-liquid surface area (cm^2) The length of the contour lines in cm, multiplied by the depth of the column (1.5 cm).

Threshold The gray value which denotes the boundary between the gas phase and the liquid phase.

2.3 Image analysis procedures

Image processing software has been developed at our laboratory to calculate bubble size distributions, specific gas-liquid interfacial areas of the gas bubbles, and bubble rise velocities. The image processing routines are programmed in Matlab 6.0 [12] and make use of standard image processing routines from the image processing toolbox. The methods and techniques used in the image analysis, are explained in the next sections. We will briefly illustrate the diversity and capabilities of the image processing techniques and methods in the study of some hydrodynamic features of bubble columns.

The images which were captured with the Dalsa CA-D6 camera are gray valued images with a size of 256x256 pixels (Figure 2.2a). This means that the images are stored as a 256x256 matrix, in which each element denotes the gray value of the corresponding pixel, ranging from 0 (black) to 255 (white). The image data is stored in the IDS format [13]. The IDS file contains only the pixel values of the captured images. A separate header file, the ICS file, contains information about the image size (256x256), the number of images in the IDS file (default 10.000 images), and additional information about the specific experiment. The IDS file is a binary file which can be opened in Matlab, after which the separate images can be plotted. Each time a 256x256 matrix is plotted using a gray value color map (Figure 2.2a). This leads to the reconstruction of the captured image. The reconstructed image can be analyzed with different techniques. All of these techniques make use of the specific gray values of the image. Therefore, only images with a good contrast between gas and liquid can be analyzed. This means for our study that the best analysis is obtained when images of carbon slurries are used. The gas phase is in that case white (gray value 255), while the liquid is gray-black. Distilled water images and images captured in electrolyte solutions have less contrast, whereas both the liquid phase as the gas phase are gray-white. These images can only be analyzed if isolated bubbles are present. This will be shown in Section 2.4.3.

In the remaining of the chapter, images of carbon particle slurries are analyzed, unless mentioned differently. The fact that a good contrast is needed for the analysis of the bubbles, implies that only bubbles which are big enough to touch both walls of the 2D column, can be analyzed. Although small bubbles in between the perspex walls can be detected visually, as seen in Figure 2.2a, they are difficult to distinguish from the liquid phase, because the gray value of these bubbles is close to the gray values of the liquid. It is visually determined from the images that bubbles smaller than the depth of the column (1.5 cm) are almost equal in size with an average diameter of about 8 mm. Based on this consideration, an image processing strategy is developed as shown in Figure 2.3, to obtain information about both the large bubble population and the small bubble population. The large bubble population is assumed to start from bubbles larger than 2 cm. Bubbles with a diameter of 2 cm have a bubble area of about 100 pixels. Objects smaller than 100 pixels are considered to be small bubbles or noise in the image, and are therefore filtered from the image by giving the pixels in these objects the value of "0" in stead of "1", before starting the image processing on the large bubbles.

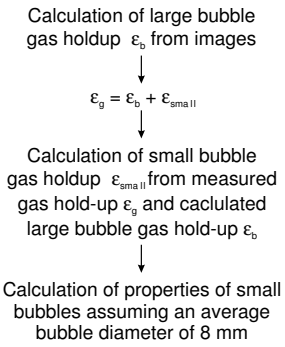

Figure 2.3: Image processing strategy to analyze bubbles touching both walls and bubbles smaller than the depth of the column.

2.3.1 Image conversion

In order to make a good distinction between the gas and the liquid phase, the gray valued image is converted to a binary image. This is achieved by choosing a threshold value, which denotes a gray value in between the gray values of the gas phase and the liquid phase. Gray values above the threshold value are turned "on" in the binary image, the pixel is given the value of 1, while gray values below the threshold value are turned "off", equaling the value of 0 in the binary image (Figures 2.4a till c). Figure 2.4c shows the pixels which correspond either with the gas phase or the liquid phase. From this binary image, the total gas fraction occupied by the large bubbles in that particular image, denoted as the large bubble gas hold-up, is calculated by counting the number of pixels with a value of 1 in the binary image, for all objects larger than 100 pixels. The actual large bubble volume is then obtained by multiplying the number of pixels by the pixel area and with the depth of the 2D bubble column hereby assuming that the bubbles have a cylindrical shape in between the perspex plates. The circumference of the bubble in between the perspex plates is thus neglected. It was calculated that the error in the estimation of the large bubble gas hold-up, which is made by assuming a cylindrical shape of the bubbles in between the perspex plates, is less than 1%. The small error is caused because the curvature

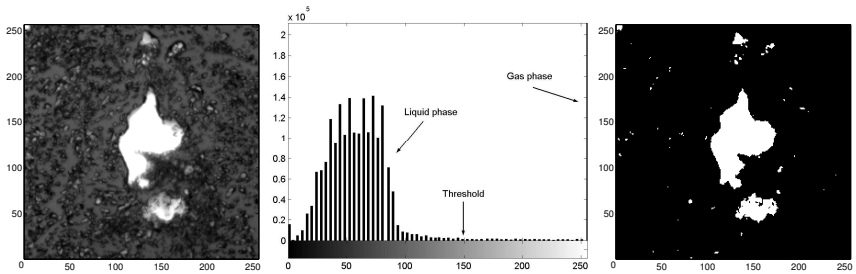

(a) Gray value image (b) Histogram plot of gray values (c) Binary image based on threshold

Figure 2.4: Separation of the gas phase and the liquid phase in a gray valued image based on a specific threshold value: (a) the gray valued image, (b) the histogram of gray values obtained from the image, and (c) the binary image.

of very large bubbles in between the perspex plates is neglected, by assuming the cylindrical shape of these bubble in between the plates. However, attention should be paid if only bubbles in between 2 and 5 cm are analyzed, because in that case the error increases to about 5%.

2.3.2 Contour plot

The circumference of the bubbles is calculated from the contour of the bubble. The contour represents an iso-threshold line which is a line connecting points of equal threshold value. An example of a bubble contour is shown in Figure 2.2b. Whereas the threshold analysis in the previous paragraph is restricted to pixels, the iso-threshold lines are represented as lines with actual coordinates. Therefore, the length of the contour can be calculated with high accuracy. The specific gas-liquid interface of the large bubbles is calculated by assuming cylindrical-shaped bubbles, as located between the perspex plates. The threshold value which provides the best representation of all bubbles in an image, is determined by trial and error. It is visually determined at which threshold value, the specific shapes and sizes of all bubbles are well described. The error that is made in this way is rather small. This was verified by calculating the average gas-liquid interfacial area in the bubble column at three different threshold values, the actual threshold value, and threshold values of +5 and -5 of the actual threshold value. This means a variation within 5% of the actual threshold value. Figure 2.5 shows that the the error in the specific gas-liquid surface area is less than 1%. From this, it is clear that the chosen threshold value describes the contour of all bubbles in the image well.

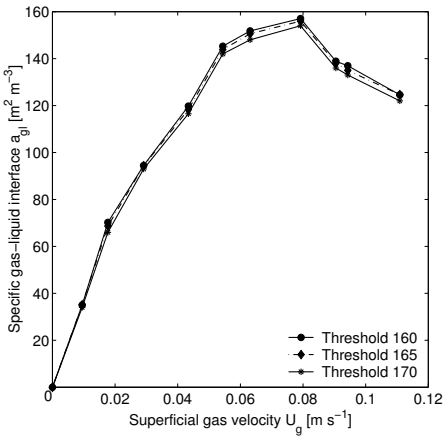

Figure 2.5: Gas-liquid interfacial area as a function of the superficial gas velocity for three different threshold values for distinguishing the gas bubbles from the liquid phase. System: 0.5 g l^{-1} carbon particles - air.

2.3.3 Image processing routine

The image processing toolbox of Matlab contains preprogrammed functions that can be used to analyze the properties of the bubbles in each of the images. With the functions included in the image processing toolbox it is possible to label single bubbles in an image with a specific number, after which specific bubble properties like the bubble area, the bubble mass middle point, and the equivalent diameter of these separate bubbles are determined. The functions of the Matlab toolbox are used in the image processing routines developed at our laboratory. These image processing routines were written to determine not only the bubble properties of bubbles in single images, but also for series of images [12]. The specific features of these image processing routines are demonstrated in view of the image processing applications as treated in Section 2.4.

2.3.4 Bubble tracking

The preprogrammed functions in the Matlab toolbox are used to determine the gas bubble properties, like equivalent diameter, mass middle point, contour, etc., of all bubbles in one image. However, in this study, images are captured at a high frequency, one after the other, and are therefore not independent but related to each other. A single rising bubble is therefore captured in multiple consecutive images. The rise velocity of the bubble determines the number of consecutive images in which the bubble will appear. If properties of individual bubbles are considered, like the average bubble diameter, the determination of the bubble properties from these images requires caution. A small bubble rising with a low rise velocity will for example appear in 50 consecutive images, while a fast rising bubble will appear only in 10 consecutive images. If e.g. the bubble diameter is determined based on analysis of the consecutive images, the bubble diameter of the slow rising bubble is

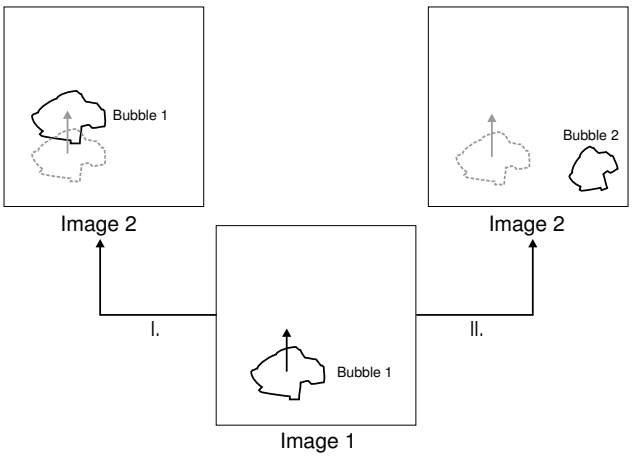

Figure 2.6: Bubble tracking procedure in which: I. the rising bubble is tracked, thus the same unique number is assigned to the bubble; II. the bubble is not tracked, thus the new bubble is assigned with a new unique number.

considered 50 times, while the bubble diameter of the fast rising bubble is considered only 10 times. This would lead to a biased result in both cases because the bubble area should only be considered once, because it concerns only one distinct bubble.

Therefore, the bubbles are to be tracked throughout the consecutive images in which they appear. The properties of each bubble are in that case only considered once, independent of the bubble rise velocity. The bubble tracking is performed according to the following procedure, and is shown in Figure 2.6:

1. A bubble entering an image is labelled with a unique number.
2. Based on the expected rise velocity of the bubble ($U_{bubble} = 0.54\sqrt{gd_{bubble}}$) [14], an estimation is made of the expected position of the bubble in the next image.
3. If an approximately equally sized ($\pm$ 2% difference in the number of pixels) bubble is detected within 4 pixels in each direction, around the estimated position in the next image, the bubble is assigned with the same unique number.
4. If a bubble is detected at the estimated position, and this bubble is not equally sized compared to the previous bubble, e.g. because the original bubble has splitted into two smaller bubbles, the new bubble is assigned with a new unique number.
5. All bubbles in the new image which are not related with bubbles in the previous image are assigned a new unique number.

This procedure is repeated for all images in the captured movie. In this way, all unique bubbles are labelled and these bubbles are only considered once, independent of the number of images in which these bubbles are present. In this way, the bubble properties are determined, without having to correct these afterwards for the difference in the number of times the bubbles appear in consecutive images in an image sequence.

2.3.5 Accuracy

The accuracy of the image processing depends on several parameters. First of all, the resolution of the images determines the accuracy of the estimated diameter or width of the bubbles. The resolution is expressed as the minimum size of an object that can be distinguished in an image. For example, if the image has a size of 30 cm square, the minimum size of objects that can be distinguished is 30 cm/256 pixels = 0.12 mm. An object smaller than this size, can not be seen, because its size falls inside a single pixel. The resolution of an image can be increased by decreasing the actual width of an image, or by increasing the number of pixels of an image. The latter option is not realistic as the number of pixels per image is determined by the hardware and cannot be changed.

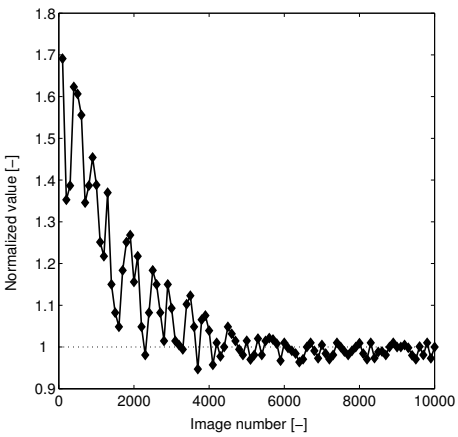

Figure 2.7: Schematic representation of the normalized value of a calculated bubble property, as a function of the number of analyzed images.

The number of images that needs to be analyzed, in order to be assured that the correct value of a parameter is determined, is obtained via the following procedure. This procedure applies for all parameters (e.g. bubble size distribution, bubble rise velocity, specific gas-liquid interfacial area, bubble gas hold-up), unless mentioned differently.

1. Each time, after processing 100 images, the time-averaged values are determined.

2. This value of the time-averaged value is compared with the previous determined value.
3. If the deviation between the present and previous value is less than 5%, it is assumed that the parameter has obtained its steady (constant) value, and is considered as independent of the remaining images.

Usually, convergence to a constant value is obtained after analyzing 4000-6000 images of the total of 10.000 images in the image sequence. This is shown in Figure 2.7. The procedure as described above concerns the determination of the value of a specific parameter from a single movie. However, the accuracy of the considered parameters is obtained from multiple and independent movies, captured under the same experimental conditions. The parameter value obtained from duplicate measurements is assumed to be accurate, if the deviation is less than 5%.

2.4 Image processing applications

The image processing techniques, as described in the previous sections can provide valuable information about several hydrodynamic phenomena in bubble columns. Five examples will be given to show the specific applications and advantages of image processing for bubble column research: estimation of the bubble gas hold-up, estimation of the bubble size distribution, estimation of the rise velocity of bubbles, estimation of the specific gas-liquid interfacial area, and the investigation of the bubble coalescence behavior of bubble pairs in a 2D bubble column.

2.4.1 Bubble hold-up

The volume occupied by gas, when it is lead through a liquid in a bubble column, is called the gas hold-up. The gas hold-up is usually expressed as the fraction of the gas volume, related to the total volume of gas and liquid. The total gas volume in a bubble column is the sum of the volume of the small bubbles (with an average bubble diameter smaller than 2.0 cm), and the volume of the large bubbles (with a diameter larger than 2.0 cm). The total gas hold-up in a bubble column can be estimated by visual determination of the liquid bed expansion. The local gas hold-up in a bubble column can be determined from differential pressure measurements done at several heights in the column. With these methods the gas hold-up of the small and the large bubbles cannot be determined separately. However, these values can be obtained from imaging which will be demonstrated below.

Images are captured in between the pressure sensor rows as indicated in Figure 2.1. The captured images are converted to binary images. Then, objects smaller than 100 pixels are filtered from the image as these objects are assumed to be smaller than 2 cm, and thus belong to the small bubble population. The resulting white pixels in the binary image after filtering (Figure 2.4c), belong to the large bubbles, and are

counted. This results in the number of pixels which are occupied by the large bubbles. While the large bubbles are assumed to have a cylindrical shape, the volume of the large bubbles per image is obtained by multiplying the number of pixels, with the actual pixel size, and with the depth of the column, viz. 1.5 cm, to obtain the large bubble volume. This procedure is repeated for all images in an image sequence, and the volumes occupied by the large bubbles are added for all images. The total volume occupied by the large bubbles in the image sequence is thus obtained. The average volume of the large bubbles per image, is determined by dividing the total volume occupied by the large bubbles in the image sequence, by the number of images in that sequence.

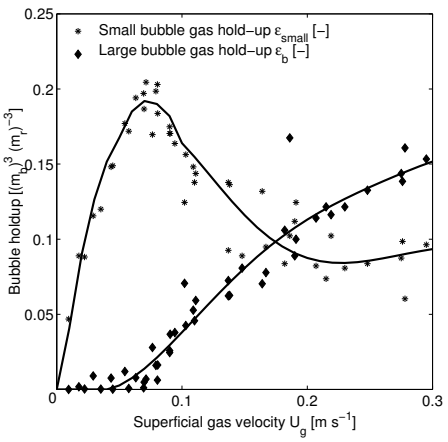

Figure 2.8: Measured data fractions large and small bubbles, in a 2D slurry bubble column, obtained at different superficial gas velocities. The lines are drawn to guide the eye, and are based on a polynomial fit of the data.

The gas hold-up of the small bubbles can then be calculated following the procedure as shown in Figure 2.3. First, the local gas hold-up ε_g at the position of the captured images is calculated from the pressure sensors above and below the position at which the images are captured (Figure 2.1), because this calculated gas hold-up is representative for the local gas hold-up in that part of the column [15]. The average volume of the large bubbles, determined from the image analysis, is divided by the total volume of the image (30 cm x 30 cm x 1.5 cm) to obtain the large bubble gas hold-up ε_{large}. The gas hold-up of the small bubbles is then obtained by subtracting the gas hold-up of the large bubbles from the local gas hold-up: $\varepsilon_{small} = \varepsilon_g - \varepsilon_{large}$.

The values of the small and large gas hold-ups can be determined at several positions in the column. For modelling purposes, it is useful to know the contributions of the large and small bubble gas hold-up to the overall gas hold-up in the bubble column. For that purpose, the gas hold-up of the small and large bubbles should be determined from images, captured at a position where the local gas hold-up is equal to the overall gas hold-up. It is shown in a previous study [15], that this is the case when the images are captured in between the sensor rows located at 83.5 and 118.5

cm above the gas sparger (Figure 2.1).

Examples of the separate values of the large and small bubble gas hold-ups as determined in this way, are shown in Figure 2.8. It is found that the small bubble gas hold-up is much larger than the large bubble gas hold-up up to superficial gas velocities of 0.1 m s^{-1}. For superficial gas velocities above 0.1 m s^{-1} the gas hold-up of the small bubbles decreases, while the gas hold-up for the large bubbles increases. At superficial gas velocities above 0.2 m s^{-1}, the gas hold-up of the small bubbles becomes constant, while the large bubble gas hold-up still increases. Krishna et al. [16] already assumed that the volume of the small bubbles becomes constant at higher superficial gas velocities. Figure 2.8 shows that this assumption is indeed valid above superficial gas velocities of 0.2 m s^{-1}.

2.4.2 Bubble size distribution

The time-averaged bubble size distribution at a certain superficial gas velocity, can be determined from images covering the whole bubble column. However, because of the large area of the bubble column, the size of the bubbles is difficult to determine from these images, because the resolution of the images will be very low. A bubble size distribution, based on these images will therefore not be very accurate (Section 2.3.5). The bubble size distribution can however be determined more accurately from images covering only a part of the bubble column, as long as the local gas hold-up in that part is equal to the total gas hold-up in the column.

To obtain a accurate estimation of the bubble size distribution in a bubble column, images should be captured covering the width of the bubble column. However, it is possible to capture the images at a certain height in the column. The image capturing of only a part of the column requires caution. Biased results are easily obtained while working at low capturing frequencies, or when not taking into account the difference in rise velocity of small and large bubbles in the image analysis, as mentioned in Section 2.3.4. In case a low image capturing frequency is employed, a large number of images needs to be recorded, due to the high velocity of large bubbles. In that case, large bubbles can pass the position at which the images are recorded, without being captured in the images. When using a high image capture frequency, at which it is assured that the fastest rising bubbles in the column are captured in at least one or more images, each bubble is taken into account, thus automatically leading to satisfactory statistics. The bubble tracking procedure as described in Section 2.3.4 is then applied on these images. The equivalent diameter of all tracked bubbles is then calculated. The bubbles are then sorted by this equivalent diameter, and added to their respective bubble classes (class width : 0.5 cm, starting from a bubble diameter of 2.0 cm). The number of bubbles in each class is then divided by the total number of bubbles, to obtain the normalized bubble size distribution.

The accuracy of the normalized bubble size distribution is determined according

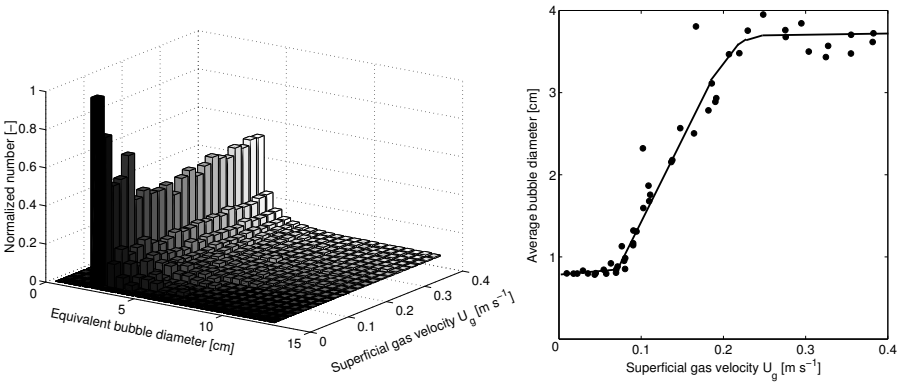

Figure 2.9: a) Normalized bubble size distribution of bubbles larger than 2 cm as a function of the superficial gas velocity. b) Average bubble diameter as a function of the superficial gas velocity. Bubble size distribution and average bubble diameter are calculated from 51 movies, each consisting of 10.000 images. Carbon particle slurries (0.1 - 2.0 g l^{-1}).

to the procedure described in Section 2.3.5. After each 100 images, the normalized bubble size distribution is calculated based on the thus far analyzed images. This new bubble size distribution is compared with the previous calculated bubble size distribution. Per bubble class, the relative deviation between the present and previous normalized distribution, is calculated. These deviations are added for all bubble classes. If the total, relative deviation is less than 5%, it is assumed that the bubble size distribution has converged. In most cases, this criterion is reached after analyzing approximately 5000 of the 10.000 images per image sequence.

An example of the thus estimated normalized bubble size distribution, as a function of the superficial gas velocity, is shown in Figure 2.9. It can be seen that the bubble size distribution hardly changes for superficial gas velocities above 0.1 m s^{-1}. The average bubble diameter as a function of the superficial gas velocity as calculated from the bubble size distribution (Figure 2.9b) at superficial gas velocities below 0.1 m s^{-1} is equal to 8 mm and increases with increasing superficial gas velocity. At superficial gas velocities above 0.25 m s^{-1} the average bubble diameter becomes approximately constant.

2.4.3 Bubble rise velocity

The gas hold-up in two-phase and three-phase systems is mainly determined by the rise velocities of the gas bubbles. Estimation of the bubble rise velocity is therefore crucial to predict the gas hold-up [11]. The bubble rise velocity can be determined with the bubble tracking procedure in Section 2.3.4. However, performing this anal-

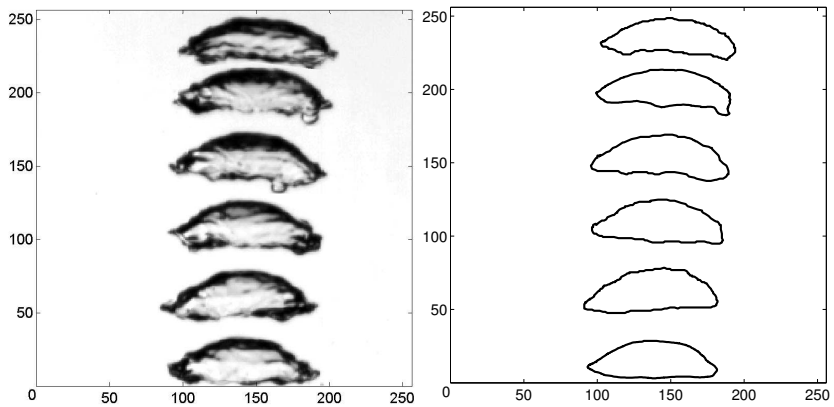

Figure 2.10: The rise of a single bubble projected in one image (a), and the reconstructed image (b). The rise velocity is determined by taking the displacement of the top of the bubble as a function of time. The bubble is plotted at respectively 0, 50, 100, 150, 200 and 240 msec. System: Air-Distilled water. Image size 15 cm x 15 cm. Bubble width approx. 5 cm.

ysis on images recorded in the heterogeneous regime where many gas bubbles are present, will not lead to an accurate value of the rise velocity as a function of the bubble diameter. The rise velocity of a gas bubble is a function of the bubble shape and especially the width of the gas bubble. The bubbles in an image however do not have a clearly defined circular or elliptical shape, as can be seen in Figure 2.2a. Furthermore, the bubble diameter as determined in the bubble tracking procedure, is the equivalent diameter. This is the diameter of a circular bubble, covering the same number of pixels as the particular bubble that is considered. This equivalent diameter is in most cases not equal to the width of the gas bubble. A long-stretched and narrow bubble, has an equivalent diameter which is much larger than the actual width of the bubble. Figure 2.2a shows that the equivalent diameter is not equal to the width of the gas bubble, and is therefore not a representative measure for the bubble width which determines the bubble rise velocity. Therefore, it was chosen to determine the bubble rise velocity of single spherical cap bubbles, which were injected with a needle, placed inside the 2D bubble column. In this case, the determination of the bubble width is more straightforward. Furthermore, with this method, the rise velocity of single spherical cap bubble can be determined, which can be verified with existing correlations, and can be applied in gas hold-up modelling studies [11].

Bubbles were released from an injection tip at the bottom of the column. The bubble trajectory in the area where the images are captured, was determined by projecting

the rising bubble in one image. This image was analyzed by determining the bubble contour as explained in Section 2.3.2. The recorded image of the rising bubble and the reconstructed image are shown in Figure 2.10. The rise velocity is calculated by measuring the bubble displacement as a function of time. The thus calculated rise velocity is plotted against the bubble width in Figure 2.11, together with rise velocity predicted from the correlation by Pyle and Harrison [14] for single bubbles in a 2D bubble column ($U_{bubble} = 0.54\sqrt{gd_{bubble}}$). It can be seen that the measured rise velocity is somewhat higher than the predicted rise velocity by Pyle and Harrison [14]. This difference may be due to the error in the determination of the bubble width. As can be seen in Figure 2.10a, the contour of the bubbles, is not sharply defined. This is caused by the shaded layer around the bubbles, caused by the curvature of the bubble surface and the movement of the bubble. The accuracy of the determined bubble width depends on the thickness of this shaded layer, which is normally 3-5 pixels. For an image with a size of 15 cm square, as used in this study, this deviation results in an error in the bubble width of about 0.5 cm, independent of the bubble width itself. The error bars in Figure 2.11 indicate this error.

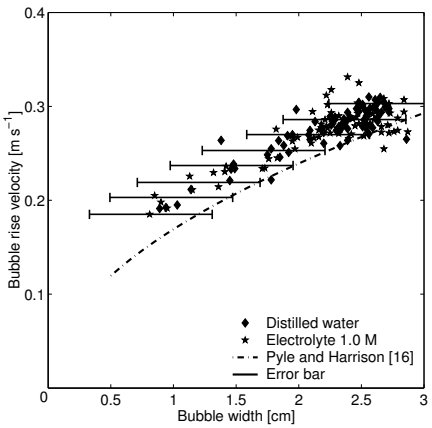

Figure 2.11: Rise velocity of single bubbles in distilled water and in a 1.0 M electrolyte solution and the predicted rise velocity calculated with the correlation of Pyle and Harrison [14] as a function of the maximum width of the spherical cap bubble. The error in the determination of the bubble width is expressed by the error bars.

2.4.4 Specific gas-liquid interfacial area

An accurate determination of the specific gas-liquid surface area in a bubble column, is useful while studying the gas-liquid mass transfer. In this way, changes in the mass transfer coefficient, which consists of a system specific constant k_l multiplied by the specific gas-liquid surface area a_{gl}, can be studied in more detail.

To calculate the specific gas-liquid interfacial area, image processing was performed on 51 movies. Each movie consists of 10.000 images. Each image was treated according to the following procedure:

1. The contour of all large bubbles in each image is determined with the procedure as described in Section 2.3.2.
2. The length of the contour of the large bubbles is calculated, and multiplied by the depth of the column (1.5 cm) to obtain the specific gas-liquid surface area of the large bubbles in each image.
3. The procedure as described in (1) and (2) is repeated for each image, and the surface areas per image are added for all images. The time-averaged surface area is then obtained by dividing the total surface area by the number of images. This is the average surface area of the large bubbles, per image.
4. The average volume of the large and small bubbles is then calculated as described in Section 2.3.2. It was determined from the images that the small bubbles have an average bubble diameter of 8 mm. Because these bubbles do not touch the walls of the 2D column, they are assumed to be spherically shaped. The surface area of the small bubbles is determined by first calculating the number of small bubbles which fit into the small bubble gas volume. The surface area of the small bubbles is then calculated by multiplying the calculated number of bubbles, with the surface area of a single small bubble of 8 mm diameter.
5. The surface areas of the small and the large bubbles are added to obtain the total specific gas-liquid surface area.

The resulting specific gas-liquid surface area is plotted as a function of the superficial gas velocity in Figure 2.12. It can be seen that at first the surface area increases for

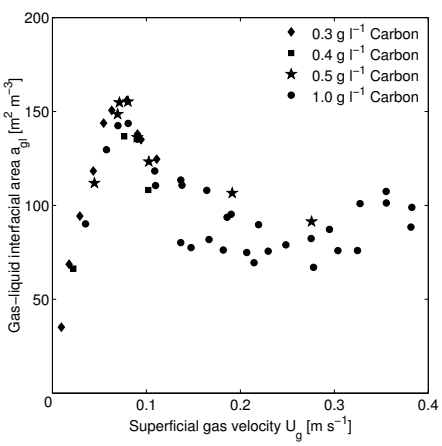

Figure 2.12: Specific gas-liquid surface area for different carbon particle slurries as a function of the superficial gas velocity.

superficial gas velocities up to 0.07 m s^{-1}. At these low superficial gas velocities, the gas volume is occupied by only small bubbles, which have a high area to volume ratio, thus resulting in a large specific surface area. At superficial gas velocities above 0.07 m s^{-1}, the number of large bubbles starts to increase, resulting in a decrease

in the specific gas-liquid surface area, because the large bubbles have a much lower area to volume ratio, compared to the small bubbles. In the heterogeneous regime, at superficial gas velocities above 0.2 m s^{-1}, the specific gas-liquid surface area becomes constant, because at these superficial gas velocities, the gas volume of both the large and the small bubbles becomes almost constant, as was already shown in Figure 2.8.

2.4.5 Bubble coalescence

The last example illustrates the use of the imaging technique to observe the coalescence of two gas bubbles rising in a liquid (as in a bubble column). Image-by-image analysis allows to observe the process of coalescence of two gas bubbles from millisecond to millisecond. Gas bubble coalescence and gas bubble break-up are important phenomena in bubble columns, because they influence the bubble size distribution, and thus the gas hold-up.

Many studies are reported in the literature [17–19] in which bubble coalescence is studied under stagnant conditions, in which the gas bubbles remain attached to the injection tip, while deliberately being pushed together. It is however more relevant for bubble column studies to observe the coalescence of these bubbles as they rise in the liquid. Therefore, coalescence is studied in the present work by releasing two gas bubbles, one after the other, from an injection needle placed inside a 2D column filled with liquid. From the recorded images of these rising bubbles, the contours of the bubbles are determined to observe their behavior and interaction during their rise in the liquid column, to measure the time period between first contact and final merging of the bubbles (coalescence time), and to quantify the probability that the bubbles coalesce to form one new bubble (coalescence probability).

Two bubbles will merge if the thickness of the liquid film separating them, decreases sufficiently fast during contact. If the thinning of this liquid film is not fast enough, the film will not break and the bubbles will bounce back without merging. The chance that the bubbles will merge, i.e. the coalescence probability, is influenced by the way the bubbles approach, by the viscosity of the liquid, by the rise velocities of the interacting bubbles, etc. [20]. The thinning and breaking of the liquid film between the bubbles as well as the collision and bouncing of the bubbles can be well observed using the imaging method.

150 bubble pairs were released from the injection needle in distilled water and in a 1.0 M electrolyte solution. The coalescence probability was calculated from the number of pairs of bubbles that do coalesce (Figure 2.13) and the number of pairs of bubbles which collide and bounce without merging (Figure 2.14). It was found that 54% of the bubble pairs in distilled water coalesced, while the coalescence probability in the electrolyte solution was 75%. However, it was also observed from visual

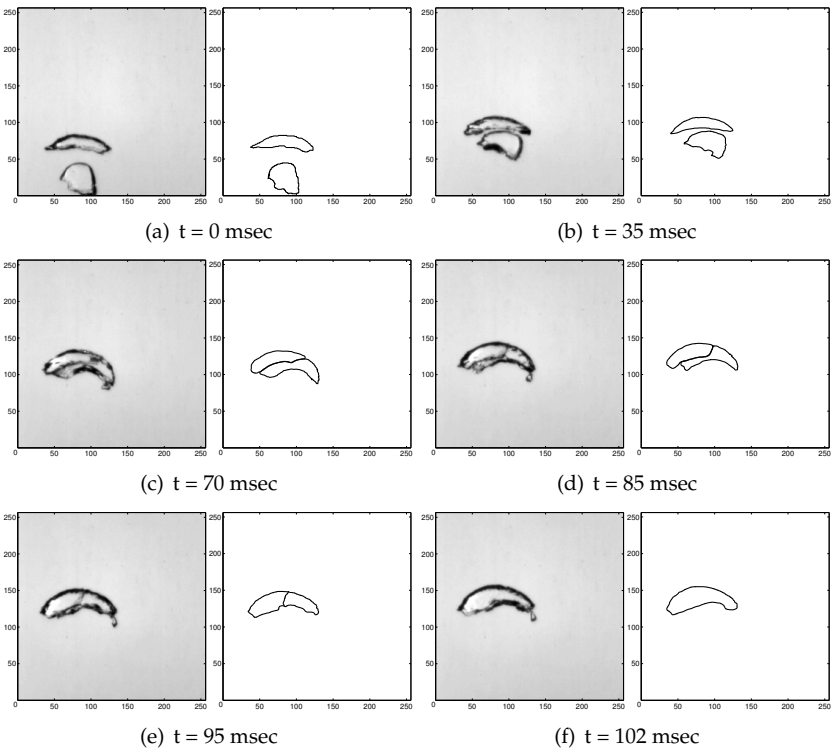

(a) t = 0 msec (b) t = 35 msec

(c) t = 70 msec (d) t = 85 msec

(e) t = 95 msec (f) t = 102 msec

Figure 2.13: Recorded and reconstructed bubble pair rising in distilled water. Bubble coalescence takes place in between t = 95 msec and t = 102 msec.

analysis of the recorded images that the way the bubbles near each other, significantly influences the probability of coalescence. In the present 2D column with the needle injection used, it was not possible to accurately reproduce for each bubble pair the bubbles' pathways and the way the bubbles near each other. This implies that the statistical significance of the reported coalescence probabilities should be further investigated.

This issue of statistical significance of the observed differences between coalescence of bubbles in distilled water and in electrolyte solution is illustrated by measuring the so-called coalescence time. This is the time period in between the first contact of the bubbles in the bubble pair, and the moment at which the two bubbles have fully merged to form one new bubble. The coalescence time is thus determined from the moment that the contour lines of the two bubbles touch and the moment that the complete contour of the new bubble has been formed. The coalescence times for all

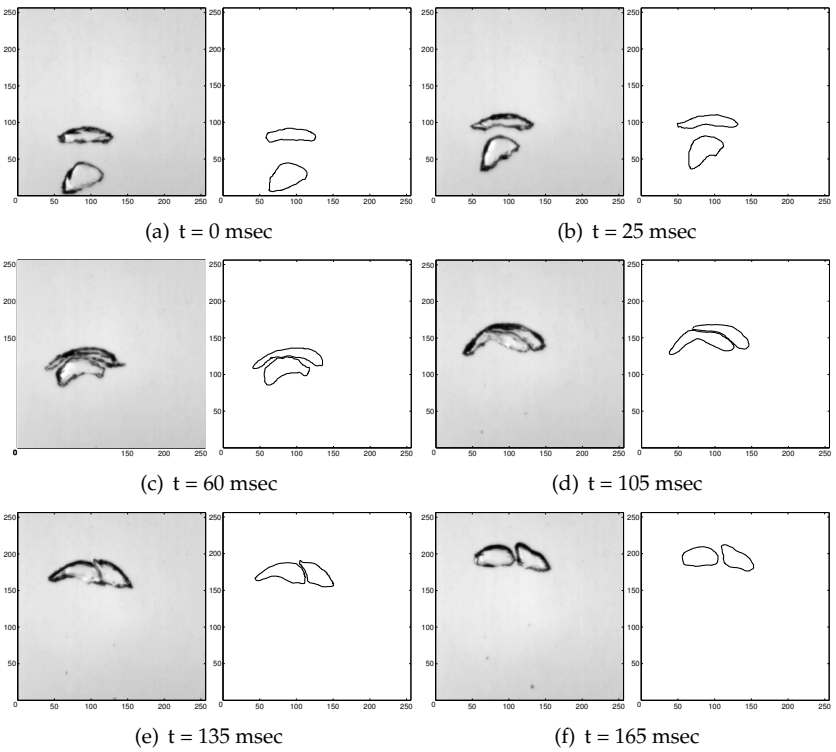

(a) t = 0 msec (b) t = 25 msec

(c) t = 60 msec (d) t = 105 msec

(e) t = 135 msec (f) t = 165 msec

Figure 2.14: Recorded and reconstructed bubble pair rising in distilled water. Bubbles touch but do not coalesce.

pairs of bubbles that coalesced, are given in Figure 2.15a. The average coalescence times shown in this figure suggest that bubble coalescence in electrolyte solutions is delayed compared to distilled water. However, the data points exhibit a large scatter. The Mann-Whitney statistical test [21] shows that these average coalescence times are not significantly different, based on a 95% confidence interval. Visual analysis of the recorded images revealed that if bubbles collided sideways, the coalescence process is much faster compared to the case in which the trailing bubble collides with the bottom of the leading bubble. Therefore, a selection was made in which only those pairs of bubbles were considered of which the mass middle points of the bubbles were aligned during the bubble approach within a width of $\pm$ 10 pixels (Figure 2.15b). Although the Mann-Whitney test result improved, the subsets can still not be statistically discriminated.

These results indicate clearly that the imaging technique can be usefully applied

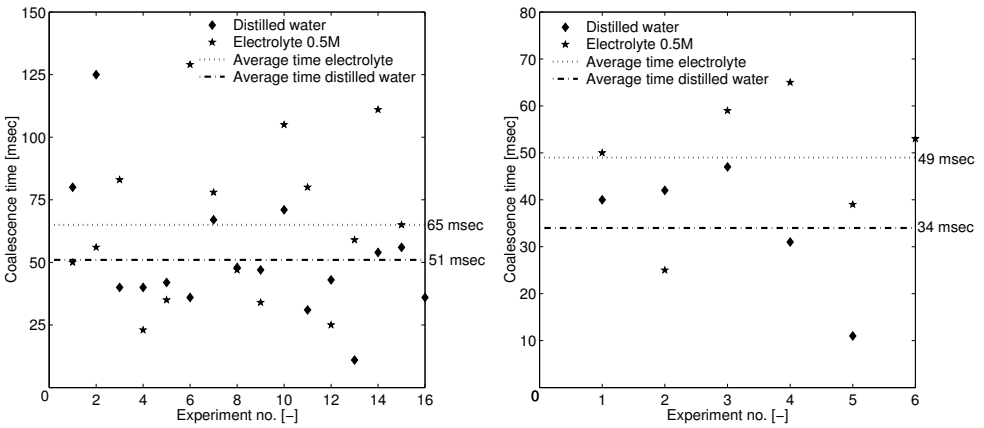

Figure 2.15: (a) Coalescence time for coalescing bubble pairs in distilled water and in a 1.0 M electrolyte solution. (b) Coalescence times for selected bubble pairs in distilled water and electrolyte solutions. The lines indicate the average coalescence times for both systems.

to observe and quantify bubble coalescence. However, in this particular case, it was found that the reproducibility of the experimental method should be improved to be able to draw conclusions on the observed differences between bubble coalescence in distilled water and in the electrolyte solution.

2.5 Concluding remarks

This study shows that the imaging technique provides valuable information for the investigation of the hydrodynamic properties of a bubble column. By analyzing the specific properties of the bubbles like the contours, the bubble areas, the bubble diameter etc. in the recorded images, it is possible to make an estimation of

- the large and small bubble gas hold-up.
- the bubble size distribution.
- the total specific gas-liquid surface area, and the separate contribution of the small and the large bubbles to the specific gas-liquid surface area.
- the rise velocity of single bubbles, as a function of the bubble diameter.
- the influence of the way two bubbles approach, on the process of bubble coalescence.

Acknowledgement

T.W.F.J van Elst is gratefully acknowledged for his contribution to the work on the coalescence behavior of bubbles in aqueous systems, as described in section 2.4.5.

Bibliography

[1] Boyer, C., Duquenne, A.M., and Wild, G., Measuring techniques in gas-liquid and gas-liquid-solid reactors, *Chem. Eng. Sci.*, 57(16), 3185-3215, 2002.

[2] Schmitz, D., and Mewes, D., Tomographic imaging of transient multiphase flow in bubble columns, *Chem. Eng. Sci.*, 77, 99-104, 2000.

[3] Chaouki, J., Larachi, F., and Dudukovic, M.P., Noninvasive tomographic and velocimetric monotoring of multiphase flows, *Ind. Eng. Chem. Res.*, 36, 4476-4503, 1997.

[4] Dudukovic, M.P., Devanathan, N., and Holub, R., Multiphase reactors: Models and experimental validation, *Rev. Inst. Fr. Pet.*, 46, 439-465, 1991.

[5] Chen, J., Kemoun, A., Al-Dahhan, M.H., Dudukovic, M.P., Lee, D.J., and Fan, L.-S., Comparative hydrodynamics study in bubble columns using computer-automated radioactive particle tracking (CARPT)/computed tomography (CT) and particle image velocimetry (PIV), *Chem. Eng. Sci.*, 54, 2199-2207, 1999.

[6] Swart, J.W.A. de, and Krishna, R., Influence of particles concentration on the hydrodynamics of bubble column slurry reactors, *Chem. Eng. Res. Des.*, 73(A3), 308-313, 1995.

[7] Letzel, H.M., Schouten, J.C., Krishna, R., and Bleek, C.M. van den, Gas holdup and mass transfer in bubble column reactors operated at elevated pressure, *Chem. Eng. Sci.*, 54(13-14), 2237-2246, 1999.

[8] Lin, T.-J., Tsuchiya, K., and Fan, L.-S., Bubble flow characteristics in bubble columns at elevated pressure and temperature, *Am. Inst. Chem. Eng. J.*, 19, 99-113, 1998.

[9] Polli, M. Stanislao, M. di, Bagatin, R., Bakr, E.A., and Masi, M., Bubble size distribution in the sparger region of bubble columns. *Chem. Eng. Sci.*, 57(1), 197-205, 2002.

[10] Mudde, R.F., Schulte, H.B.M., and Akker, H.E.A. van den, Analysis of a bubbling 2D gas-fluidized bed using image processing, *Powder Technol.*, 81(2), 149-159, 1994.

[11] Kluytmans, J.H.J., Wachem, B.G.M. van, Kuster, B.F.M., Krishna, R., and Schouten, J.C., 2D bubble column hydrodynamic phenomena clarified with a 3D gas-liquid model. *Accepted for presentation at the GLS 6 conference, Vancouver, Canada, submitted for publication in Can. J. Chem. Eng.*, 2003.

[12] Matlab 6.0, Matlab 6.0 image processing toolbox, and Matlab image processing scripts: **seriesofmovies.m** : routine to analyze multiple IDS movie files, **mainmeasure.m** : main routine to calculate specific gas-liquid surface area of gas bubbles, in one movie file, **analysesurface.m**: calculation routine which is called to calculate specific gas-liquid surface area of gas bubbles, **measfeauture.m**: calculation routine to measure the equivalent diameter, the position and the area of gas bubbles in an image, **makebinary.m**: routine to convert images from gray value images to binary images, based on a threshold value, **surfacesmall.m**: routine to calculate the surface area of the total volume of small bubbles, **bubblefollow.m**: routine to track bubbles troughout image sequences, **sortandcalc.m**: routine to determine bubble size distribution from the tracked bubbles Image processing scripts and documentation available on http://www.chem.tue.nl/scr/

[13] Dean, P., Mascio, L., Ow, D., Sudar, D., and Mullikin, J., Proposed standard for image cytometry data files, *Cytometry*, 11, 561-569, 1990.

[14] Pyle, D.L., and Harrison, D., The rising velocity of bubbles in two-dimensional fluidized beds, *Chem. Eng. Sci.*, 22(4), 531-535, 1967.

[15] Kluytmans, J.H.J., Wachem, B.G.M. van, Kuster, B.F.M., and Schouten, J.C., Gas holdup in a slurry bubble column: Influence of electrolyte and carbon particles, *Ind. Eng. Chem. Res.*, 40(23), 5326-5333, 2001.

[16] Krishna, R., Baten, J.M. van, Urseanu, M.I., and Ellenberger, J., A scale up strategy for bubble column slurry reactors, *Cat. Today*, 66(2-4), 199-207, 2001.

[17] Zahradnik, J., Fialova, M., Kastanek, F., Green, K.D., and Thomas, N.H., The efect of electrolytes on bubble coalescence and gas holdup in bubble column reactors, *Trans IChemE*, 73(A), 341-346, 1995.

[18] Marrucci, G., A theory of coalescence. *Chem. Eng. Sci.*, 24, 975-985, 1969.

[19] Drogaris, G., and Weiland, P., Coalescence behavior of gas bubbles in aqueous solutions of n-alcohols and fatty acids, *Chem. Eng. Sci.*, 38(9), 1501-1506, 1983.

[20] Smith, J.M., Coalescence phenomena. UK, Hemisphere Publishing Corporation, 1991.

[21] Spiegel, M.R., Chapter 17 in Schaum's outline of theory and problems of statistics, 373-374, 1988.

3

Gas hold-up in a slurry bubble column: Influence of carbon particles and electrolyte

This chapter has been published as:
Kluytmans, J.H.J., Wachem, B.G.M. van, Kuster, B.F.M., Schouten, J.C., Gas hold-up in a slurry bubble column: Influence of carbon particles and electrolyte, *Ind. Eng. Chem. Res.*, 40(23), p. 5326, 2001.

Abstract

This study deals with the effects of electrolyte and particle concentrations on the gas hold-up in both the homogeneous and the heterogeneous flow regimes in a slurry bubble column. Gas hold-up measurements and video recordings of the bubble behavior were carried out in a 2D slurry column (0.015x0.30x2.00m) at ambient conditions. The addition of electrolyte (sodium gluconate, 0.05-0.2M) and of solid carbon particles (diameter 30 μm, 0.1-1.0 g l^{-1}) both show a considerable increase in gas

hold-up. In both cases critical concentrations exist above which no further increase of gas hold-up is observed. The transition from the homogeneous to the heterogeneous regime is significantly affected by the presence of electrolyte as well as by the presence of carbon particles. Three mechanisms are proposed which might account for the gas hold-up increase due to particle and electrolyte addition. It is suggested that a layer of carbon particles around the gas bubbles results in a lower average bubble rise velocity. Both the addition of carbon particle and electrolyte lead to bubble stabilization, a decreased rate of coalescence, and thus a higher gas hold-up. It is further suggested that the presence of electrolyte changes the surface tension, leading to smaller bubbles, a lower average bubble rise velocity, and thus a higher gas hold-up. The combined addition of electrolyte and carbon particles confirms these hypotheses.

3.1 Introduction

Increasingly, bubble columns find their application in chemical industries, for example in Fischer-Tropsch processes or in biological wastewater treatment. Bubble columns incorporate many advantages like easy construction, easy operation, and severe mixing of the phases by gas aeration only. The hydrodynamic behavior, governed by bubble-bubble, bubble-particle and bubble-liquid interactions, is still a major research topic, judging upon the recent review of Joshi et al. [1], covering 253 references on bubble column reactors.

In literature, attention for gas hold-up prevails because gas hold-up affects mixing and mass transfer and therefore the performance of the system. Gas hold-up is influenced by many parameters, like particle concentration [2–4], electrolyte concentration [5], liquid viscosity, and surface tension. Increase in gas hold-up was reported due to addition of electrolyte [5] and addition of wettable particles [2–4]. Although many mechanisms are proposed for this gas hold-up increase, still there is no agreement upon which mechanism prevails.

3.2 Objective

In literature, many gas hold-up studies are performed with model systems using distilled water as a liquid phase, air as a gas phase, and silica or glass beads as the solids phase. Because the present study is part of a research project that aims at the investigation of an actual reaction system [6], the effect of carbon particles and electrolyte concentration on the hydrodynamics was studied. Both particle and electrolyte concentrations were kept low to study the effect of particles and electrolyte on bubble-bubble and bubble-particle interactions, without significantly changing the bulk properties of the liquid. With a combination of experimental techniques, like local and overall gas hold-up measurement and high-speed video imaging, the

mechanisms accounting for the increase in gas hold-up due to electrolyte and particle addition were investigated.

3.3 Experimental set-up and procedures

Gas hold-up experiments were carried out with different carbon particle and electrolyte concentrations. All experiments were carried out in a 2D slurry bubble column as shown in Figure 3.1. Carbon particles with a mean diameter of 30 μm were used and sodium gluconate was used to study electrolyte concentration effects.

3.3.1 Gas hold-up measurement

The pressure difference between two pressure sensors represents the local gas hold-up according to Equation 3.1:

$$\varepsilon_{i,j}^{local} = \frac{(\bar{p_j} - \bar{p_i})_0 - (\bar{p_j} - \bar{p_i})_{aerated}}{(\bar{p_j} - \bar{p_i})_0} \qquad with\, i,j\, =\, 1,2,3,4 \tag{3.1}$$

Also, the overall gas hold-up in the column was measured, both visually and with a float. The float accurately follows the movement of the liquid surface. The movement of the float is measured with a Honeywell K180E ultrasonic distance sensor. Signals of the float position and the four pressure signals were measured for two minutes with a sample frequency of 50 Hz. The time series were averaged to obtain average pressures and average liquid heights. The total gas hold-up is calculated with Equation 3.2:

$$\varepsilon_G^{total} = \frac{H_1 - H_0}{H_1} \tag{3.2}$$

with H_0 the non-aerated liquid height and H_1 the average aerated liquid height.

3.3.2 Transition point measurement

The homogeneous regime is characterized by a low superficial gas velocity, a narrow bubble size distribution, small bubbles, and a low rate of bubble coalescence. When the superficial gas velocity is increased, the homogeneous regime changes into the heterogeneous regime. The heterogeneous regime is characterized by a higher rate of bubble coalescence, a wider bubble size distribution, in which both large and small bubbles exist. The superficial gas velocity at which the homogeneous regime changes into the heterogeneous regime is called the transition velocity. Changes at the transition point between the homogeneous and heterogeneous flow regimes can give insight in the mechanisms of gas hold-up increase. Several techniques have been proposed to determine the transition point. Vial et al. [7] compared different techniques to estimate the transition point from pressure signals. Part of their findings are in agreement with work of Letzel et al. [8]. Letzel et al. employ the

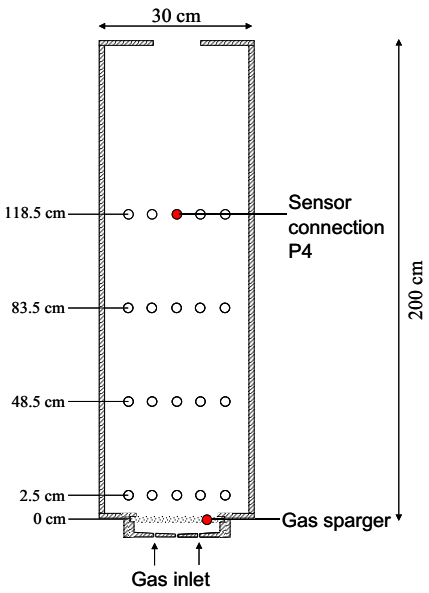

*Figure 3.1: 2D perspex bubble column d*w*h 0.015*0.30*2.00 m, with 20 sensor connections located at 2.5, 48.5, 83.5, and 118.5 cm above the gas sparger. If the sensor connections were not used, they were closed flush with the wall. Four Drck PTX 400 pressure sensors were connected in the middle position of each sensor row, from bottom to top numbered from P1 to P4.*

Kolmogorov entropy to determine the transition point, where Vial et al. prefer the relative standard deviation of the pressure signal. In the present study the relative standard deviation and the average cycle frequency are used. Although, the average cycle frequency is directly related to the Kolmogorov entropy as used by Letzel et al., the average cycle frequency is much quicker and easier to calculate, which is the reason that we used it in this work.

Using the average cycle frequency, the transition point between the homogeneous and the heterogeneous flow regimes is estimated from a graph of the average cycle frequency fc of the measured pressure signals as a function of the superficial gas velocity. The average cycle frequency is defined as $f_c = n_t/(2*t_m)$, where t_m is total measuring time of the pressure signal and n_t is the number of events the pressure signal crosses it's mean value. The average cycle frequency provides a characteristic measure of the bubble dynamics and therefore serves as an indicative measure of regime transition.

3.3.3 Experimental conditions

In the review of Joshi et al. [1] it can be seen that gas hold-up in a bubble column is affected by many parameters, like the liquid viscosity, the gas density, the initial liquid height or the type of gas which is used. However, from several experiments in this study it was observed that within a small range of liquid viscosity (1.0 to 2.0 kg m^{-1} s^{-1}), gas density (0.17 to 1.3 kg m^{-3}), and type of gas (nitrogen, oxygen, and

air) do not influence the gas hold-up significantly. Therefore all experiments in this paper were carried out with nitrogen. Initial liquid height (H_0) did not influence the gas hold-up significantly if it was above 1 m. Therefore initial liquid height in all experiments was between 1.0 and 1.5 meter. All experiments were carried out at ambient pressure and temperature. Distilled water is preferred over tap water because the properties of tap water are poorly defined.

Sodium gluconate was used as electrolyte in concentrations of 0.05-0.5M. Sodium gluconate is one of the products formed during glucose oxidation. This oxidation reaction is used as model reaction in further research.

Surface tension and viscosity of the electrolyte solutions were measured. Viscosity varied between $1.0.10^{-3}$ and $1.2.10^{-3}$ kg m^{-1} s^{-1} for all solutions. The surface tension was measured using a Wilhelmy plate with a Digital Tensiometer. From Table 3.1 it is shown that the surface tension decreases with increasing electrolyte concentration. At first the decrease in surface tension is high but it becomes smaller at higher electrolyte concentrations. The decrease in surface tension with increasing electrolyte concentration is contradicting compared with many electrolytes used in gas hold-up studies. It is expected that the sodium gluconate acts as a kind of surface active agent, therefore decreasing the surface tension with increasing electrolyte concentration.

Table 3.1: Surface tension of distilled water, carbon slurries and different electrolyte solutions at 298 K.

	Surface tension [mN m^{-1}]
Distilled water	74 ± 2
0.05 - 2.0 g l^{-1} Carbon	74 ± 2
0.05 M Electrolyte	68 ± 2
0.1 M Electrolyte	61 ± 2
0.2 M Electrolyte	55 ± 2
0.5 M Electrolyte	48 ± 2

Carbon particles (Engelhard Q500-130) with a mean particle diameter of 30 μm were used. The carbon particles are similar to the carrier material of the Pt/carbon catalyst, which will be employed in the actual reaction system [6]. Prior to each experiment, the carbon particles were washed with distilled water and dried at 378 K, to clean them from organic contaminations. Because the carbon particles tend to be hygroscopic, they were stored at 378 K. It was verified with conductivity measurements and surface tension measurements that addition of the carbon particles in distilled water did not lead to contamination of the water, or a change in the surface tension of the distilled water as can be seen in Table 3.1. The wettability of the carbon particles is one of the main parameters influencing the gas hold-up in a bubble column. To make sure that all particles are completely wetted at the start of each measurement, the particles were mixed with distilled water for one hour, in the column.

3.3.4 Spargers

Two spargers were used. The first sparger is a porous plate with a mean pore size of 30 μm. The second sparger was a perforated plate with 49 holes, of 0.5 mm diameter. The holes were positioned in three parallel rows and were positioned as shown in Figure 3.2. Both spargers were 0.2m x 0.01m (length x width) and located in the bubble column as shown in Figure 3.1. If not mentioned differently, the 0.5 mm sparger was used in all experiments.

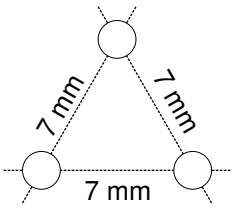

Figure 3.2: 0.5 mm sparger holes located equidistant from each other at 7 mm distance.

3.3.5 Bubble size imaging

Video images were taken with an image size of 0.15x0.15 m, using a Dalsa CA-D6 high-speed camera, taking 955 frames per second. Due to the high shutter speed, severe illumination of the imaged surface is required. For this purpose, ten halogen lamps of 500 W each are pointed at a white screen behind the 2D column of Figure 3.1. All lamps can be dimmed between 0-100% of their capacity. Ten light sensors, located at the back of the 2D bubble column, measure the amount of light falling on the imaged surface, assuring that the same amount of light was used at each video image.

3.3.6 Error analysis of gas hold-up data

Reproducibility and measurement error were estimated for each average pressure value, obtained from a time series of two minutes that was sampled with a frequency of 50 Hz. Each of these average points suffers from an error, which is given by:

$$\begin{aligned} \text{Error} = {} & \text{Measured pressure*Accuracy of the sensor} \\ & + \text{read out error + reproducibility error} \end{aligned} \tag{3.3}$$

The accuracy of the sensor is expressed as 0.25% percent of the measured value. For P1 and P2 a read-out error of 0.25 mbar and a reproducibility error of 0.353 mbar were measured (95% confidence interval). For P3 and P4 a read-out error of 0.08 mbar and a reproducibility error of 0.615 mbar were measured. Hence, the maximal error in each gas hold-up point is 15%. When interpreting the data, this maximum error has been taken into account.

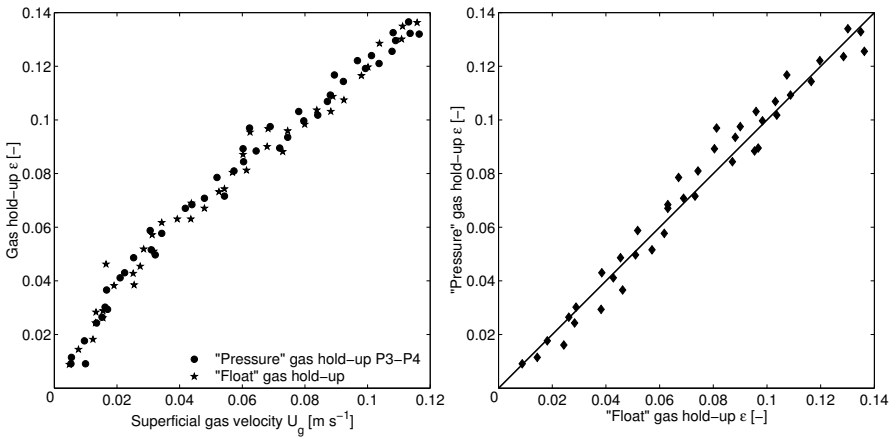

(a) (b)

Figure 3.3: a) Gas hold-up in distilled water measured with float and pressure sensors P3-P4. b) Parity plot of the gas hold-up calculated from pressure signals P3-P4, compared to gas hold-up calculated from float signals. Sparger in both figures: 0.5 mm perforated plate.

3.4 Experimental results

3.4.1 Distilled water

Figure 3.3a shows the pressure hold-up measured at positions 3 and 4 and the gas hold-up measured with the float. The parity plot of these gas hold-up data is shown in Figure 3.3b. The local gas hold-up calculated from the pressure signals is in agreement with the overall gas hold-up obtained from the float measurements. The gas hold-up determined with the pressure sensors is more accurate than the gas hold-up calculated from the bed expansion, because the dynamic movement of the float is disturbed by interactions of the float with the walls of the column. The observation that the "float" gas hold-up is equal to the gas hold-up calculated pressure sensors P3 and P4, allows us to use the gas hold-up calculated from these pressure sensors as representative for the overall gas hold-up in the column. In the remainder of this chapter, the thus calculated gas hold-up is used, unless mentioned differently.

The deviation from the overall "float" gas hold-up compared to the local "pressure" gas hold-up, is due to a somewhat lower gas hold-up below pressure sensor 3 and a slightly higher gas hold-up above pressure sensor 4, due to gas expansion. Hold-up data obtained from pressure sensors 1 and 2 show a deviation from the overall gas hold-up due to acceleration and impulse effects as a result of the air entering the bottom of the column. It can be seen from Figure 3.3b that these effects can be neglected above pressure sensor P3.

3.4.2 Electrolyte concentration

Figure 3.4 shows the increase in gas hold-up with increasing electrolyte concentration. No changes in gas hold-up take place above a critical concentration. The critical concentration is between 0.05M and 0.1M. These results are in accordance with literature [7–9]. Above an electrolyte concentration of 0.1M, no significant changes in gas

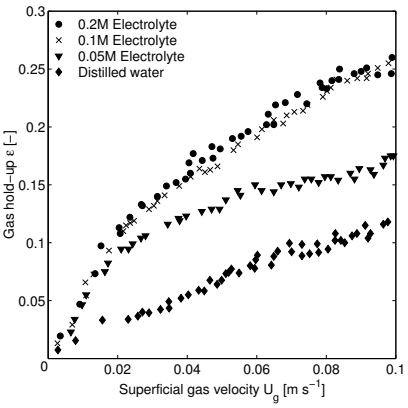

Figure 3.4: Gas hold-up measured with pressure sensors 3 and 4 with different electrolyte solutions and distilled water. Sparger: 0.5 mm perforated plate.

hold-up with increasing electrolyte concentration were observed. 1000 video images (approx. 1 sec.) were captured at a superficial gas velocity of 0.07 m s^{-1}. The pictures shown in Figure 3.5 are representative for each of the series of 1000 images. In each image in Figure 3.5 a large bubble of approximately 5 cm diameter can be seen. In the electrolyte solutions many more, smaller, bubbles with a diameter of less than 0.5 cm, are present compared to the image of distilled water. The number density of small bubbles increases with increasing electrolyte concentration.

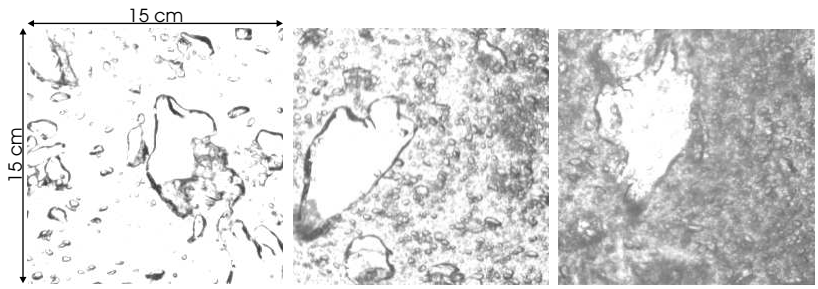

Figure 3.5: Video images taken at a superficial gas velocity of approx. 0.07 m s^{-1} at 70 cm above the sparger. Image size is 15x15cm. a) Distilled water, b) 0.05 M Electrolyte solution, c) 0.2 M electrolyte solution. Sparger: 0.5 mm perforated plate.

3.4.3 Carbon particle concentration

Gas hold-up in different carbon particle slurries was measured as a function of the superficial gas velocity. Figure 3.6 shows that a critical concentration exists above which no changes in gas hold-up take place. This critical carbon particle concentration is found between 0.2 g l^{-1} and 0.5 g l^{-1}. Video images of different slurries were

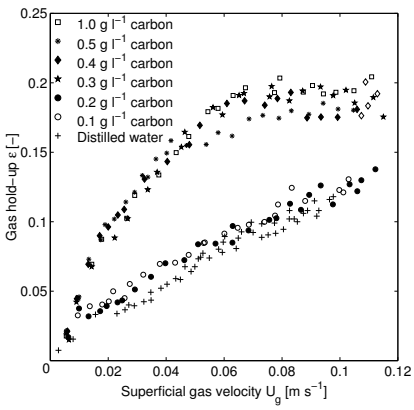

Figure 3.6: Gas hold-up measured with pressure sensors 3 and 4 with different carbon particle solutions and distilled water. Sparger: 0.5 mm perforated plate.

recorded at a superficial gas velocity of approximately 0.07 m s^{-1}. Characteristic pictures are shown in Figure 3.7. The images in Figure 3.7 are clearly different from the images in Figure 3.5. For both the distilled water and for the suspension containing 0.1 g l^{-1} carbon particles, a large bubble with a diameter of approximately 5 cm is observed. This typical size bubble is not present in the picture of the suspension containing 0.5 g l^{-1} slurry. For the 0.5 g l^{-1} suspension, many more, smaller bubbles exist compared to the 0.1 g l^{-1} carbon slurry and distilled water cases. However,

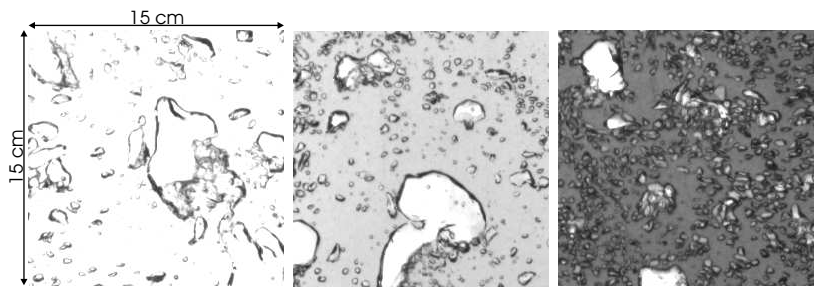

(a) (b) (c)

Figure 3.7: Video images taken at a superficial gas velocity of approx. 0.07 m s^{-1} at 70 cm above the sparger. Image size is 15x15cm. a) Distilled water, b) 0.1 g l^{-1} Carbon slurry, c) 0.5 g l^{-1} Carbon slurry. Sparger: 0.5 mm perforated plate.

these small bubbles are larger compared to the small bubbles observed in the 0.2M electrolyte picture from Figure 3.5.

3.4.4 Joint effect of carbon particle and electrolyte concentrations

Experiments were carried out with addition of both particles and electrolyte well above the critical concentrations. This led to a very high gas hold-up, which exceeded the hold-up of the two separate cases (see Figure 3.8). Due to the limited height of the column, it was not possible to measure at superficial gas velocities higher than 0.1 m s^{-1}. At low gas velocities, in the homogeneous flow regime, the addition of carbon particles and electrolyte results in the same gas hold-up as for the separate cases. At high gas velocities, in the heterogeneous flow regime, the gas hold-up clearly exceeds the hold-up of the two separate cases.

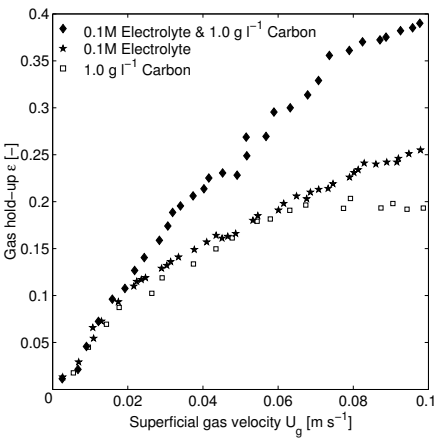

Figure 3.8: Gas hold-up measured with pressure sensors P3-P4 in 0.1M electrolyte solution, 1.0 g l^{-1} carbon particle slurry and in a combined experiment with 0.1 M electrolyte and 1.0 g l^{-1} carbon particles. Sparger: 0.5 mm perforated plate.

3.4.5 Initial bubble size

The initial bubble size, immediately above the sparger, was changed using a 30 μm porous plate instead of the 0.5 mm perforated plate. It was observed form the video image recordings that the initial bubble size was considerably smaller (approx. 0.2-0.5 mm) than in case of the perforated plate (approx 1-2 mm). Figure 3.9a shows that the initial bubble size affects the gas hold-up in case of the electrolyte solution. Apparently, in the homogeneous regime, there is no change in gas hold-up as a function of the initial bubble size. However, in the heterogeneous regime, a smaller initial bubble size leads to a higher gas hold-up. At a gas velocity of about 0.5 m s^{-1}, coalescence starts resulting in a steep gas hold-up decrease. At higher gas velocities initial gas hold-up in the case of Figure 3.9b shows that there is no effect of the initial bubble size on gas hold-up in case of the carbon particle slurry.

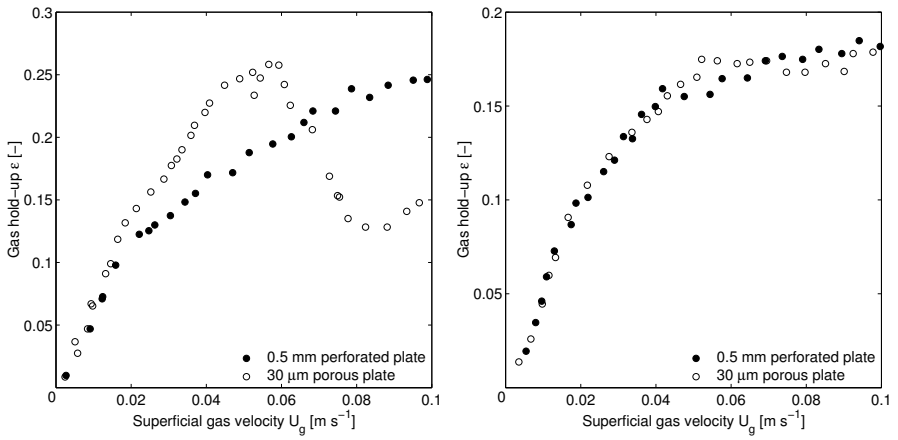

Figure 3.9: a) Local gas hold-up P3-P4 as a function of the superficial gas velocity in 0.1M electrolyte solution with two different spargers; b) Local gas hold-up P3-P4 as a function of the superficial gas velocity in 1 g l^{-1} carbon slurry with two different spargers.

3.4.6 Transition point

Carbon particles and electrolyte may have an effect on the transition between the homogeneous and heterogeneous flow regimes. Figures 3.10a and 3.10b show the relative standard deviation (σ/μ) of the pressure signals in respectively 1 g l^{-1} carbon particle suspension and in distilled water. Vial et al. [7] suggest that a measured value of the relative standard deviation of 1.5 (dotted lines in Figures 3.10a and 3.10b) indicate that the end of the homogeneous regime is reached. In case of distilled water, this would be around a superficial gas velocity of 0.03 m s^{-1}, which is in agreement with the average cycle frequency measurement of pressure sensor 3 (Figure 3.10d). For the carbon particle slurry, however, the transition point proposed by Vial et al. [7] would predict an incorrect transition point at a superficial gas velocity of 0.06 m s^{-1} (Figure 3.10a). The average cycle frequency of the pressure signals in Figure 3.10c however, shows a clear transition point around a superficial gas velocity of 0.035 m s^{-1} which is significantly different from the transition point obtained form Figure 3.10a.

In general, Figures 3.10c and 3.10d show that it is possible to estimate a regime transition point by means of pressure signal analysis, using the average cycle frequency. Comparing both figures shows that bubble dynamics influences the average cycle frequency. In the case of figure 10c, many small bubbles were present, resulting in a sharp transition point. This effect is caused by the passage of the small bubbles along the pressure sensor, which results in a higher frequency in the pressure time

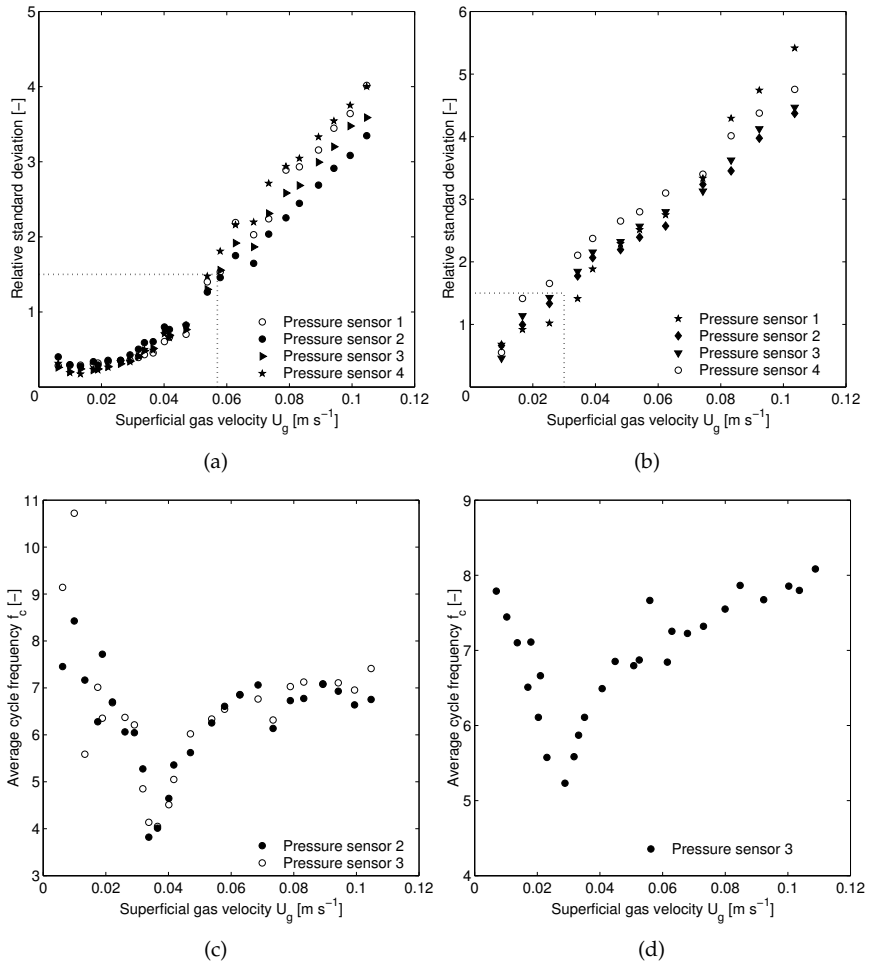

Figure 3.10: a) Relative standard deviation of pressure signals measured in 1 g l^{-1} carbon slurry, b) Relative standard deviation of pressure signals measured in distilled water, c) Average cycle frequency of pressure signals measured in 1 g l^{-1} carbon slurry, d) Average cycle frequency of pressure signals measured in distilled water.

series than the passage of a large bubble. When more small bubbles are present, the frequency changes more drastically upon appearance of large bubbles. This results in a sharp transition point.

With the average cycle frequency, transition points were determined. This resulted in a transition point for distilled water at a superficial gas velocity of 0.03 ± 0.005 m s^{-1}. For all carbon slurries a slight shift in transition velocity was measured of about 0.005 m s^{-1}, resulting in a transition velocity of 0.035 ± 0.005 m s^{-1}. For all electrolyte solutions above 0.1 M, a transition velocity of 0.04 ± 0.005 m s^{-1} was measured. The transition point for the experiment with both carbon particles and electrolyte could not be found within the range of superficial gas velocities studied, due to severe foam formation.

3.5 Mechanisms for gas hold-up increase

From Figures 3.4 and 3.6 it is concluded that addition of carbon particles and electrolyte leads to a significant increase in gas hold-up in a bubble column. This conclusion is underlined by the images depicted in Figures 3.5 and 3.7, where the addition of electrolyte and carbon particles shows a large increase in the volume occupied by bubbles, caused by a change in bubble size distribution.

Three possible mechanisms may account for this gas hold-up increase. A hold-up increase can be attributed to one or to a combination of these mechanisms. First, these possible mechanisms will be briefly outlined. Subsequently, in the next section, these mechanisms are used to explain the experimental results.

Mechanism 1: Effect of surface tension on gas hold-up

It is possible that the presence of electrolyte or particles changes the surface tension of the slurry as well as the surface properties of the gas-liquid interface. This change leads to a change in bubble size distribution: as the surface tension is a measure for the stability of the gas-liquid interface, a smaller surface tension leads to a less stable gas-liquid interface and thus to a smaller average bubble size over the whole bubble column. The residence time of a small bubble is larger than that of a large bubble, because the rise velocity of a bubble increases with the square root of its size. Hence, a smaller average bubble size leads to an increase in gas hold-up. The average bubble size is primarily dictated by the surface tension of the liquid.

Mechanism 2: Effect of wettability of particles and ionic forces on gas hold-up

Another possible effect of the addition of electrolyte and active carbon particles is the stabilization or destabilization of bubbles. This (de)stabilization is the result of the formation of a layer of particles or electrolyte around the gas bubble, which hinders or promotes bubble coalescence. Jamialahmadi and

Muller-Steinhagen [2] described this effect for wettable and non-wettable particles. As shown in Figure 3.11a, wettable particles tend to repel the gas interface, therefore acting as a buffer between two adjacent gas bubbles, resulting in a decreased rate of coalescence. Non-wettable particles have the opposite effect (Figure 3.11b).

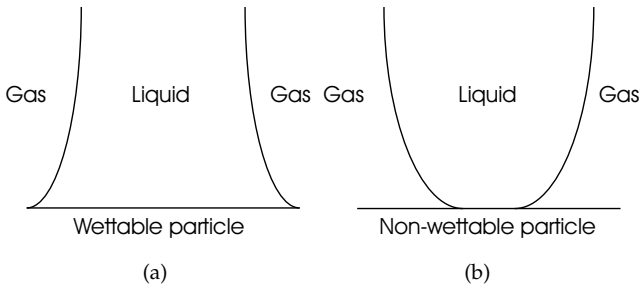

Figure 3.11: a) Gas-Liquid adsorption on a wettable particle, b) Gas-Liquid adsorption on a non-wettable particle.

Marrucci [10] has performed small-scale experiments with two approaching bubbles in electrolyte solutions. It was proposed that due to ionic forces the film drainage speed between two approaching bubbles is slowed down, resulting in a lower rate of coalescence and thus a higher gas hold-up. According to this theory, electrolyte decreases the liquid film drainage speed between two approaching bubbles, thus decreasing the rate of coalescence.

In this mechanism, the initial bubble size affects the average bubble size and thus the gas hold-up. A different initial bubble size results in a different bubble size distribution, leading to a higher or lower gas hold-up. This mechanism causes the transition between the homogeneous and the heterogeneous regimes to occur at a larger or smaller superficial gas velocity. For example, wettable particles will stabilize small bubbles and, therefore, delay the formation of large bubbles by coalescence.

Mechanism 3: Effect of viscosity and density on gas hold-up

Electrolyte and carbon particles influence the rise velocity of the bubbles. The rise velocity of a single bubble will be lowered, resulting in a higher gas hold-up, when the density or viscosity of the liquid-slurry layer around the bubble is significantly increased due to the presence of electrolyte or carbon particles. The initial bubble size does not affect the gas hold-up when only mechanism 3 prevails. The bubble size distribution is not affected by local changes in viscosity of density around the bubbles.

3.6 Discussion of results

3.6.1 Electrolyte

Figure 3.4 shows a significant increase in gas hold-up in electrolyte solutions. The images in Figure 3.5 show clearly this increase is caused by an increase in the number of small bubbles compared to distilled water. Changing the initial bubble size by applying a different sparger shows a significant increase in the gas hold-up in the presence of electrolyte. Moreover, the transition from the homogeneous regime to the heterogeneous regime in systems containing electrolyte is delayed, compared to systems with distilled water. The difference in gas hold-up with different initial bubble sizes is due to the effect that small bubbles are more stabilized than large bubbles. When the coalescence starts, at a superficial gas velocity of about 0.05 m s^{-1}, the collision probability is larger in the experiment with a smaller initial bubble size, therefore resulting in a higher rate of coalescence than in the case of the perforated plate, where already larger bubbles are present. This causes a steep decrease in gas hold-up in the experiment with the porous plate.

Also, electrolyte changes the bubble size distribution because of the decrease in surface tension. This is supported by the images in Figure 3.5. At low superficial gas velocity many more small bubbles are formed, an effect which can only be attributed to the change in surface tension, because coalescence and break-up of bubbles at these low superficial gas velocities is negligible. These observations show mechanisms 1 and 2 to explain the gas hold-up increase with addition of electrolyte. A reduced rise velocity as explained in mechanism 3 is not likely, because the viscosity of the electrolyte solutions hardly changes with increasing electrolyte concentration.

Prince and Blanch [9] have calculated the critical electrolyte concentration in electrolyte solutions for different electrolytes. Their calculations were based on the model of Marrucci [10]. This critical concentration is in the same order of magnitude as found in our study. Marrucci [10] and Prince and Blanch [9] conclude that a decreased rate of coalescence, due to a reduced film drainage speed between two approaching bubbles, is responsible for the increase in gas hold-up. Our study shows that besides this effect, also a smaller bubble size distribution, due to a change in surface tension of the liquid, accounts for a gas hold-up increase upon electrolyte addition.

3.6.2 Carbon particles

Figure 3.9b shows that the gas hold-up is not affected when changing the initial bubble size in a slurry of carbon particles. However, the gas hold-up shown in Figure 3.6 increases upon addition of particles and the transition from the homogeneous to the heterogeneous regime occurs at a larger gas velocity in systems with carbon particles compared to distilled water. These observations are in favor of mechanism 2. If only

bubble stabilization would account for the higher gas hold-up due to particle addition, one would not expect a higher gas hold-up compared to distilled water, already in the homogeneous regime, where bubble coalescence is almost absent. However, Figure 3.6 shows the opposite. Therefore it is expected that the density of the layer around a bubble is significantly increased by the addition of carbon particles, lowering the rise velocity of a single bubble. This puts forward mechanism 3. The surface tension is hardly influenced by the presence of carbon particles and thus mechanism 1 is less likely to occur. Hence, upon adding carbon particles it is suggested that a combination of mechanisms 2 and 3 describes the increase in gas hold-up.

3.6.3 Electrolyte and carbon particles

The experiment with both carbon particles and electrolyte in Figure 3.8, shows the joint effect of the suggested mechanisms. Smaller bubbles are formed due to the addition of electrolyte, which are stabilized by the carbon particles, resulting in a considerable increase of the gas hold-up.

3.7 Conclusions

In this study we have shown that:

- The addition of electrolyte changes the bubble size distribution and leads to an increase of the gas hold-up in a bubble column reactor. Experiments show that addition of electrolyte changes the surface tension of the solution, thus leading to a smaller average bubble size. Adding electrolyte also stabilizes bubbles, decreasing the rate of coalescence and therefore increases the gas hold-up in a bubble column. The postponing of the transition point going from the homogeneous to the heterogeneous regime supports this conclusion. It was not found that addition of electrolyte significantly changes the density or viscosity of the liquid layer around a bubble.

- The addition of carbon particles changes the bubble size distribution due to bubble stabilization. Experiments show that adding carbon particles leads to postponing of bubble coalescence and thus to an increase of the superficial gas velocity at which the transition from the homogeneous to the heterogeneous regime occurs. Also, due to particle addition, the density of the liquid layer around the bubbles significantly increases, decreasing the rise velocity of a bubble, thus increasing the gas hold-up. Conductivity and surface tension measurements showed that the surface tension of the liquid is hardly influenced by the presence of carbon particles.

- The addition of both carbon particles and electrolyte increases the gas hold-up significantly, due to a joint effect. Smaller bubbles are formed due to addition

of electrolyte, while these bubbles are stabilized and slowed down due to the presence of carbon particles.

- The average cycle frequency is a very powerful tool to determine the transition point between the homogeneous and the heterogeneous regimes. The standard deviation of the pressure signals does not provide this information.

Table 3.2: List of symbols

p	pressure measured by P1 to P4	[N m^{-2}]
ε_g	gas hold-up	[-]
f_c	average cycle frequency	[s^{-1}]
n_t	the number of occasions the pressure signal crosses it's mean value	[-]
t_m	measuring time	[s]
H	liquid height	[m]

Bibliography

[1] Joshi, J.B., Parasu Veera, U., Prasad, Ch.V., Phanikumar, D.V., Deshphande, N.S., Thakre, S.S., and Thorat, B.N., Gas hold-up structure in bubble column reactors. *PINSA*, 64A, 441-567, 1998.

[2] Jamialahmadi, M., and Muller-Steinhagen, H., Effect of solid particles on gas hold-up in bubble columns. *Can. J. Chem. Eng.*, 69, 390-393, 1991.

[3] Koide, K., Design parameters of bubble colum reactors with and without solid suspensions. *J. Chem. Eng. J.*, 29(5), 745-759, 1996.

[4] Krishna, R., Swart, J.W.A. de, Ellenberger, J., Martina, G.B., and Maretto, C., Gas holdup in slurry bubble-columns - effect of column diameter and slurry concentrations. *AIChE J.*, 43(2), 311-316, 1997.

[5] Jamialahmadi, M., and Muller-Steinhagen, H., Effect of electrolyte concentration on bubble size and gas hold-up in bubble columns. *Trans IChemE*, 68(A), 202-204, 1990.

[6] Kluytmans, J.H.J., Markusse, A.P., Kuster, B.F.M., Marin, G.B., and Schouten, J.C., Engineering aspects of the aqueous noble metal catalyzed alcohol oxidation. *Cat. Today*, 57(1-2), 143-155, 2000.

[7] Vial, C., Camarasa, E., Poncin, S., Wild, G., Midoux, N., and Bouillard, J., Study of hydrodynamic behaviour in bubble columns and external loop airlift reactors through analysis of pressure fluctuations. *Chem. Eng. Sci.*, 55, 2957-2973, 2000.

[8] Letzel, H.M., Schouten, J.C., Krishna, R., and Bleek, C.M. van den, Characterisation of regimes and regime transitions in bubble columns by chaos analysis of pressure signals. *Chem. Eng. Sci.*, 52, 4447-4459, 1997.

[9] Prince, M.J., and Blanch, H.W., Transition electrolyte concentrations for bubble coalescence. *AIChE J.*, 36(9), 1425-1429, 1990.

[10] Marrucci, G., A theory of coalescence. *Chem. Eng. Sci.*, 24, 975-985, 1969.

4

2D bubble column hydrodynamic phenomena clarified with a 3D gas-liquid model

This chapter is submitted for publication as:
Kluytmans, J.H.J., Wachem, B.G.M. van, Kuster, B.F.M., Krishna, R., Schouten, J.C., 2D bubble column hydrodynamic phenomena clarified with a 3D gas-liquid model, *Can. J. Chem. Eng.*, in conjunction with the Gas-Liquid-Solid (GLS) 6 conference, August 2003, Vancouver, Canada, 2002.

Abstract

In this study the gas hold-up in a 2D bubble column is modelled using a 3D gas hold-up model. The influence of the scale of 2D bubble columns on several parameters, for instance transition gas hold-up, transition gas velocity, and bubble rise velocities is investigated and related to 3D bubble columns. It is shown that by adapting the rise velocity of the large bubbles of an existing 3D bubble column model [1], the gas

hold-up in both the homogeneous and the heterogeneous regime can be described satisfactorily. By adapting the transition points only, it is also possible to describe the gas hold-up in systems containing small amounts of carbon particles and electrolyte. It is found that the smallest dimension of the 2D slurry bubble column, the column depth, influences the location of the regime transition point. In the heterogeneous regime however, it is only the largest column dimension, the column width, that influences the gas hold-up. These observations together enable proper 2D/3D bubble column comparison in future studies.

4.1 Introduction

Modelling of gas hold-up as a function of operating parameters in two and three phase systems is an important subject in multiphase reactor engineering [1–6]. Many correlations have been proposed to describe the gas hold-up in two and three phase systems to predict the effect of addition of surfactants [7, 8], electrolyte [9, 10], and several other substances. However, a fundamental understanding of the physical and hydrodynamic parameters and mechanisms, determining the gas hold-up in these multiphase systems is still lacking. Generally, the application of empirical, engineering correlations to systems outside the experimental window in which they were determined, is questionable. Furthermore, model assumptions are sometimes difficult to verify because of restrictions on measuring techniques.

A transparent 2D bubble column can increase the insight in multiphase hydrodynamics, by enabling video recording and image analysis of flow patterns, bubble size distributions, bubble rise velocities, and many other flow characteristics. The insight is indeed increased if the gas hold-up and the effect of the scale of the bubble column can be modelled and clarified with a comprehensive model. This study aims to quantify the gas hold-up in a 2D bubble column, based on a 3D model, and to evaluate the effect of the scale of a bubble column on several hydrodynamic parameters.

The gas hold-up in a bubble column is determined by many parameters, for instance the physical properties of the gas, the liquid, and the solids, the rates of bubble coalescence and break-up, the position of the transition point, the rise velocity of the bubbles in the homogeneous and heterogeneous regimes, the extent of mixing and circulation and the column scale. The latter one is one of the most important parameters, because it affects many of the others. To understand the influence of the scale of the bubble column on gas hold-up, the effect of scale on these parameters should be known. Many of the engineering correlations for the prediction of gas hold-up do not predict the effect of the scale of the column, because these correlations are usually based on dimensionless groups which are fitted on experimental data obtained in one column only. However, in the recent years, Krishna et al. have developed a model consisting of separate correlations for the rise velocity of the gas bubbles, the

gas hold-up and the superficial gas velocity at the transition point, including the effect of bubble-bubble interactions and the effect of bubble-column wall interactions. This model was published in many articles [1, 11–14] and was comprehensively published in the thesis of Urseanu [15]; further reference to this model will be made to Krishna et al. [13].

The model of Krishna et al. [13] includes most of the above mentioned aspects, influencing the gas hold-up in a 3D bubble column, and is therefore at current the most reliable model for the gas hold-up prediction in a 3D system. However, the effect of scale of a 2D column on the gas hold-up prediction is not considered in this model. Therefore, the model of Krishna is taken as starting point to investigate the effect of the scale of a bubble column on model parameters like the bubble rise velocity, including bubble-bubble interactions and bubble-wall interactions, and to describe the gas hold-up in a 2D bubble column. First the experimental set-up is introduced in which the gas hold-up measurements were performed. Secondly, the 3D model of Krishna et al. [13] is treated comprehensively. Hereafter all model parameters are evaluated more closely to determine to what extent these are affected by the scale of a 2D column (viz., column width and column depth). The model parameters which are clearly most affected are adapted accordingly. Finally, the resulting model with the modified parameters is verified experimentally by comparison with measured gas hold-up data in the 2D bubble column in three different systems.

4.2 2D experimental set-up

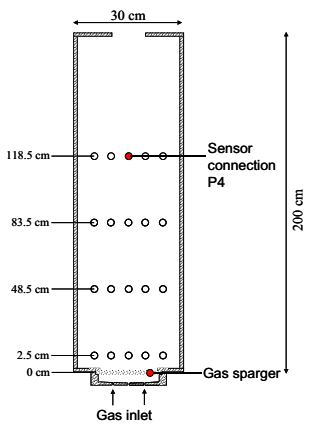

Figure 4.1: 2D perspex bubble column dxwxh 0.015x0.30x2.00 m, with 20 sensor connections located at 2.5, 48.5, 83.5, and 118.5 cm above the gas sparger, for gas hold-up measurements. Two gas spargers were used, a 0.5 mm perforated plate and a 30 μm porous plate. If not mentioned differently the 0.5 mm perforated plate was used in the experiments.

A 2D bubble column is used to study the bubble flow pattern, bubble size distribution, and bubble rise velocity during gas hold-up measurements, with a high-speed video camera. The 2D laboratory scale reactor as shown in Figure 4.1 consists of two perspex plates with a height of 2 m and a width of 0.3 m. The two walls of the

column are placed 0.015 m apart from each other. Gas hold-up measurements are performed under ambient conditions (1 bar, 293 K), with distilled water, with small amounts of catalyst particles (carbon particles, $\bar{d}_p \approx 30$ μm, 0.1 - 20 g l^{-1}) and with electrolyte (sodium gluconate, 0.05 M - 2.0 M). From several experiments it is observed that a small range of liquid viscosity (1.0 to 2.0 kg m^{-1} s^{-1}), gas density (0.17 to 1.3 kg m^{-3}), and type of gas (nitrogen, oxygen, and air) do not influence the gas hold-up significantly. All experiments in this paper are therefore carried out with nitrogen gas. Initial liquid height does not influence the gas hold-up if it is kept above 1 m. Therefore in all experiments the initial liquid height is between 1.0 and 1.5 m. Distilled water is preferred over tap water because the properties of tap water are poorly defined. Local and overall gas hold-up are calculated from pressure sensors which are connected at the back wall of the 2D column at sensor positions as shown in Figure 4.1. If the sensors are not used, the sensor connections are closed flush with the wall to prevent disturbances in the flow behavior. The regime transition point is determined from the dynamic pressure signal. Changes in the average cycle frequency of the pressure signal are a measure for the transition from the homogeneous regime to the heterogeneous regime [16]. Video images are recorded with a high speed Dalsa CA-D6 camera at a frequency of 955 frames per second. The video images are analyzed with image processing software developed at the Eindhoven University of Technology, to obtain quantitative data about bubble size distributions and bubble rise velocities.

4.3 3D gas hold-up correlations and models

Many models and empirical correlations are available to predict the gas hold-up in two and three phase bubble columns. The models and correlations of Hikita et al. [17], Reilly et al. [18], Wilkinson et al. [19], Ellenberger and Krishna [20], and Krishna et al. [13], are compared with the experimental data obtained in the 2D bubble column (section 4.2). The experimental conditions for which these correlations were developed, mostly resemble the experimental conditions of those in the 2D gas hold-up measurements [16]. Figure 4.2a shows that the gas hold-up in the homogeneous regime, below a superficial gas velocity of 0.015 m s^{-1}, is reasonably well described by the selected models and correlations. However, the gas hold-up in the heterogeneous regime is over-predicted by all models, although the shape and slope of some curves resemble the measured data quite well. Besides the deviation in the predicted and measured gas hold-up, a large difference exists between the calculated transition points from the 3D models and the measured transition points in the 2D bubble column, as shown in Table 4.1. The gas hold-up correlations and models then result in the curves as shown in Figure 4.2b. This comparison shows that the correlation of Hikita et al. [17], and the models of Ellenberger and Krishna [20] and Krishna et al. [13] are most promising to predict the gas hold-up in the 2D slurry bubble column. The correlation of Hikita et al. [17] is however purely empirical and does not offer much possibilities to explore the effect of the scale of the 2D column on sepa-

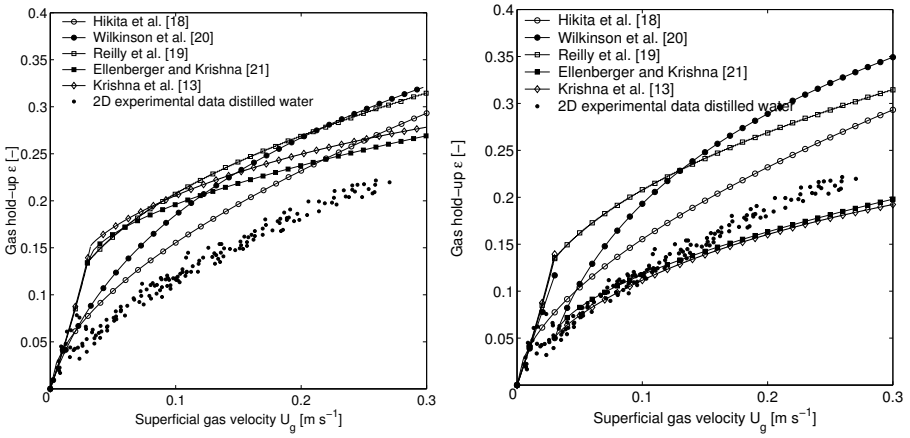

(a) "Using calculated transition points" (b) "Using measured transition point"

Figure 4.2: Comparison of literature models and correlations with experimental data of gas hold-up obtained in a 2D bubble column. a) Transition points as calculated by the models and correlations, b) Experimentally determined transition point in the 2D bubble column, see Table 4.1.

rate model parameters, like bubble rise velocity and transition points. Therefore this correlation is not further considered. The Krishna et al. [1, 15, 20] model is built on fundamental and semi-empirical correlations describing separate parameters, like the rise velocity of a single bubble, the rise velocity of a bubble swarm, the transition point, etc. By adapting these sub-correlations to fit the 2D gas hold-up data, insight can be obtained to what extent the separate model parameters are affected by the scale of the 2D bubble column compared to the 3D case.

Table 4.1: Calculated and measured transition parameters for the transition from the homogeneous to the heterogeneous regime. Distilled water-Nitrogen or Distilled water-Air, Experimental study: 2D bubble column; literature values: 3D bubble columns.

	ε_{trans} [-]	U_{trans} [m s^{-1}]
Wilkinson et al. [19]	0.01	0.0026
Reilly et al. [18]	0.1342	0.0296
Krishna et al. [13]	0.1517	0.0305
Experimental study [16]	0.05 ± 0.01	0.03 ± 0.01

4.4 Gas hold-up model by Krishna et al. [13]

Ellenberger and Krishna [20] studied the analogy between gas-solid fluidized beds and gas-liquid-solid bubble column reactors. Their model is based on the two-phase model for gas-solid systems of May [21] and van Deemter [22], in which the gas phase is divided in a large bubble phase and a dense phase, containing only small bubbles. This distinction was made to account for the different behavior of small and large bubbles in multiphase reactors. Based on these considerations, Ellenberger and Krishna [20] developed a model for the prediction of the gas hold-up in the heterogeneous regime in gas-liquid bubble columns. Krishna et al. [13] extended this model with a correlation for the gas hold-up in the homogeneous regime. The model of Krishna et al. [13] consists of separate sets of equations for the homogeneous and the heterogeneous regime. The model parameters are treated in the next sections, and evaluated on their potential to be affected by the column dimensions. This evaluation leads to the insight about which model parameters need to be adapted based on the 2D/3D scale difference.

4.4.1 Homogeneous regime

In the homogeneous regime it is assumed that only equally sized gas bubbles are present. It is assumed that these small gas bubbles rise with the same and constant velocity throughout the column and have little interactions with each other. Once the rise velocity of these small bubbles has been estimated, the gas hold-up can be calculated with:

$$\varepsilon_g = \frac{U_g}{U^{\infty}_{small,b}(1-\varepsilon_g)} \qquad \text{for} \qquad U_g < U_{trans} \tag{4.1}$$

The average diameter of the small gas bubbles in the homogeneous regime is considered to be in between 4 and 8 mm [1]. Therefore it is expected that if the 2D column depth exceeds 1 cm, it will hardly affect the rise velocity of the small bubbles, and therefore will not affect the gas hold-up in the homogeneous regime.

4.4.2 Transition regime

The transition region separating the homogeneous regime and the fully developed heterogeneous regime is not considered in the model of Krishna et al. [13]. In the model of Krishna et al. [13] this regime is reduced to a transition point, which is located at the intersection of the gas hold-up correlation for the homogeneous regime and the gas hold-up correlation for the heterogeneous regime. Generally, it is found that the transition regime lies in between superficial gas velocities of 0.05 m s^{-1} and 0.15 m s^{-1}. At low superficial gas velocities in the transition regime, the first large bubbles are formed due to mutual interactions of the small bubbles while at higher superficial gas velocities larger bubbles start to interact. The location of the transition

point thus strongly depends on its definition as well as on the measuring technique or the calculation procedure.

The transition point is one of the critical parameters in the model of Krishna et al. [13], because it determines the end point of the correlation describing the gas hold-up in the homogeneous regime and the starting point of the correlation for the heterogeneous regime, especially in the range of superficial gas velocities used in this study (U_g = 0 - 0.3 m s^{-1}).

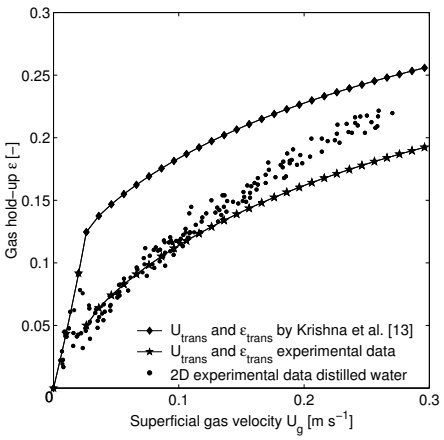

Figure 4.3: Gas hold-up prediction with the model of Krishna et al. [13] using the measured transition point in a 2D bubble column [16] and the calculated transition parameters as starting parameters for the gas hold-up prediction, compared with experimental hold-up data measured in the 2D laboratory column.

Using an experimentally determined transition point can lead to a discontinuity in the prediction of the gas hold-up, as shown in Figure 4.3, in which both the experimentally determined transition point and the calculated transition point are used. Therefore, Krishna et al. [13] proposed an empirical correlation for the transition hold-up using dimensional analysis:

$$\varepsilon_{trans} = 0.012 Re_b^{0.4} We^{-0.2} \left(1 - exp\left(-0.04 \frac{D_T}{d_b}\right)\right) \tag{4.2}$$

Here the Reynolds number is based on the average bubble diameter d_b at the transition point, and is defined as $Re_b = (\rho_{liquid} \overline{U_b} d_b)/\eta_{liquid}$, while the Weber number is described as We=$(g d_b^2 \rho_{liquid})/\sigma$. The transition gas velocity is defined by Reilly et al. [18]:

$$U_{trans} = U^{\infty}_{small,b} \varepsilon_{trans} (1 - \varepsilon_{trans}) \tag{4.3}$$

Both equations were found to predict the transition gas hold-up and superficial gas velocity in air-water systems and air-tellus oil systems in several 3D columns. It is expected that the scale of the column will have a large influence on both the superficial gas velocity and the gas hold-up at the transition point. For example, interactions of the bubbles with the column walls are assumed to promote bubble coalescence. This consideration is expressed in Equation 4.2 in which both the bubble diameter and

the column diameter are included. However, for a 2D system it is unknown which column dimension should be used in this equation in order to calculate the correct gas hold-up at the transition point.

4.4.3 Heterogeneous regime

The gas hold-up in the heterogeneous regime is obtained by addition of the gas hold-up in the homogeneous regime, the dense phase gas hold-up, and the gas hold-up of the large bubbles. It is assumed that the gas hold-up of the small bubbles (dense phase) is equal to the gas hold-up at the transition point, and is constant throughout the heterogeneous regime. The gas hold-up for the heterogeneous regime is then given as:

$$\varepsilon_g = \varepsilon_{l,b} + \varepsilon_{trans}\left(1 - \varepsilon_{l,b}\right) \qquad \text{for} \qquad U_g > U_{trans} \tag{4.4}$$

By definition, the gas hold-up of the large bubbles is given by

$$\varepsilon_{l,b} = \frac{U_g - U_{trans}}{U_{l,b}} \tag{4.5}$$

The velocity of the large bubbles $U_{l,b}$ is related to the rise velocity of a single bubble in an infinite medium as given by Davies and Taylor [23]:

$$U_{l,b}^{\infty} = \Phi\sqrt{g d_b} \tag{4.6}$$

with Φ=0.71. However, in a bubble column bubbles have mutual interactions as well as interactions with the column walls. The rise velocity of a single bubble, interacting with other gas bubbles and with the column walls, is therefore expressed as:

$$U_{l,b} = 0.71\sqrt{g d_b}(SF)(AF) \tag{4.7}$$

SF is expressed the so called scale factor and AF is the acceleration factor. The scale factor SF was introduced by Collins [24] to account for the bubble-wall interactions. The scale factor is given by an empirical correlation and is a function of the ratio between the bubble diameter and the diameter of the column:

$$\begin{aligned} SF &= 1 && \text{for} && \frac{d_b}{D_T} < 0.125 \\ SF &= 1.13 exp\left(-\frac{d_b}{D_T}\right) && \text{for} && 0.125 < \frac{d_b}{D_T} < 0.6 \\ SF &= 0.496\sqrt{\frac{D_T}{d_b}} && \text{for} && \frac{d_b}{D_T} > 0.6 \end{aligned} \tag{4.8}$$

The mutual interactions of the gas bubbles are accounted for by Krishna et al. [13] through the acceleration factor (AF). This empirical parameter was fitted for low viscous fluids, resulting in the following correlation:

$$AF = 2.73 + 4.505\left(U_g - U_{trans}\right) \tag{4.9}$$

Combining Equations 4.7 and 4.5 provides the prediction of the large bubble gas hold-up in the heterogeneous regime:

$$\varepsilon_{l,b} = \frac{U_g - U_{trans}}{0.71\sqrt{gd_b}(SF)(AF)} \tag{4.10}$$

From the above equations it can be seen that the gas hold-up in the heterogeneous regime is mainly determined by the gas velocity at the transition point, the rise velocity of the large gas bubbles in the column and the average bubble diameter. The bubble diameter can be estimated from high speed video imaging as can be seen in Figure 4.5. It is not known to what extent the rise velocity of the large bubbles and the bubble-bubble interactions expressed by the acceleration factor are affected by the column diameter. Furthermore, the applicability of the scale factor correlation of Collins [24] for 2D bubble columns requires further investigation.

4.5 2D modelling

As raised in the previous section, the basic question in the modelling of the gas hold-up in a 2D bubble column with the 3D model by Krishna et al. [13], is which characteristic column size (viz., column width, column depth or a combination of the two) should be used in the calculation of the transition point, the scale factor, and the rise velocity of the large bubbles. To answer this question, first a model sensitivity analysis is performed to determine which parameters influence the gas hold-up most. This is done by comparing gas hold-up model predictions with the gas hold-up data that were measured in the 2D laboratory scale column (section 4.2). Subsequently, the influence of column size on the model parameters that affect the hold-up most is determined and these model parameters are adapted accordingly.

4.5.1 Sensitivity analysis

Four parameters are selected which are assumed to be most affected by the scale of the column, viz. the transition superficial gas velocity (U_{trans}), the transition gas hold-up (ε_{trans}), the scale factor (SF), the rise velocity of the large bubbles ($U_{l,b}^{\infty}$), and the acceleration factor (AF). The sensitivities of the gas hold-up prediction to changes in these parameters are shown in Figures 4.4a till d. These figures show that the effect of the transition parameters and the acceleration factor on the gas hold-up prediction is relatively limited. The scale factor however, influences the gas hold-up prediction to a large extent.

4.5.2 Homogeneous regime

The gas hold-up in the homogeneous regime is governed by the rise velocity of the small bubbles, which is determined in experimental studies of Krishna et al. [13],

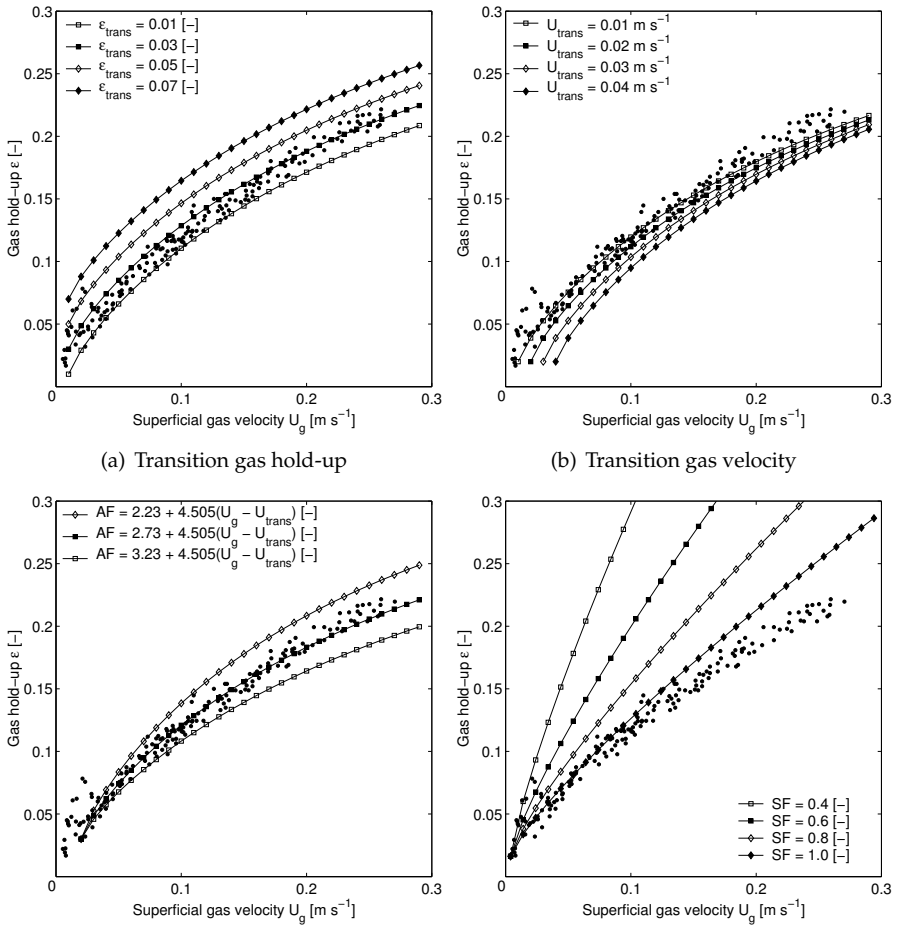

(a) Transition gas hold-up

(b) Transition gas velocity

(c) Acceleration factor

(d) Scale factor

Figure 4.4: Evaluation of model parameters of the 3D model of Krishna et al. [13] with respect to experimental data obtained in a 2D bubble column. Model parameters were changed to evaluate the sensitivity of the gas hold-up prediction with respect to these parameters. a) the transition hold-up, b) the superficial gas velocity at the transition point, c) the acceleration factor, d) the scale factor. System: nitrogen-distilled water.

Reilly et al. [18], and Wilkinson et al. [19]. The rise velocity of the small bubbles in the 2D bubble column is measured with high speed video imaging. The results are compared with these literature values in Table 4.2. It is clear that the rise velocity of the small bubbles and thus the gas hold-up is not affected by the column size.

Table 4.2: Literature values of the rise velocities of small bubbles in the homogeneous regime (3D) and measured rise velocity of small bubbles in the 2D bubble column (ambient conditions; system: distilled water-air), average bubble size 6-8 mm.

	$U_{small,b}$ [m s^{-1}]
Wilkinson et al. [19]	0.26
Reilly et al. [18]	0.24-0.26
Krishna et al. [13]	0.23-0.25
This study (2D column)	0.25 ± 0.02

4.5.3 Heterogeneous regime

Equations 4.5 and 4.7 show that the rise velocity of the large bubbles, the scale factor, and the acceleration factor determine the gas hold-up in the heterogeneous regime. A sensitivity analysis shows that the acceleration factor has only a minor influence on the gas hold-up prediction while the scale factor has a much larger influence. These parameters will be treated separately.

Acceleration factor

The acceleration factor accounts for the mutual interactions of bubbles, on the rise velocity of gas bubbles. The acceleration factor depends on the superficial gas velocity, because the contribution of the large and small bubbles to the gas hold-up changes with increasing gas velocity. The parameters in the AF correlation (Equation 4.9) were fitted by Krishna et al. [13] on 3D experimental data. Figure 4.4c shows that this correlation describes the measured 2D gas hold-up data reasonably. This supports the idea that the mutual bubble interactions which the acceleration factor accounts for, are not affected by the size of the column. Therefore, Equation 4.9 can be used for the prediction of the gas hold-up in a 2D bubble column.

Scale factor

The scale factor (SF) introduced by Collins [24] has been derived explicitly for 3D bubble columns. This scale factor adapts the factor $\Phi = 0.71$ in the theoretical equation of Davies and Taylor [23] for the rise velocity of a single bubble in an infinite

medium, to account for the effect of the column size. Krishna et al. (2000) have derived a scale factor for 2D columns, based on experiments and CFD modelling on the rise velocity of single bubbles, in a 2D column with a column depth of 5 mm. Using this 2D scale factor for the estimation of the gas hold-up in the 2D column in the present work, does not give a satisfactory description of the measured gas hold-up data. This is possibly due to the difference in the depths of the 2D columns that were used in both studies, viz. 5 mm in the study of Krishna et al. (2000) and 15 mm in the 2D column in the present work. The mutual interactions between the small and large bubbles will most probably be influenced by this distance between the column walls. In the work of Krishna et al. (2000), the column depth is in the order of magnitude of the size of the small bubbles (4-8 mm), while in the 2D setup in the present work, the column depth is at least twice as large as this small bubble size. It is expected that while using the 2D scale factor as derived by Krishna et al. (2000), also the acceleration factor AF needs to be adapted to properly describe the gas hold-up in 2D columns. However, the parameter sensitivity analysis as presented in Figure 4.4c indicates that the acceleration factor as taken from the 3D hold-up model of Krishna et al. (1999) already provides a proper description of the 2D gas hold-up. Therefore, in this case, the rise velocity of the large bubbles has to be adapted differently to account for the effect of the column size, than by the 2D scale factor as was introduced by Krishna et al. (2000).

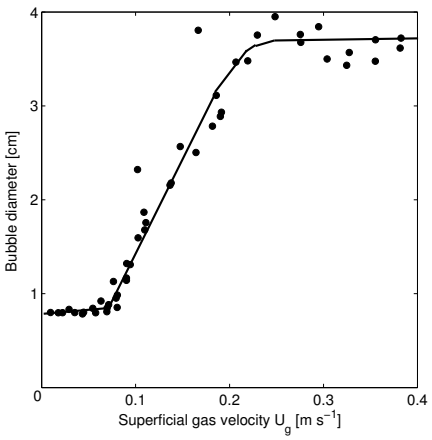

Figure 4.5: Average bubble size as a function of the superficial gas velocity, calculated from video images captured during gas hold-up experiments at a frame rate of 955 Hz. System : Nitrogen-Carbon particle slurries 0.1 - 2.0 g l^{-1}.

Pyle and Harrison [25] have adapted the factor $\Phi = 0.71$ for a 2D column with a depth of 1 cm, to $\Phi = 0.54$. The latter value adapts the rise velocity of a single bubble under influence of the smallest dimension of the 2D column, viz. the depth of the column. In their case the 2D column depth is also larger than the size of the small bubbles. Applying this to the correlation of Krishna et al. [13] results in a rise velocity of the large bubbles of

$$U_{l,b} = 0.54\sqrt{gd_b}(SF)(AF) \tag{4.11}$$

The scale factor of Collins [24] should in this case only correct for the influence of the width of the 2D column on the rise velocity of the large bubbles. To calculate the value of the scale factor according to Equation 4.8, the average bubble size in the heterogeneous regime is required. The average bubble size is estimated from video images recorded with a high speed video camera. Figure 4.5 shows that the average bubble diameter never exceeds the size of approximately 4 cm for gas velocities up to 0.4 m s^{-1}. Therefore, the ratio d_b/D_T in Equation 4.8 is always smaller than 0.125 for a column diameter of 0.3 m; the scale factor in that case is equal to 1. This is in agreement with Figure 4.4d which shows that scale factors smaller than 1 do not describe the experimental data satisfactorily. This analysis shows that indeed the rise velocity of the large bubbles in the heterogeneous regime is affected by the size of the 2D bubble column.

4.6 2D gas hold-up model validation

The values of the model parameters to calculate the gas hold-up in a 2D column are summarized in Table 4.3. The gas hold-up model predictions are compared with the experimental data obtained in the 2D bubble column as described in section 4.2. The

Table 4.3: Values and equations of the model parameters for the modelling of the gas hold-up in a 2D bubble column.

Parameter	Value/Equation
$U_{small,b}$	0.25 [m s^-]
AF	2.73 + 4.505(U_g-U_{trans}) [-]
SF	1 [-]
$U_{l,b}$	$0.54\sqrt{gd_b}$(SF)(AF) [m s^{-1}]
d_b	Values according to Figure 4.5 [m]

transition points are chosen such that the gas hold-up in the three systems in the homogeneous regime and the heterogeneous regime ($U_g > 0.15$ m s^{-1}) is well described. The gas hold-up prediction for carbon particles is optimized for the carbon particle concentrations above 0.3 g l^{-1} because the gas hold-up at lower concentrations is equal to the gas hold-up data of distilled water, as shown in Figure 4.6a. The resulting prediction of the gas hold-up for the three experimental systems is shown in Figures 4.6a till c. For the three systems the gas hold-up is well described in both the homogeneous as the heterogeneous regime. It can be seen that the gas hold-up in the transition regime for electrolyte solutions (Figure 4.6b) and carbon particle slurries (Figure 4.6c) in between superficial gas velocities of 0.02-0.12 m s^{-1} is not predicted at all. These transitions regimes are reduced to the transition point. The determined transition points are listed in Table 4.4. The transition hold-up deviates quite extensively from the transition hold-up predicted with Equation 4.2, when the width of the 2D column (0.3 m) is used as column diameter D_T. Equation 4.2 gives

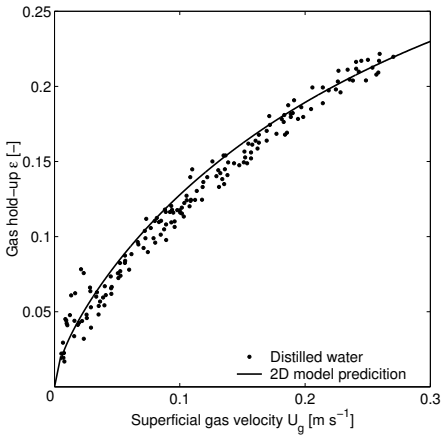

(a) Distilled water

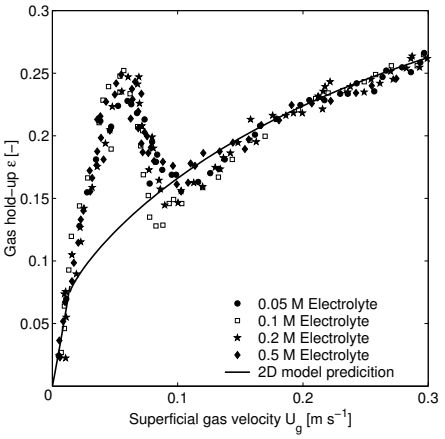

(b) Electrolyte solutions

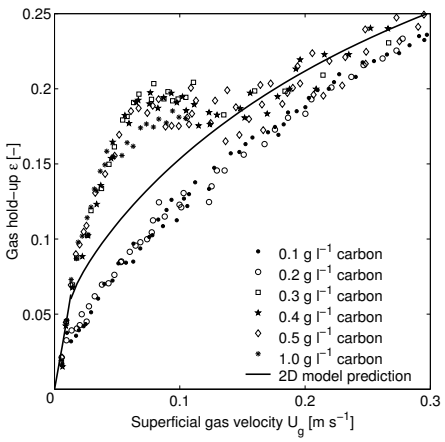

(c) Carbon slurries

Figure 4.6: Measured gas hold-up data in a 2D slurry bubble column modelled with the adapted 3D gas hold-up model of Krishna et al. [13] for a) Distilled water, b) Electrolyte solutions, and c) Carbon slurries. Data was modelled with SF = 1, AF = 2.73 + 4.505(U_g - U_{trans}), and the Pyle an Harrison [25] factor of 0.54 for the rise velocity of the large bubbles, see Table 4.3.

Table 4.4: Transition points determined from the optimized gas hold-up prediction in the homogeneous regime and the heterogeneous regime as shown in Figures 4.6a till c.

System	ε_{trans} [-]	U_{trans} [m s^{-1}]
Distilled water	0.017	0.005
Electrolyte solution	0.075	0.014
Carbon slurry	0.06	0.013

a transition gas hold-up of ε_{trans} = 0.10 - 0.15, which is approximately twice the gas hold-up as given in Table 4.4. This demonstrates that the transition point is influenced by the size of the column. It is expected that the formation of the first large bubbles at the start of the transition regime is influenced by the smallest dimension of the column. This idea is confirmed when calculating the column diameter D_T from Equation 4.2 using the transition gas hold-up as given in Table 4.4. This calculation results in a column diameter for the three transition points (viz., distilled water, electrolyte solution, and carbon slurry) in between 3 and 5 cm, which is of the order of magnitude of the smallest dimension of the 2D column (viz., the column depth of 1.5 cm). Apparently, the depth of the 2D column influences the development of the first large bubbles by pushing the small bubbles together, therefore forcing the small bubbles to interact and coalesce to form large bubbles. The width of the 2D column has evidently no pronounced effect on this process.

4.7 2D - 3D gas hold-up comparison

In the previous sections, we have shown that the gas hold-up in a 2D bubble column is predicted quite well by the model of Krishna et al. [13] after adapting the calculation of the transition point and the rise velocity of the large bubbles to account for the proper scale of the column (viz., column width or column depth). The way these parameters had to be adapted allowed insight in the hydrodynamic behavior of a 2D bubble column. Using both models, we can now make a proper comparison between the gas hold-up in a 2D bubble column and the gas hold-up in a 3D bubble column, at the same operating conditions (viz., superficial gas velocity). This comparison is shown in Figure 4.7a. It is evident that there is quite a difference in the gas hold-up in the 2D and 3D cases up to a superficial gas velocity of approximately 0.2 m s^{-1}, above which the gas hold-up predictions become quite similar. At higher gas velocities, the 2D and 3D gas hold-up predictions still remain very close (see Figure 4.7b). This would suggest that hold-up data that are measured at sufficiently high superficial gas velocity in a 2D bubble column, offer a reasonable prediction of the hold-up in the actual 3D case. However, it is expected that this will not be true for any 2D bubble column. Especially the choice of the depth of the 2D column is crucial in this respect, to properly account for the presence of small bubbles that are approximately 4 to 8 mm in size. A column depth of at least more than 1 cm, but preferably 1.5 cm, will allow the small bubbles to flow freely with the liquid, without being pushed upward due to interactions with the column walls. This does justice to the considerations of the two-fluid model. It is in this light that the rise velocity of the small bubbles in the homogeneous regime is not affected by the depth of the column. However, it is expected that for 2D columns with a depth of less than 1 cm, this may not be true anymore. In that case, the analysis of the model parameters needs further evaluation.

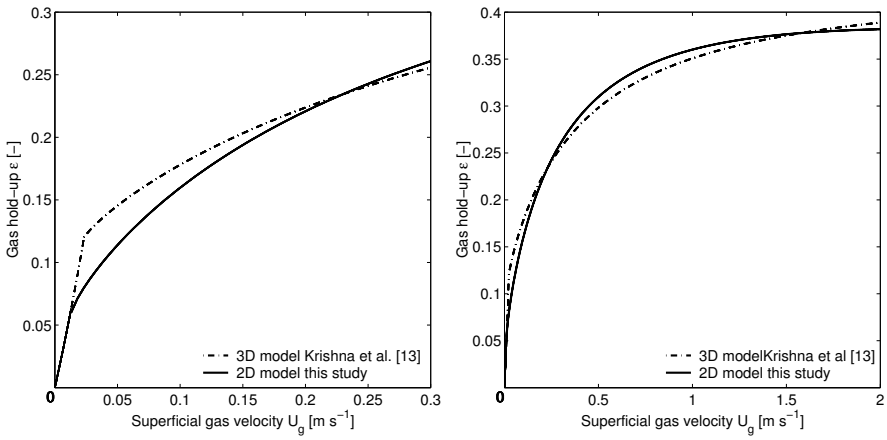

(a) U_g = 0 - 0.2 m s^{-1} (b) U_g = 0 - 2.0 m s^{-1}

Figure 4.7: Comparison of the 3D model of Krishna et al. [13] and the adapted model for a 2D column at a) superficial gas velocities up to 0.3 m s^{-1} and b) superficial gas velocities up to 2.0 m s^{-1}.

4.8 Concluding remarks

The 3D model of Krishna et al. [13] can be adapted to properly describe the gas hold-up in a 2D bubble column. The following considerations and model adaptations have been discussed (see also Table 4.3):

- The 2D column should have a depth of at least 1 cm, but preferably 1.5 cm, to prevent that the rise velocity of the small bubbles is affected by the column walls.
- The rise velocity of the small bubbles in the homogeneous regime equals 0.25 m s^{-1} and is independent of the size of the bubble column for bubbles with an average diameter of 6-8 mm.
- The transition gas hold-up is affected by the depth of the 2D column. This means that if the transition gas hold-up is calculated with Equation 4.2, the characteristic column size D_T in this equation should be taken equal to the depth of the column and not equal to the width of the column.
- The rise velocity of the large bubbles should be adapted to account for the width of the 2D column by using the factor Φ=0.54 as was suggested already by Pyle and Harrison [25].
- The scale factor SF in case of a 2D column can be calculated with Equation 4.8 in which the characteristic column size D_T should be taken equal to the column width of the 2D column.

- The acceleration factor AF is not affected by the scale of the column and is similar for the 2D and 3D cases.
- The 2D gas hold-up model can be applied on several different systems (distilled water, carbon slurries with small amounts of carbon particles, electrolyte solutions) by adapting the transition points only.

Acknowledgement

B.A.J. Tilborghs is gratefully acknowledged for his contribution to the experimental work as well as the development of the 2D gas hold-up model as presented in this chapter.

Table 4.5: List of symbols

AF	acceleration factor	[-]
d_b	bubble diameter	[m]
g	acceleration constant	[m s^{-2}]
Re_b	Reynolds number based on bubble diameter $(\rho_{liquid}\overline{U_b}d_b)/\eta_{liquid}$	[-]
U_{trans}	transition gas velocity	[m s^{-1}]
$U_{l,b}$	large bubble rise velocity	[m s^{-1}]
$U_{l,b}^{\infty}$	large bubble rise velocity in a infinite medium	[m s^{-1}]
U_g	superficial gas velocity	[m s^{-1}]
$U_{small,b}$	small bubble rise velocity	[m s^{-1}]
$U_{small,b}^{\infty}$	small single bubble rise velocity in a infinite medium	[m s^{-1}]
SF	Scale factor	[-]
We	Weber number $((gd_b^2\rho_{liquid})/\sigma)$	
Greek and Roman symbols		
ε_{trans}	transition gas hold-up	[-]
$\varepsilon_{l,b}$	large bubble gas hold-up	[-]
ε_g	gas hold-up	[-]
η_{liquid}	liquid viscosity	[kg m^{-1} s^{-1}]
ρ_{liquid}	liquid density	[kg m^{-3}]

Bibliography

[1] Krishna, R., Baten, J.M. van, Urseanu, M.I., and Ellenberger, J., A scale up strategy for bubble column slurry reactors, *Catal. Today*, 66(2-4), 199-207, 2001.

[2] Bauer, M., and Eigenberger G., Multiscale modeling of hydrodynamics, mass transfer and reaction in bubble column reactors. *Chem. Eng. Sci.*, 56(3), 1067-1074, 2001.

[3] Camarasa, E., Meleiro, L.A.C., Carvalho, E., Domingues, A., Maciel Filho, R., Wild, G., Poncin, S., Midoux, N., and Bouillard, J., A complete model for oxidation air-lift reactors. *Comput. Chem. Eng.*, 25(4-6), 577-584, 2001.

[4] Khinast, J.G., Impact of 2D bubble dynamics on the selectivity of fast gas-liquid reactions. *AIChE J.*, 47(10), 2304-2319, 2001.

[5] Maretto, C., and Krishna, R., Modeling of a bubble column slurry reactor for Fischer-Tropsch synthesis. *Catal. Today*, 52(2-3), 279-289, 1999.

[6] Meikap, B.C., Kundu, G., and Biswas, M.N., Modeling of a novel multi-stage bubble column scrubber for flue gas desulfurization. *Chem. Eng. J.*, 86(3), 331-342, 2002.

[7] Zahradnik, J., Kuncova, G., and Fialova, M., The effect of surface active additives on bubble coalescence and gas holdup in viscous aerated batches. *Chem. Eng. Sci.*, 54(13-14), 2401-2408, 1999.

[8] Zhang, Y., McLaughlin, J.B., and Finch, J.A., Bubble velocity profile and model of surfactant mass transfer to bubble surface. *Chem. Eng. Sci.*, 56(23), 6605-6616, 2001.

[9] Kellermann, H., Juttner, K., and Kreysa, G., Dynamic modeling of gas hold-up in different electrolyte systems. *J. Appl. Electrochem.*, 28(3), 311-319, 1998.

[10] Zahradnik, J., Fialova, M., Kastanek, F., Green, K.D., and Thomas, N.H., The effect of electrolytes on bubble coalescence and gas holdup in bubble column reactors. *Trans. IChemE.*, 73A, 341-346, 1995.

[11] Krishna, R., Baten, J.M. van, and Urseanu, M.I., Scale effects on the hydrodynamics of bubble columns operating in the homogeneous flow regime. *Chem. Eng. Technol.*, 24(5), 451-458, 2001.

[12] Krishna, R., Baten, J.M. van, Urseanu, M.I., and Ellenberger, J., Rise velocity of single circular-cap bubbles in two-dimensional beds of powders and liquids. *Chem. Eng. Process.*, 39(5), 433-440, 2000.

[13] Krishna, R., Urseanu, M.I., Baten, J.M. van, and Ellenberger J., Influence of scale on the hydrodynamics of bubble columns operating in the churn-turbulent regime: experiments vs. Eulerian simulations. *Chem. Eng. Sci.*, 54(21), 4903-4911, 1999.

[14] Krishna, R., Urseanu, M.I., Baten, J.M. van, and Ellenberger, J., Rise velocity of a swarm of large gas bubbles in liquids. *Chem. Eng. Sci.*, 54(2), 171-183, 1998.

[15] Urseanu, M.I., *Scaling Up Bubble Column Reactors*. Thesis/Dissertation, University of Amsterdam, The Netherlands, 2000.

[16] Kluytmans, J.H.J., Wachem, B.G.M. van, Kuster, B.F.M., and Schouten, J.C., Gas holdup in a slurry bubble column: Influence of electrolyte and carbon particles. *Ind. Eng. Chem. Res.*, 40(23), 5326-5333, 2001.

[17] Hikita, H., Asai, S., Tanigawa, K., Segawa, K., and Kitao, M., Gas hold-up in bubble columns. *Chem. Eng. J.*, 20, 59-67, 1980.

[18] Reilly, I.G., Scott, D.S., Bruijn, T. de, Jain, A., and Piskorz, J., A correlation for gas holdup in turbulent coalescing bubble columns. *Can. J. Chem. Eng.*, 64, 705-717, 1986.

[19] Wilkinson, P.M., Spek, A.P., and Dierendonck, L.L. van. Design parameters estimation for scale-up of high-pressure bubble columns. *AIChE J.*, 38(4), 544-554, 1992.

[20] Ellenberger, J., and Krishna, R., A unified approach to the scale-up of gas-solid fluidized bed and gas-liquid bubble column reactors. *Chem. Eng. Sci.*, 49(24B), 5391-5411, 1994.

[21] May, W.G. Fluidized-bed reactor studies. *Chem. Eng. Prog.*, 55(12), 49-56, 1959.

[22] Deemter, J.J. van, Mixing and contacting in gas-solid fluidized beds. *Chem. Eng. Sci.*, 13, 143-154, 1961.

[23] Davies, R.M., and Taylor, G.I., The mechanics of large bubbles rising through extended liquids and through liquids in tubes. *Proc. Royal Soc. London*, A200, 375-390, 1950.

[24] Colins, R., The effect of containing cylindrical boundary on the velocity of a large gas bubble in a liquid. *J. Fluid. Mech.*, 28, 91-112, 1967.

[25] Pyle, D.L., and Harrison, D., The rising velocity of bubbles in two-dimensional fluidized beds. *Chem. Eng. Sci.*, 22(4), 531-535, 1967.

5

Mass transfer in sparged and stirred reactors: Influence of carbon particles and electrolyte

This chapter is submitted for publication as:
Kluytmans, J.H.J., Wachem, B.G.M. van, Kuster, B.F.M., Schouten, J.C., Mass transfer in sparged and stirred reactors: Influence of carbon particles and electrolyte, *Chem. Eng. Sci.*, 2002.

Abstract

Mass transfer in multiphase systems is one of the most studied topics in chemical engineering. However, in three-phase systems containing small particles, the mechanisms playing a role in the increased rate of mass transfer compared to two-phase systems without particles, are still not clear. Therefore, mass transfer measurements were carried out in a 2D slurry bubble column reactor (0.015x0.30x2.00m), a stirred tank reactor with a flat gas-liquid interface, and in a stirred tank reactor with a gas

inducing impeller. The rate of mass transfer in these reactors was investigated with various concentrations of active carbon particles (average particle size of 30 μm), with electrolyte (sodium gluconate), and with combinations of these. In the bubble column, high-speed video recordings were captured from which the bubble size distribution and the specific bubble area were determined. In this way, the specific mass transfer area a_{gl} was determined separately from the mass transfer coefficient k_l. Mechanisms proposed in literature to describe mass transfer and mass transfer enhancement in stirred tank reactors and bubble columns are compared. It is shown that the increased rates of mass transfer in the 2D bubble column and in the stirred tank reactor with the gas inducing impeller are completely caused by an increased gas-liquid interfacial area upon addition of carbon particles and electrolyte. It is suggested that an increased level of turbulence at the gas-liquid interface caused by carbon particles accounts for a smaller effective boundary layer thickness and an enhancement of mass transfer in the flat gas-liquid surface stirred tank reactor.

5.1 Introduction

5.1.1 Gas-liquid mass transfer

In industry, three-phase systems are applied in the Fischer-Tropsch synthesis, biological wastewater treatment, and in many production processes in the fine chemicals sector. Mass transfer is one of the key parameters determining the performance of these three-phase systems. A good understanding of mass transfer is relevant to obtain adequate reactor designs. Most mass transfer phenomena can be well described with the two-film model of Whitman [1]. Because the two-film model is essentially a steady state model, various dynamic models were developed, to model non-stationary mass transfer phenomena as well. These models are generally addressed as penetration models or surface renewal models. Depending on the hydrodynamics of a certain system, several age distribution functions for the liquid elements at the surface have been developed, of which the models of Higby [2] and Danckwerts [3] are the best known. These models have been used to describe mass transfer phenomena in many gas-liquid contactors. Alper et al. [4, 5] suggested that for three-phase systems with small particles, suspended in the liquid, the two-film model and the penetration model could not describe the observed mass transfer phenomena. Therefore, Alper et al. introduced the concept of enhancement of mass transfer, which is due to the presence of the small particles in three-phase systems. The particles are supposed to adsorb an additional amount of gas at the gas-liquid interface, after which this adsorbed gas desorbs from the particles, in the liquid bulk. This effect has been described as the so-called "shuttle" or "grazing" effect. Alper et al. [4, 5] and many others [6-11] have measured an increased rate of mass transfer in several three-phase systems [12, 13]. However, as shown in the review of Beenackers and van Swaaij [14], the exact cause of this mass transfer enhancement is not clear.

Aim of this chapter is to investigate which mechanism accounts for the measured increase in the rate of gas-liquid mass transfer in a 2D bubble column reactor, upon addition of carbon particles and electrolyte. Mechanisms which possibly account for this increased rate of gas-liquid mass transfer, were obtained from literature. The validity of these mechanisms for our system was investigated by performing mass transfer measurements in three different stirred and sparged reactors.

5.1.2 Mass transfer mechanisms

The mechanism of mass transfer enhancement by the shuttle or grazing effect is closely related to the mechanism of mass transfer as described by the penetration theory: the refreshment of small particles adsorbing gas at the gas-liquid interface after which the gas is desorbed in the liquid bulk, is very similar to the refreshment of liquid phase elements at the gas-liquid interface. Holstvoogd et al. [15] attempted to model the mass transfer enhancement as described by Alper et al. [4, 5] with the penetration model. They modelled the increased rate of gas-liquid mass transfer by assuming a decreased effective diffusion layer at the gas-liquid interface, caused by adsorption of gas by the particles in the diffusion layer. They concluded that only a very high adsorption capacity of the carbon particles could account for the mass transfer enhancement as suggested by Alper et al. [4, 5]. More recently, Van der Zon et al. [16] used the two-film model to calculate mass transfer enhancement during reaction in a three-phase system. They also found that mass transfer was enhanced by the catalyst particles and that the enhancement was a function of the hydrophobicity of the particles used. Although the rate of mass transfer is predicted well by the models of both Holstvoogd et al. [15] and Van der Zon et al. [16], the exact cause of the mass transfer enhancement is still not understood. Both models neglect other possible mechanisms leading to an increased rate of gas-liquid mass transfer. Other mechanisms have been published in many articles and reviews like those of Lee and Foster [17] and Beenackers and van Swaaij [14] and are also supported by recent studies in our laboratory [18]. From these studies three mechanisms can be identified, which may account for an increased rate of mass transfer in three-phase systems. In this work, three different reactors, a 2D slurry bubble column, a stirred tank reactor with a gas inducing impeller, and a stirred tank reactor with a flat gas-liquid interfacial area, were used to study these mechanisms.

Mechanism 1: Shuttle or grazing effect

This mechanism has been described by Alper et al. [4, 5]: the particles are supposed to transport an additional amount of gas to the liquid bulk through adsorption of the dissolved gas in the gas-liquid diffusion layer and desorption in the liquid bulk. As mentioned before, the shuttle or grazing effect is very similar to the penetration theory. Therefore, it is expected that with increasing carbon particle concentration and with increasing the stirrer speed in a stirred tank reactor, the refreshment rate of carbon particles at the gas-liquid interface will increase, leading to an increased transport of gas from the gas-liquid in-

terface to the liquid bulk, which will result in a larger gas-liquid mass transfer coefficient k_l.

Mechanism 2: Hydrodynamic effects in the gas-liquid boundary layer
The presence of particles can affect the hydrodynamic behavior of three-phase systems. Particles can collide with the gas-liquid interface or may induce turbulence at the gas-liquid interface, leading to a smaller effective diffusion layer. Diffusion of gas into the liquid film, and mixing of gas into the bulk liquid can therefore be increased by the presence of particles, leading to an increase in the mass transfer coefficient k_l. Increasing the stirrer speed in a stirred tank reactor or increasing the superficial gas velocity in a bubble column, will increase the shear stress in the system. Eventually, the shear stress in the system will be much higher compared to the forces induced by the small particles. The relative effect of carbon particles on the increase of the gas-liquid mass transfer will therefore decrease, if the shear stress in the system becomes higher. The number of collisions of carbon particles with the gas-liquid interface or the degree of induced turbulence at the gas-liquid interface, is not necessarily dependent on the concentration of the particles in the bulk liquid. More important in this case are the number of particles present at the interface and the nature of the particle interactions with the interface, which are mainly determined by the affinity of the particles for the gas-liquid interface, as expressed by the hydrophobicity or hydrophilicity of the particles.

Mechanism 3: Changes in the specific gas-liquid interfacial area
The increase of gas-liquid mass transfer is generally expressed by an increase in the combined mass transfer coefficient $k_l a_{gl}$. The increase in mass transfer can thus be due to a change in the mass transfer coefficient k_l or due to a change in the specific gas-liquid interfacial area a_{gl}. Previous studies [18] showed that carbon particles and electrolyte affect the gas hold-up and therefore the gas-liquid interfacial area in a 2D bubble column. Besides changes in the specific gas-liquid interfacial area, no additional increase in the gas-liquid mass transfer coefficient k_l is expected upon changing the carbon particle concentration, stirrer speed or superficial gas velocity, if only this mechanism is present. Also for this mechanism, with increasing superficial gas velocity or stirrer speed, the shear stresses in the system increase, decreasing the effect of electrolyte and carbon particles on the increased gas-liquid interfacial area, and thus decreasing the effect on the rate of gas-liquid mass transfer [18].

The objective of this work is to clarify which mechanism leads to the observed increased rate of gas-liquid mass transfer in sparged and stirred three-phase reactors. By definition, mass transfer enhancement as considered in this chapter, is defined as the increased rate of gas-liquid mass transfer due to an increase in the mass transfer coefficient k_l (mechanisms 1 and 2) while measuring the rate of oxygen depletion from the liquid phase.

5.2 Experimental setup and procedures

Experiments were carried out at ambient conditions. It was found that the type of gas (nitrogen, oxygen, air) did not influence mass transfer significantly. In all three reactors, experiments were carried out with distilled water, carbon particles, electrolyte, and combinations of carbon particles and electrolyte solutions. Sodium gluconate was used as electrolyte in concentrations of 0.05-0.5M. Carbon particles (Engelhard Q500-130) with a mean particle diameter of 30 μm and a BET surface area (CO adsorption) of approx. 1150 m^2g^{-1} were used. Prior to each experiment, the carbon particles were washed with distilled water and dried at 378 K, to clean them from organic contaminations. Because the carbon particles tend to be hygroscopic, they were stored at 378 K. The wettability of the carbon particles is one of the main parameters influencing the gas hold-up [18]. To make sure that all particles are completely wetted at the start of each experiment, the particles were mixed with distilled water for one hour preceding each experiment.

5.2.1 2D slurry bubble column

The 2D slurry bubble column consists of two parallel perspex plates (h x w : 200 cm x 30 cm) at a distance of 1.5 cm apart from each other. Gas hold-up was measured with four pressure sensors and with a float on top of the column [18]. Gas hold-up and gas-liquid mass transfer were measured simultaneously. Mass transfer was measured using the saturation method described by Letzel et al. [19]. The electrolyte solutions and carbon particle slurries were saturated with oxygen after which the gas feed was switched to nitrogen, whilst maintaining a constant gas hold-up. The oxygen depletion from the liquid was measured in a sample loop connected at the bottom of the column. This sample loop consisted of a sample chamber with an Ingold oxygen electrode and a pump to circulate the liquid. A constant liquid circulation rate resulted in a residence time of the liquid in the sample chamber of less than 0.2 s, ensuring a sufficiently accurate measurement of the oxygen depletion in the column.

5.2.2 Stirred tank reactor with flat gas-liquid surface

Experiments with a known gas-liquid interfacial area a_{gl} in a flat-surface stirred tank reactor were performed, to be able to measure the mass transfer coefficient k_l separately. The mass transfer was measured by adsorption of oxygen into the liquid according to the following procedure. The liquid was first degassed where after fresh gas was let into a further closed reactor. Then the stirrer was started, inducing the diffusion of the gas into the liquid. The mass transfer was measured by recording the pressure of the gas in the vessel as a function of time. Assuming the two-film model, the rate of mass transfer is obtained from the slope of the pressure-time curve.

5.2.3 Stirred tank reactor with gas inducing impeller

Experiments in the 2D bubble column and in the stirred tank reactor with a flat gas-liquid interface give insight in the effect of carbon particles and electrolyte on mass transfer in a sparged and in an agitated reactor. A reactor with stirrer through which gas bubbles are sparged into the stirred reactor, is used to complete the set of experiments. It enables to study the combined effect of stirring and sparging in one reactor. Mass transfer measurements were carried out using the pressure step method described by Letzel et al. [19]. Gas is sucked in through the impeller, creating gas bubbles in the liquid. The reactor is pressurized with oxygen until equilibrium between the gas phase and the dissolved oxygen in the liquid phase has been established. Releasing the pressure results in an oxygen depletion from the liquid to the gas phase from which the rate of mass transfer is determined.

5.2.4 Mass transfer modelling

The two-film model is used to describe the rate of mass transfer in all three reactors. In both the 2D bubble column and the stirred tank reactor with gas inducing impeller the liquid was saturated with nitrogen after which the gas feed was switched to nitrogen, while measuring the oxygen depletion from the liquid. In the stirred tank reactor with flat gas-liquid surface area the diffusion of oxygen was measured into a fully degassed liquid. It is assumed that both the gas and liquid phases are each fully mixed. This assumption was verified by measuring the rate of mass transfer at various heights in the 2D bubble column and by verifying the assumptions as given by Letzel et al. [19], which apply for the two-film model in a slurry bubble column. Letzel et al. [19] also showed that the increase in oxygen gas-phase concentration in the bubble column and the stirred tank reactor was small, and could therefore be neglected. The liquid side mass transfer is represented by $k_l a_{gl}$ and determines in most cases the overall rate of gas-liquid mass transfer, while the gas side mass transfer resistance is negligible. The rate of change of the gas concentration in the liquid bulk is then given by Equation 5.1:

$$\frac{dC_{l,bulk}}{dt} = k_l a_{gl} \left(C_{l,i} - C_{l,bulk}\right) \tag{5.1}$$

When the liquid bulk is first saturated with oxygen after which the gas feed is switched to nitrogen, Equation 5.1 can be integrated with the initial condition stating that $C_{l,bulk}$=$C_{l,i}$ at t=0 and $C_{l,i}$=0 for t>0. The latter condition was verified for a bubble with a diameter of 1 cm rising through the bubble column with a velocity of 0.2 m s^{-1}, and having a mass transfer coefficient of k_l = $5.0.10^{-4}$. With Equation 5.1, it was calculated that the increase in the oxygen gas phase concentration, for this bubble, during its residence time in the liquid was less than 4%, showing that the increase in gas phase concentration can be neglected. Integration of Equation 5.1 then leads to:

$$C_{l,bulk} = C^0_{l,bulk} e^{-k_l a_{gl} t} \tag{5.2}$$

The volumetric mass transfer coefficient $k_l a_{gl}$ can then be determined by a least squares fit of Equation 5.2 to the experimentally obtained values of $C_{l,bulk}(t)$.

5.2.5 Oxygen sensor response time

The Ingold oxygen sensor measures the amount of dissolved oxygen in a liquid with an electrochemical cell. The response of the oxygen sensor to a change of the oxygen concentration has a finite delay, which can be described by a first order process. Because this delay in response is of the order of magnitude of the time constant of the gas-liquid mass transfer, the sensor response time should be incorporated in the overall mass transfer model as described by Letzel et al. [19]. Equation 5.3 represents the first-order response of the oxygen sensor:

$$\frac{dC_{sensor}}{dt} = k_{sensor}\left(C_{sensor} - C_{l,bulk}\right) \tag{5.3}$$

The sensor constant k_{sensor}, is a function of the medium in which the oxygen depletion is measured, the stirrer speed, and the degree of turbulence at the membrane surface. Therefore, the sensor constant was independently measured in a setup in which the liquid feed could be switched from a saturated oxygen solution to a saturated nitrogen solution without oxygen present, under the exact flow conditions as during the measurements in the 2D slurry bubble column and in the stirred tank reactors. It was found that the response time changes under influence of the presence of carbon particles and electrolyte. This effect was the most pronounced in the stirred tank reactor with gas inducing impeller because in that case the degree of turbulence at the sensor membrane was much lower than in the sample loop of the 2D slurry bubble column. Sensor constants ranging from 0.8 - 0.98 s^{-1} in distilled water, carbon slurries, and electrolyte solutions were obtained in the stirred tank reactor, while in the 2D bubble column the sensor constant ranges between 0.95 - 0.99 s^{-1}.

5.2.6 Image processing

To calculate the specific gas-liquid interface a_{gl} in the 2D bubble column, high-speed video recordings were made with a Dalsa CA-D6 camera at a frame-rate of 955 frames s^{-1}. The image processing is performed assuming a distinction between the small and large bubble populations as proposed by Krishna [20]. The distance between the perspex plates in the 2D bubble column is 1.5 cm, therefore only bubbles larger than 2 cm, touching both walls, can be detected in carbon particles slurries, which are classified as large bubbles. The volume of the small bubbles is calculated by subtracting the volume of the large bubbles from the total gas volume calculated from the measured gas hold-up. Based on the bubble size classification of Krishna [20], it was assumed that the volume of the small bubbles consisted of bubbles with a mean bubble diameter of 8 mm. The total gas-liquid specific surface area is then calculated by addition of the specific gas-liquid interfacial area of the large

bubbles and the gas-liquid interfacial area of the small bubbles. In distilled water and electrolyte solutions, the contrast between the gas phase and the liquid phase was too small to even observe the large bubbles by the automatic image processing. However, to obtain estimations for the bubble size distributions in distilled water and electrolyte, randomly chosen images from these movies were analyzed by hand.

5.3 Experimental results

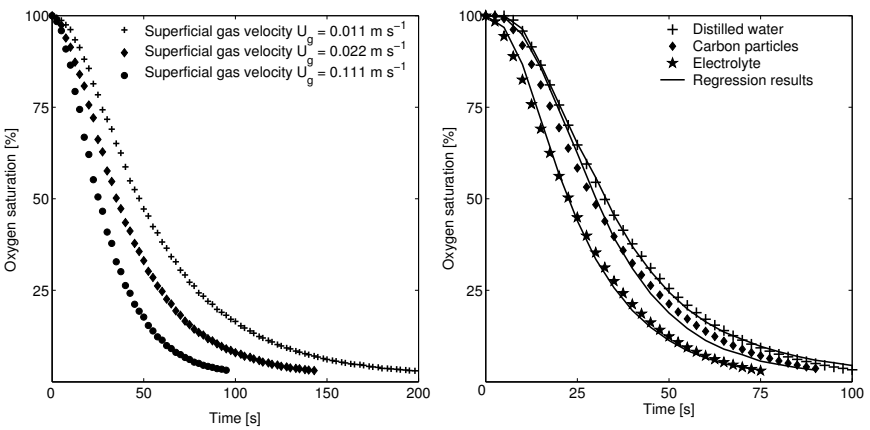

(a) (b)

Figure 5.1: Measured oxygen saturation in the liquid, in the 2D slurry bubble column: a) at different superficial gas velocities in distilled water; b) at a superficial gas velocity of 0.011 m s^{-1} for distilled water, a 0.5 g l^{-1} carbon particles slurry, and an 0.5 M electrolyte solution. The lines indicate the fitted oxygen saturation curves.

5.3.1 Mass transfer in a 2D bubble column

The rate of mass transfer was measured at different superficial gas velocities and in different carbon particles slurries and electrolyte solutions. Measurements in solutions containing both carbon particles and electrolyte did not give reliable data, because of severe foaming. As shown in Figure 5.1, the rate of mass transfer increases with increasing superficial gas velocity and under influence of addition of carbon particles and electrolyte. The $k_l a_{gl}$ values were calculated from the oxygen depletion curves by orthogonal distance regression using the two-film model described in section 5.2. The regression results obtained using Equations 5.2 and 5.3 is in good agreement with the measured oxygen depletion (Figure 5.1b). Figure 5.2 shows that $k_l a_{gl}$ increases with increasing superficial gas velocity and gas hold-up. The carbon particles concentration in these measurements was varied from 0.1 g l^{-1}

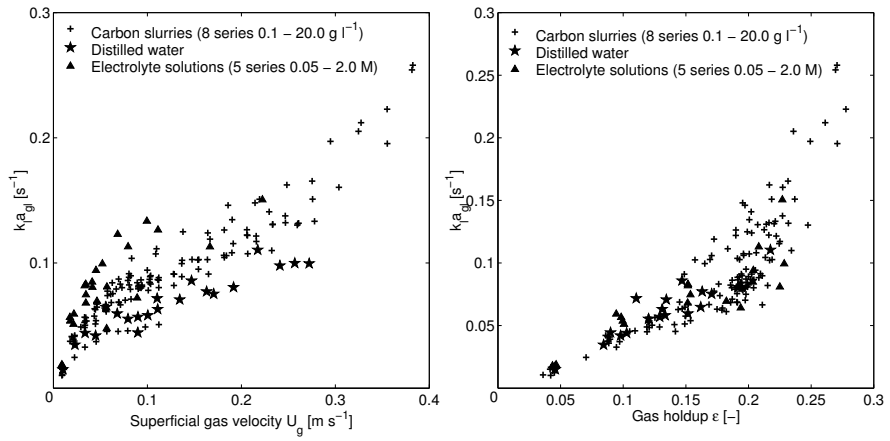

(a) (b)

Figure 5.2: Measured values of $k_l a_{gl}$ in the 2D bubble column, in distilled water, carbon particle slurries [0.1 - 1.0 g l^{-1}], and electrolyte solutions [0.05 - 2.0 M] as a function of a) the superficial gas velocity, and b) the measured gas hold-up.

to 20 g l^{-1}. However, within the measurement error of $\pm$ 10%, no dependency was found between the mass transfer coefficient and the carbon particles concentration in between 0.1 g l^{-1} - 2.0 g l^{-1}. As shown in Figure 5.2b, measurements in electrolyte solutions and in distilled water are equally scattered as the measurements for the carbon particle slurries. To determine the mass transfer coefficient k_l, the gas-liquid specific surface area a_{gl} is measured with image processing (see section 5.2.6).

5.3.2 Determination of a_{gl} and k_l

Image processing has been performed on 51 movies each consisting of 10.000 images, made of different carbon particles slurries. Bubble size, bubble volume, and specific gas-liquid surface area were determined using image processing routines. The vertical lines in Figure 5.3 show that up till a superficial gas velocity of 0.075 m s^{-1} no large bubbles are present; the small bubbles are homogeneously distributed in the liquid phase and have a mean bubble diameter of 8 mm. Further analysis of the movies of the carbon particle slurries showed that the specific gas-liquid interfacial area a_{gl} is not dependent on the carbon particle concentration (Figure 5.4a). The overall mass transfer coefficient k_l was calculated using the total gas volume obtained from the gas hold-up measurements and from the measured $k_l a_{gl}$ values (Figure 5.2). The thus calculated k_l values are shown in figure 5.4b. The values are in the same order of magnitude as calculated with several correlations for the calculation of the mass transfer coefficient k_l in bubble columns, as summarized in the review of Shah et al. [21]. It can be seen from figure 5.4b that the mass transfer

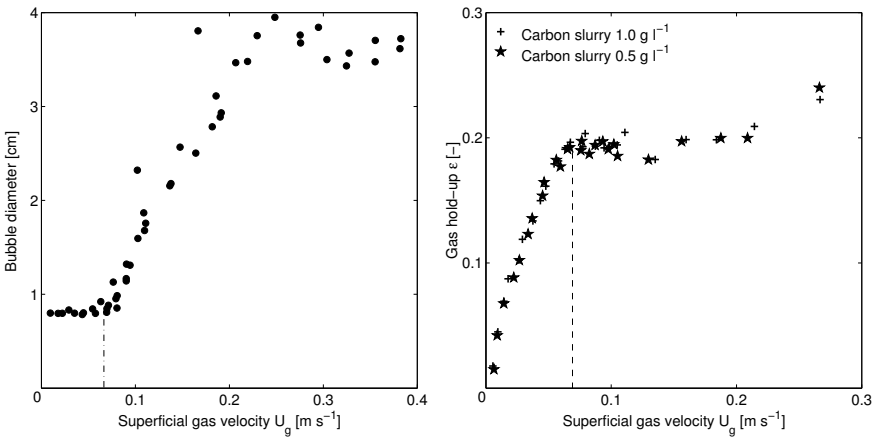

(a) (b)

Figure 5.3: a) Bubble size as a function of the superficial gas velocity, calculated from 51 movies of carbon particle slurries with carbon particle concentrations ranging from 0.1 g l^{-1} to 1 g l^{-1}. b) Corresponding gas hold-up of the carbon particle slurries determined with image processing. The vertical lines in both graphs show that up to a superficial gas velocity of 0.07 m s^{-1} the bubble diameter is approximately 8 mm.

coefficient k_l is not dependent on the carbon particle concentration. However, k_l increases with increasing superficial gas velocity above 0.075 m s^{-1}, because at this point large bubbles start to develop. This is as expected based on the fact that small bubbles have a rigid gas-liquid interface while large bubbles have a more developed movement of the gas-liquid interface, leading to a higher refreshment rate of liquid at the interface and thus a higher mass transfer coefficient. Also, the large bubbles are not entrained into the liquid, resulting in a higher shear at the outside of the bubbles and therefore in a smaller effective gas-liquid diffusion layer [20], compared to small bubbles. With the information obtained from the image processing, the overall value of k_l for carbon particle slurries can be separated in a mass transfer coefficient for the small bubbles ($k_{l,small}$) and a value for the mass transfer coefficient of the large bubbles ($k_{l,large}$). These calculations showed that the mass transfer coefficient k_l for small bubbles in carbon slurries was $5.3.10^{-4}$ m s^{-1}. The mass transfer coefficient of the large bubbles could then be calculated for superficial gas velocities above 0.075 m s^{-1} from: $k_l a_{gl} = k_{l,large} a_{large} + k_{l,small} a_{small}$. This resulted in an average mass transfer coefficient for the large bubbles of $k_{l,large} = 8.0.10^{-3}$ m s^{-1}.

As mentioned before, the movies captured during distilled water experiments could not be analyzed with the automatic image processing routines because of a lack of contrast between the gas and the liquid phase. Analyzing the movies of distilled water by hand showed that up to a superficial gas velocity of 0.06 m s^{-1} no large

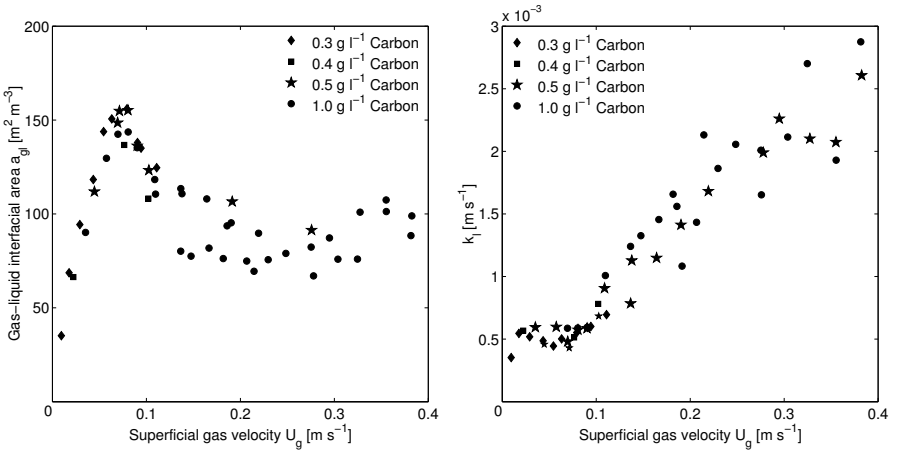

(a) (b)

Figure 5.4: a) Specific gas-liquid surface area in 7 carbon slurries in the 2D slurry bubble column, with concentrations between 0.3-1.0 g l^{-1}. b) k_l calculated with the gas-liquid surface area from Figure 4a and the measured $k_l a_{gl}$ values of Figure 2a.

bubbles were present. The corresponding specific gas-liquid surface area was then calculated, assuming that the total gas volume consisted of bubbles with an average diameter of 8 mm. With this information, the mass transfer coefficient of small bubbles in distilled water up to a superficial gas velocity of 0.06 m s^{-1} could be calculated. It was found that the mass transfer coefficient of these small bubbles was equal to the mass transfer coefficient of the small bubbles in carbon slurries and equals $5.3.10^{-4}$ [m s^{-1}].

5.3.3 Mass transfer in a stirred tank reactor with flat gas-liquid interface

Figure 5.5a shows that the experiments with carbon slurries result in a higher value of k_l compared to the experiments with distilled water and electrolyte solutions. The combined experiment with carbon particles and electrolyte shows an increase of k_l only at higher stirring speeds. These experiments clearly show that carbon particles tend to increase the mass transfer coefficient k_l in the stirred tank reactor with flat gas-liquid interface. However, the calculation of k_l in the 2D bubble column showed that carbon particles and distilled water have the same value of k_l at superficial gas velocities up to 0.06 m s^{-1}. This will be discussed in section 5.4.

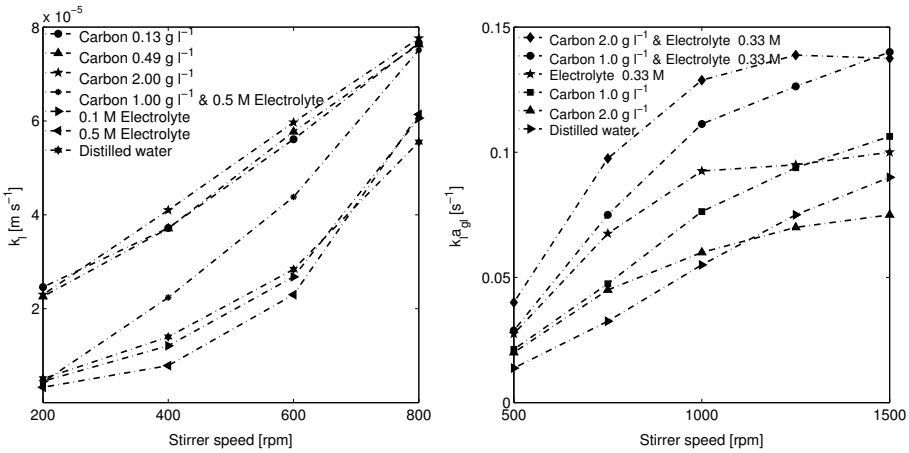

(a) (b)

Figure 5.5: a) k_l values determined from mass transfer measurements in the stirred tank reactor with a flat gas-liquid surface, for distilled water, carbon slurries (0.1-2.0 g l^{-1}), electrolyte solutions (0.1 - 1.0M), and a combined carbon particle and electrolyte experiment (1 g l^{-1} and 0.5 M); b) Mass transfer coefficient $k_l a_{gl}$ as a function of stirrer speed in the stirred tank reactor with gas inducing impeller, for distilled water, different carbon slurries (1.0 and 2.0 g l^{-1}), electrolyte solution (0.33 M), and combined carbon particles and electrolyte solutions.

5.3.4 Mass transfer in a stirred tank reactor with gas inducing impeller

Mass transfer experiments in the stirred tank reactor with a gas inducing impeller were carried out to study the effect of the carbon particles and electrolyte on a system in which gas is sparged into the reactor by the stirrer. Figure 5b shows for distilled water, carbon particle slurries, electrolyte solutions and combined experiments with carbon particles and electrolyte that the rate of mass transfer increases with increasing carbon particle concentration. The increase in gas-liquid mass transfer is even more pronounced in the experiment with carbon particles and electrolyte, in which the rate of mass transfer increases with a factor of 3 to 4. Table 5.1 shows that at constant carbon concentration, the increase in the rate of gas-liquid mass transfer becomes smaller with increasing stirrer speed. This is in agreement with the observed effects in the stirred tank reactor with flat gas-liquid interfacial area. However, at a stirrer speed above 1000 rpm the increase of the rate of gas-liquid mass transfer for most carbon slurries is negligible or even decreases compared to distilled water.

Table 5.1: Ratio between the rate of mass transfer in carbon particle slurries and in distilled water ($(k_l a_{gl})_{carbon}/(k_l a_{gl})_{distilledwater}$) for various concentrations of carbon particles as a function of the stirrer speed in the stirred tank reactor with gas inducing impeller. All values ± 2%

Carbon concentration [g l^{-1}]	500 rpm	750 rpm	1000 rpm	1250 rpm	1500 rpm
0.0	1.00	1.00	1.00	1.00	1.00
0.5	1.17	1.15	1.05	0.98	0.94
1.0	1.54	1.46	1.10	1.25	1.18
2.0	1.44	1.38	1.09	0.93	0.83
3.0	1.45	1.39	1.21	1.03	0.89
4.0	1.45	1.23	1.14	1.03	0.92

5.4 Discussion

From the experiments it is not straightforward to appoint one of the mechanisms described in section 5.1.2, as being responsible for the observed increased rate of mass transfer in all three reactors. The observed phenomena in each reactor should therefore be compared with the expected phenomena for each mechanism as described in section 5.1.2.

5.4.1 Mass transfer mechanism in the 2D bubble column

The results point out that within the measurement error of about 10% no dependency was found of the rate of mass transfer on carbon concentration. Mechanism 1 (the shuttle or grazing effect) is therefore unlikely to account for the increased rate of gas-liquid mass transfer, because a concentration dependency is expected when this mechanism is present. Despite of the large BET area (1150 m^2 g^{-1} of the carbon particles, no evidence was found for gas adsorption at the carbon particle interface, however, it is not excluded that gas adsorption occurs, however, the experiments show that this effect does not contribute significantly to the increase in the rate of gas-liquid mass transfer. It was found that the mass transfer coefficient is only a function of the superficial gas velocity. Up to a superficial gas velocity of 0.06 m s^{-1}, it was found that the mass transfer coefficient k_l for distilled water and carbon slurries was exactly the same ($k_l = 5.3.10^{-4}$ m s^{-1}). This is not expected if mechanism 2 (a hydrodynamic effect) is supposed to be responsible for the increased rate of mass transfer. It can be concluded that the increase in gas-liquid mass transfer is only caused by an increase in the specific gas-liquid interfacial area a_{gl}, upon addition of carbon particles and electrolyte (mechanism 3).

5.4.2 Mass transfer mechanism in the stirred tank reactor with flat interfacial area

An increased mass transfer coefficient upon addition of carbon particles was measured in the stirred tank reactor with flat gas-liquid interfacial area (Figure 5.5a). No dependency of the mass transfer coefficient on the carbon particle concentration was found. Therefore, the shuttle effect as described in mechanism 1 is unlikely to account for the increased rate of mass transfer in this reactor. Moreover, increasing the stirrer speed, decreases the effect of the carbon particles, which is also not expected with mechanism 1. Based on the observations in Figure 5.5a, a hydrodynamic effect (mechanism 2) is more likely to account for the increased rate of mass transfer in this reactor. It is suggested that carbon particles enforce the level of turbulence at the gas-liquid interface, therefore mixing the gas-liquid boundary layer into the bulk liquid, resulting in a smaller effective boundary layer thickness, and thus in a higher rate of gas-liquid mass transfer. The effective diffusion layer can be calculated from the correlation for k_l in stirred tank reactors, $(k_l \delta_{eff})/D = a\, Re^{1/3} Sc^{1/2}$. At constant liquid properties and stirrer speed, Reynolds (Re) and Schmidt (Sc) numbers are unchanged, therefore the ratio of the effective diffusion layers can be written as:

$$f_{eff} = \frac{\delta_{eff,water}}{\delta_{eff,carbon}} = \frac{k_{l,carbon}}{k_{l,water}} \tag{5.4}$$

As shown in Table 5.2, the effective diffusion layer in the carbon particle slurry is always smaller compared to distilled water. At higher stirrer speeds, the shear stress at the gas-liquid interface increases, leading to a decreased effect of the carbon particles on the reduction of the effective film layer. The factor f_{eff} for the combined experiment with carbon particles and electrolyte shows a maximum at 400 rpm. It is known that electrolyte promotes carbon particle agglomeration [16], therefore it is assumed that an increased rate of mass transfer for the combined experiment is only measured at higher stirrer speeds, where the particle agglomerates have enough energy to induce the same mixing effect as the small particles. However, at stirrer speeds above 600 rpm, the increase in the rate of gas-liquid mass transfer decreases because of the increased shear stress at higher stirring speeds.

Table 5.2: Ratio of the size of the effective film layer thickness in carbon particle slurries and combined carbon particle and electrolyte solutions compared with distilled water in the stirred tank reactor with flat gas-liquid interfacial area, calculated with Equation 5.4.

Stirrer speed [rpm]	$f_{eff,carbon}$ [-]	$f_{eff,combined}$ [-]
200	4.71	0.85
400	2.74	1.60
600	2.01	1.54
800	1.38	1.35

5.4.3 Mass transfer mechanism in the stirred tank reactor with gas inducing impeller

As shown in previous work [18] and section 5.3.1, carbon particles, electrolyte, and combinations of carbon particles and electrolyte increase the gas hold-up, the gas-liquid interfacial area, and therefore the rate of gas-liquid mass transfer in a 2D bubble column. However, the effect of carbon particles and electrolyte decreases at higher superficial gas velocities, where the shear stresses become higher. The experiments in the stirred tank reactor with gas inducing impeller show the same behavior upon addition of carbon particles and electrolyte as observed in the 2D bubble column. This increase of the rate of mass transfer upon electrolyte addition can only be ascribed to the increase in gas-liquid interfacial area. Therefore, it is concluded that the increase in gas-liquid mass transfer upon addition of carbon particles and electrolyte in this reactor is caused by an increased gas-liquid interfacial area a_{gl} (mechanism 3).

5.5 Conclusions

This chapter shows that finding the cause of an increased rate of mass transfer in three-phase systems is not straightforward. In most cases it is not well possible to measure the parameters to clarify the exact mechanisms, like the effective diffusion layer, the adsorption and desorption rates of oxygen on a carbon interface in a liquid, the oxygen transport by particles, and the specific gas-liquid interfacial area. However, we have shown that by combining the results of experiments in three different reactors, it is possible to give more insight in the mechanisms leading to an increased rate of mass transfer or mass transfer enhancement. Summarizing, we have found that:

- For the carbon particles used in this study it is rather unlikely that mass transfer enhancement takes place due to the shuttle or grazing effect as described by Alper et al. [4, 5] (mechanism 1).
- Carbon particles may increase the degree of turbulence at the gas-liquid interface, resulting in a reduced effective gas-liquid diffusion layer and in a mass transfer enhancement (mechanism 2) at low stirrer speeds, where the shear stresses due to stirring are relatively low.
- The rate of mass transfer in the 2D slurry bubble column and in a sparged stirred tank reactor is increased upon addition of carbon particles and electrolyte, due to an increase in the specific gas-liquid interfacial area a_{gl} (mechanism 3).
- The mass transfer coefficient $k_{l,small}$ for small bubbles in a 2D slurry bubble column, for distilled water and carbon particles slurries, is equal to $5.3.10^{-4}$ m s^{-1}, up to a superficial gas velocity of 0.06 m s^{-1}.

- The mass transfer coefficient $k_{l,large}$ for large bubbles in a 2D slurry bubble column, for carbon particles slurries, is equal to $8.0.10^{-3}$ m s^{-1}

Table 5.3: List of symbols

a_{gl}	Specific gas-liquid interfacial area	[m^2 m^{-3}]
U_g	Superficial gas velocity	[m s^{-1}]
k_l	Overall mass transfer coefficient	[m s^{-1}]
$k_{l,small}$	Mass transfer coefficient of the small bubbles	[m s^{-1}]
$k_{l,large}$	Mass transfer coefficient of the large bubbles	[m s^{-1}]
α	Constant	[-]
$C_{l,bulk}$	Concentration in the liquid bulk	[mol m^{-3}]
d_{eff}	Effective diffusion layer thickness	[m]
$C_{l,i}$	Concentration at the gas-liquid interface in the liquid	[mol m^{-3}]
Re	Reynolds number	[-]
C_{sensor}	Concentration measured by sensor	[mol m^{-3}]
Sc	Schmidt number	[-]
t	Time	[s]
D	Diffusion coefficient	[m^2 s^{-1}]
k_{sensor}	Sensor constant	[s^{-1}]
f_{eff}	Ratio between effective diffusion layers	[-]

Bibliography

[1] Whitman, W.G., Preliminary experimental confirmation of the two-film theory of gas absorption, *Chem. Metal. Eng.*, 29, 146-148, 1923.

[2] Higbie, R., The rate of absorption of a pure gas into a still liquid during short periods of exposure, *Trans. Am. Inst. Chem. Eng.*, 31, 365-389, 1935.

[3] Danckwerts, P.V., Significance of liquid-film coefficients in gas absorption, *Ind. Eng. Chem.*, 43, 1460-1467, 1951.

[4] Alper, E., Wichtendahl, B., and Deckwer, W.D., Gas absorption mechanism in catalytic slurry reactors, *Chem. Eng. Sci.*, 35(1-2), 217-222, 1980.

[5] Alper, E. and Ozturk, S., The effect of activated carbon loading on oxygen absorption into aqueous sodium sulfide solutions in a slurry reactor, *Chem. Eng. J.*, 32(2), 127-130, 1986.

[6] Dagaonkar, M.V., Beenackers, A.A.C.M., and Pangarkar, V.G., Gas absorption into aqueous reactive slurries of calcium and magnesium hydroxide in a multiphase reactor, *Cat. Today*, 66(2-4), 495-501, 2001.

[7] Dagaonkar, M.V., Beenackers, A.A.C.M., and Pangarkar, V.G., Enhancement of gas-liquid mass transfer by small reactive particles at realistically high mass transfer coefficients: absorption of sulfur dioxide into aqueous slurries of $Ca(OH)_2$ and $Mg(OH)_2$ particles, *Chem. Eng. J.*, 81(1-3), 203-212, 2001.

[8] Demmink, J.F., Mehra, A., and Beenackers, A.A.C.M., Gas-absorption in the presence of particles showing interfacial affinity - case of fine sulfur precipitates, *Chem. Eng. Sci.*, 53(16), 2885-2902, 1998.

[9] Zahradnik, J., Kuncova, G., and Fialova, M., The effect of surface active additives on bubble coalescence and gas holdup in viscous aerated batches, *Chem. Eng. Sci.*, 54(13-14), 2401-2408, 1999.

[10] Tinge, J.T., and Drinkenburg, A.A.H., Absorption of gases into activated carbon-water slurries in a stirred cell, *Chem. Eng. Sci.*, 47(6), 1337-1345, 1992.

[11] Tinge, J.T., and Drinkenburg, A.A.H., The enhancement of the physical absorption of gases in aqueous activated carbon slurries, *Chem. Eng. Sci.*, 50(6), 937-942, 1995.

[12] Quicker, G., Alper, A., and Deckwer, W.-D., Effect of fine activated carbon particles on the rate of CO_2 adsorption, *AIChE J.*, 33(5), 871-875, 1987.

[13] Quicker, G., Alper, A., and Deckwer, W.-D., Gas adsorption rates in a stirred cell with plane interface in the presence of fine particles, *Can. J. Chem. Eng.*, 67, 32-38, 1989.

[14] Beenackers, A.A.C.M., and Swaaij, W.P.M. van, Mass transfer in gas-liquid slurry reactors, *Chem. Eng. Sci.*, 48(18), 3109-3139, 1993.

[15] Holstvoogd, R.D., Swaaij, W.P.M. van, and Dierendonck, L.L. van, The adsorption of gases in aqeous activated carbon slurries enhanced by adsorbing or catalytic particles, *Chem. Eng. Sci.*, 43(8), 2181-2187, 1988.

[16] Zon, M. van der, Hamersma, P.J., Poels, E.K., and Bliek, A., Gas-solid adhesion and solid-solid agglomeration of carbon- supported catalysts in 3-phase slurry reactors, *Cat. Today*, 48(1-4), 131-138, 1999.

[17] Lee, J.H., and Foster, N.R., Measurement of gas-liquid mass transfer in multiphase reactors, *Applied Cat.*, 63,1-36, 1990.

[18] Kluytmans, J.H.J., Wachem, B.G.M. van, Kuster, B.F.M., and Schouten, J.C., Gas holdup in a slurry bubble column: Influence of electrolyte and carbon particles, *Ind. Eng. Chem. Res.*, 40(23), 5326-5333, 2001.

[19] Letzel, H.M., Schouten, J.C., Krishna, R., and Bleek, C.M. van den, Gas holdup and mass transfer in bubble column reactors operated at elevated pressure, *Chem. Eng. Sci.*, 54(13-14),2237-2246, 1999.

[20] Krishna, R., Chapter 8 : Analogies in multiphase reactor hydrodynamics, p. 239-297 *in Encyclopedia of Fluid Mechanics, Supplement 2, Advances in Multiphase Flow, N P Cheremisinoff (Editor),*, Gulf Publishing, Houston, 1993.

[21] Shah, Y.T., Kelkar, B.G., Godbole, S.P., and Deckwer, W.-D., Design parameters estimations for bubble column reactors, *AIChE J.*, 28(3), 353-379, 1982.

6

Design of an industrial size airlift loop redox cycle (ALRC) reactor for catalytic alcohol oxidation and catalyst reactivation

This chapter is submitted for publication as: Kluytmans, J.H.J., Wachem, B.G.M. van, Kuster, B.F.M., Schouten, J.C., Design of an industrial size airlift loop redox cycle (ALRC) reactor for catalytic alcohol oxidation and catalyst reactivation, *Ind. Eng. Chem. Res.*, 2002

Abstract

An industrial size airlift loop redox cycle (ALRC) reactor has been designed for the selective oxidation of alcohols. Selective catalytic alcohol oxidation can produce valuable products for fine chemistry applications. However, the catalyst looses activity with a factor of 10 within hours, due to overoxidation of the catalyst. The catalyst

can be reactivated by contacting it with a reducing environment. This modelling and reactor design study shows that the ALRC reactor is a suitable option for achieving the alternating contact of the catalyst with a reducing and oxidizing environment. It is shown that the superficial slurry velocity and the inlet partial pressure of oxygen, mainly determine the reactor performance. A reactor design is made based on kinetic, hydrodynamic, and economic considerations, in which the catalyst activity remains high during the presence in the reactor. Finally, the ALRC reactor is compared with a stirred tank reactor process involving alternating gas feed streams. It is shown that the ALRC is much cheaper in reactor operation compared to the stirred tank reactor process, and is thus a feasible solution to be applied in the selective oxidation of alcohols, whilst maintaining a high catalyst activity.

6.1 Introduction

6.1.1 Airlift reactors

Airlift loop reactors are a collection of reactors which consist of a riser and a downcomer. The liquid and/or solid phase in the riser is transported through the reactor, due to a gas stream entering at the bottom of the column, while in the downcomer the liquid and/or solid phase is recirculated due to the difference in density between the phases in the riser and the downcomer. A schematic drawing of an internal airlift loop reactor is shown in Figure 6.1. Airlift reactors are found in many different configurations, like external or internal airlift reactors [1, 2], agitated airlift reactors [3], or more advanced airlift reactors like the biofilm airlift suspension reactor [4].

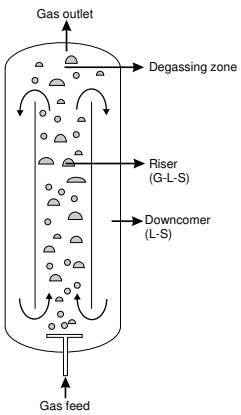

Figure 6.1: Scheme of a three phase airlift loop reactor. The riser is a three phase system, the gas leaves the column at the degassing zone, the liquid and solids are recirculated via the downcomer.

The airlift reactor has multiple advantages, like improved liquid mixing because of the internal or external recycle stream. Furthermore, the airlift loop reactor is suitable to create different hydrodynamic and/or kinetic regimes in the riser and downcomer, within one reactor. During recent years, much research has been devoted to the application of the airlift loop reactor in many different processes. Modelling and experimental studies [5–9] show that the application of the airlift loop reactor in chemical processes is very diverse.

The airlift loop reactor is selected for this particular design study because it allows the creation of an oxidative and reductive zone within one reactor. The creation of these zones is beneficial to maintain a high catalyst activity during the selective oxidation of alcohols. This type of airlift loop reactor will be addressed as the airlift loop redox cycle (ALRC) reactor. The hydrodynamic properties of an ALRC reactor are investigated in this chapter, in conjunction with the kinetics of the MGP oxidation and the catalyst deactivation and reactivation. Finally, industrial size reactor calculations are performed, to investigate the feasibility of the ALRC reactor in practice, including a cost analysis.

6.1.2 Platinum catalyzed oxidation of alcohols

The oxidation of methyl-α-D-glucopyranoside (MGP) towards 1-O-methyl-α-D-glucuronic acid (NaMG) on a carbon supported platinum catalyst,

$$MGP + O_2 + NaOH \rightarrow NaMG + 2H_2O, \tag{6.1}$$

can be considered as a typical model reaction for many selective alcohol oxidation reactions. The selective oxidation of alcohols can provide valuable products for a variety of applications in fine chemistry. For example, 1-O-methyl-α-D-glucuronic acid can be used as an intermediate in an alternative synthesis route for the production of vitamin C. Although the process routes seem very promising due to the mild process conditions (293 - 323 K, at atmospheric pressure) and the rather high selectivity, major problems still have to be overcome. One of these problems is the fast deactivation of the platinum catalyst due to over-oxidation of the platinum surface. Over-oxidation results in a loss of catalyst activity with a factor of 10 within hours [10]. However, the catalyst deactivation is reversible by contacting the catalyst with a reducing, oxygen-free, environment. In this environment, the adsorbed oxygen and the oxide that is formed at the platinum surface, are consumed, regenerating the catalyst to its initial activity. This so called redox cycle requires a process design allowing the catalyst to maintain a high catalyst activity. Generally, three possibilities exist to achieve this goal:

1. Periodically switching the gas feed from an oxygen rich gas feed to a gas feed containing no oxygen. This option was explored by Markusse et al. [11] using a continuous stirred tank reactor.

2. Design of a reactor in which the catalyst alternately travels through an oxidizing zone and a reducing zone, with a constant gas feed.

3. A combination of the above mentioned reactors.

Other options, like operating the reactor under mass transfer limiting conditions or at very low dissolved oxygen concentrations, are not considered. In these cases the reaction rates and thus the efficiency of the reactor are very low. Furthermore,

Markusse et al. [11] showed that under these conditions, additional catalyst deactivation may occur due to poisoning of the catalyst surface. The second option, a reactor in which both a reductive and an oxidative zone are present, was also addressed by Markusse et al. [11], who pointed to the airlift loop reactor as being possibly suitable for selective oxidation of alcohols with a Pt/C catalyst, in continuous operation. The present study aims to show the feasibility of the airlift loop reactor for this purpose, while maintaining a high catalyst activity.

6.2 Reactor design considerations

The aim of this work is to design an ALRC reactor to produce 1-O-methyl-α-D-glucuronic acid out of methyl-α-D-glucopyranoside with a carbon supported platinum catalyst. The ALRC reactor is designed based on several considerations. These considerations are a result of previous studies on the selective oxidation of MGP towards NaMG, and due to the general views concerning the process layout and reactor operation of an airlift loop redox cycle reactor. These considerations and the consequences for the reactor modelling and design, are treated in the following paragraphs.

6.2.1 Process specifications and model parameters

The feasibility of the airlift loop process is demonstrated by comparison with the stirred tank process with switching gas feed composition as described by Markusse et al. [11]. The yearly production capacity for the airlift loop reactor is therefore chosen equal to the process of Markusse et al. [11]. This yearly production rate is chosen arbitrarily, since NaMG is at current not produced at a large scale, whereas no comparison with other processes is possible. However, the production rate of 1.27 10^7 mol NaMG per year in the process of Markusse et al. [11], is equal to 2% of the yearly production capacity of vitamin C, when this would be produced completely via the synthesis route of methyl-α-D-glucopyranoside (based on 50% synthesis efficiency and a yearly production capacity of vitamin C of 100.000 tons). To facilitate a good comparison between the two processes, the ALRC reactor is designed at the same operating conditions as the stirred tank process of Markusse et al. [11].

The airlift loop reactor is designed at a reactor temperature of 323 K operating under atmospheric pressure. The catalyst concentration is taken equal to 14 kg m^{-3}. The catalyst used is a 3.7 wt% Pt/C catalyst with a specific platinum surface of 0.073 mol kg_{cat}^{-1}. It is expected that it is beneficial to work at low bulk liquid concentrations. Experimental and modelling studies (Markusse et al. [11], Gangwal et al. [12]) showed that at oxygen bulk concentrations below 0.2 mol m^{-3}, the reaction is best performed if an egg-shell distribution for the platinum is used. The reactor is operated at a maximum MGP conversion of 10% because at this conversion the selectivity towards NaMG is about 95%. At higher conversions, the production of MGP suffers

from the formation of side products due to oxidation of secondary alcoholic groups and because of rupture of C-C bonds [13]. The liquid feed stream contains 1000 mol m^{-3} of MGP. The gas feed stream consists of air or oxygen/nitrogen mixtures.

Markusse et al. [11] showed that the stirred tank reactor design is primarily determined by the oxygen content in the bulk liquid and at the catalyst surface, which is affected by the mass transfer properties of the system. Markusse et al. [11] did not consider the effect of oxygen diffusion limitation inside the catalyst particle. However, as Gangwal et al. [12] showed, this is an important phenomenon and should therefore be taken into consideration. Model parameters regarding the diffusion and the reaction in the catalyst particle, like the liquid-solid mass transfer coefficient, porosity and tortuosity of the particle, and the intra-particle diffusivities of MGP and oxygen, are taken from the modelling study of Gangwal et al. [12], which will be treated in section 6.3.3. All hydrodynamic model parameters like the large bubble gas hold-up, the small bubble gas hold-up, the mass transfer coefficients of the small and large bubbles, and the specific gas-liquid interfacial area, which are used in the design of the ALRC reactor, are measured as a function of the superficial gas velocity in a laboratory scale 2D slurry bubble column reactor. The hydrodynamic parameters were measured with no net liquid flow. The ALRC reactor is however operated with an upward superficial liquid velocity. Therefore, the hydrodynamic parameters used in the present study were taken at the 2D laboratory scale superficial gas velocity which corresponds to the difference in superficial gas velocity and the superficial liquid velocity in the ALRC reactor simulations. The validity of the above mentioned model parameters to 3D systems and to large reactor size is shown in a 2D/3D comparison study [14].

6.2.2 Process layout

The choice for an internal or external draft tube in the airlift loop reactor mainly determines the process layout and thus the modelling equations. Each of these configurations has its own benefits: while the construction of an internal draft tube is rather easy, an external draft tube has multiple advantages in the redox cycle reactor design. For this study it is necessary to create a reductive zone in the downcomer part of the reactor, therefore, the inlet of the downcomer should preferably be completely gas free. If gas is entrained in the liquid flow entering the downcomer, a large amount of oxygen will be entrained with this gas. A gas-free downcomer is easier to achieve with an external recycle stream, especially when the riser is operated in the heterogeneous regime [5]. Furthermore, the reaction from MGP towards NaMG is exothermic (-409 kJ mol^{-1}). According to calculations of Markusse et al. [11] the reactor needs an additional cooling power of 125 kW at an average reaction rate of 3.52 mmol kg_{cat}^{-1} s^{-1} and a liquid feed stream of 0.524 kg s^{-1}. With a wall heat transfer coefficient of about 200 - 400 W m^{-2} K^{-1} [20] this results in a required cooling area of about 20 m^2. This surface area available for both the riser and the downcomer if an external loop reactor is applied. However, cooling of the riser from the outside wall

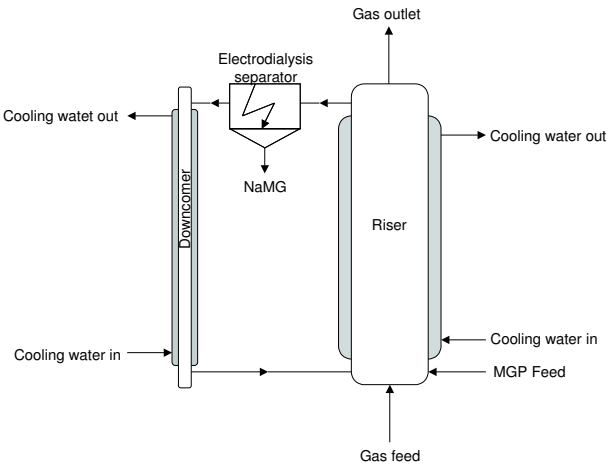

Figure 6.2: Simple process scheme of an external airlift loop reactor for the oxidation of methyl-α-D-glucopyranoside.

becomes difficult if an internal loop is applied. In the industrial size reactor design in this work, it is therefore chosen to apply an external downcomer.

Based on the above considerations, the simple process scheme for the airlift loop reactor is shown in Figure 6.2. Both riser and downcomer are tubular reactors. The riser part is aerated with the gas feed stream, entering at the bottom of the column through a gas sparger. The liquid feed stream containing the reactant MGP enters the reactor above the gas sparger and is mixed with the liquid and the catalyst particles in the riser, due to the aeration of the gas. The gas leaves the column at the top of the riser, while the liquid and the catalyst are recirculated through the electrodialysis separator and the downcomer. The electrodialysis separator separates each 1 m^3 of riser outlet stream (containing 100 mol m^{-3} NaMG and 900 mol m^{-3} MGP) in 0.1 m^3 1000 mol m^{-3} NaMG and 0.9 m^3 1000 mol m^{-3} MGP [15]. Because the reaction still continues in the downcomer at the catalyst surface, oxygen is consumed in the downcomer. Finally, after all oxygen has been transferred from the bulk liquid to the catalyst particles, the oxygen and oxide at the platinum surface are consumed, thereby regenerating the catalyst activity.

6.2.3 Model assumptions

The model equations describing the hydrodynamics in the riser and in the downcomer of the ALRC reactor are formulated and solved in conjunction with the reaction kinetics [10]. The following model assumptions need to be made:

a) The liquid phase in the riser is completely mixed.

b) Catalyst particles with a diameter of 15 μm and a density of the dry catalyst of 900 kg m^{-3} are used. The catalyst particles are evenly distributed in the liquid.

In the riser they are considered to be perfectly mixed.

c) All catalyst particles have the same residence time in the riser. The effect of differences in residence time of the particles can be neglected. Therefore, the behavior of one catalyst particle is considered to represent the average behavior of all catalyst particles in the riser.

d) In the homogeneous regime, the small bubbles in the reactor rise in plug flow.

e) In the heterogeneous regime, the small bubbles are backmixed with the liquid phase and the large bubbles are in plug flow.

f) The flow of the liquid and the catalyst particles in the downcomer is characterized as plug flow.

g) The conversion of MGP is limited to 10% to prevent side product formation.

h) The experimental data on mass transfer coefficients, specific gas-liquid interfacial area, and gas bubble hold-up as measured in a 2D slurry bubble column can be used for 3D modelling [14].

The validity of these assumptions will be verified in section 6.3.6.

6.2.4 Design approach

The purpose of the model simulations is to find the conditions at which the highest average reaction rates in both the riser and downcomer are reached. High reaction rates reduce the volume of the reactor which reduces the capital costs. All simulations are therefore compared by the MGP oxidation rate. To find the conditions at which the highest reaction rate is reached, and to find the optimal reactor configuration, the following approach is used:

- The model assumptions raised in section 6.2.3 are verified.
- Simulations are performed using the measured hydrodynamic data from a 2D laboratory scale reactor, to determine the superficial gas velocity at which the highest oxidation rate in the reactor is reached.
- The sensitivity of the simulation results is determined for the most relevant model parameters, like gas hold-up, inlet oxygen concentration, superficial slurry velocity, and mass transfer properties of the system.
- Based on the sensitivity analysis, the main design parameters are selected for which the industrial scale ALRC reactor design is made.
- A cost estimation is made for both the stirred tank process of Markusse et al. [11] and the airlift loop redox cycle design in order to compare the feasibility of both processes.

The hydrodynamic parameters as measured in a 2D slurry bubble column reactor are used in the simulations and parameter studies. As indicated in Section 6.2.3 the usage of these parameters is allowed based on a 2D-3D comparison study [14]. The model simulations and parameter sensitivity study is performed for a 3D pilot ALRC reactor (H=1.5 m, D_{riser} = 0.3 m, $D_{downcomer}$ = 0.1 m).

The 3D pilot scale simulations and the parameter sensitivity study are carried out with a catalyst concentration of 1 kg m^{-3}. The simulations of the industrial size ALRC reactor are performed with a catalyst concentration of 14 kg m^{-3}, to allow easy comparison with the reactor design of Markusse et al. [11]. A catalyst concentration of 1 kg m^{-3} in the simulations and sensitivity study is applied because the differences in calculated reaction rate for the parameter values considered, are larger and thus easier to compare. A higher catalyst concentration will only lead to a faster decrease of the oxygen concentration in the bulk liquid. This can be compensated by a smaller reaction volume and higher superficial gas and slurry velocities.

6.3 Model equations

6.3.1 Riser

The hydrodynamics of the riser part of the airlift loop reactor is modelled using the axial dispersion model for the gas phase, while the slurry phase is considered to be perfectly mixed. De Swart and Krishna [16] have shown that the gas flow in a three-phase bubble column is well described with the axial dispersion model, as long as the gas phase is divided into a dense phase, containing only small bubbles, and a phase which consists of only large bubbles. This division was made, to account for the large difference in residence time of both bubble phases. Furthermore, small bubbles exhibit a different behavior in the homogeneous regime, at low superficial gas velocities, where the small bubbles travel in plug flow through the riser, compared to the heterogeneous regime, in which the small bubbles are entrained in the liquid. The division of the gas phase in a small bubble and a large bubble phase, is even more justified based on observations from mass transfer studies, which clearly show a large difference in mass transfer characteristics between the large and small bubble phases [17]. The slurry phase is modelled as being completely mixed, which appears to be valid based on the work of De Swart and Krishna [16]. The validity of these assumptions will be addressed in Section 6.3.6.

Simulations of the behavior of the catalyst particle by Gangwal et al. [12] showed that because of the much lower oxygen concentration in the liquid compared to the concentration of MGP, oxygen is the rate limiting component. Therefore only oxygen is considered in the mass balances.

Based on these considerations, the unsteady-state mass balances for each phase in

the riser are given as follows:

- The oxygen mass balances over the large and the small bubbles read:

$$\begin{aligned}\varepsilon_{large}\frac{\partial C_{O_2,large}}{\partial t} = \varepsilon_{large}E_{large}\frac{\partial^2 C_{O_2,large}}{\partial h^2} - (U_g - U_{df})\frac{\partial C_{O_2,large}}{\partial h} \\ - k_{l,O_2,large}a_{large}\left(\frac{C_{O_2,large}}{H_{O_2}} - C_{O_2,l}\right)\end{aligned} \tag{6.2}$$

$$\begin{aligned}\varepsilon_{small}\frac{\partial C_{O_2,small}}{\partial t} = \varepsilon_{small}E_{small}\frac{\partial^2 C_{O_2,small}}{\partial h^2} - U_{df}\frac{\partial C_{O_2,small}}{\partial h} \\ - k_{l,O_2,small}a_{small}\left(\frac{C_{O_2,small}}{H_{O_2}} - C_{O_2,l}\right)\end{aligned} \tag{6.3}$$

These mass balances denote the change in oxygen concentration in respectively the large and the small bubbles as a consequence of axial dispersion (first term at the right hand side), convective transport (second term), and mass transfer to the liquid bulk (third term). The interaction between the large and small bubble phase is neglected, which appears to be valid based on considerations as addressed by De Swart and Krishna [16].

- The oxygen mass balance over the liquid phase is then:

$$\begin{aligned}\varepsilon_{liquid}\frac{\partial C_{O_2,l}}{\partial t} = \frac{U_{ss}}{H}\left(C^0_{O_2,l} - C_{O_2,l}\right) + k_{l,O_2,large}a_{large}\left(\frac{C_{O_2,g,large}}{H_{O_2}} - C_{O_2,l}\right) \\ + k_{l,O_2,small}a_{small}\left(\frac{C_{O_2,g,small}}{H_{O_2}} - C_{O_2,l}\right) \\ - k_{s,O_2}a_{part}\left(C_{O_2,l} - \frac{C_{O_2,s}}{m_{part}}\right)\end{aligned} \tag{6.4}$$

In this equation only convective transport of oxygen (first term) and mass transfer of oxygen from the large gas bubble phase to the liquid (second term), from the small gas bubble phase to the liquid (third term), and from the liquid to the catalyst particle are considered (fourth term). The flux of oxygen to the catalyst particle governed by the mass transfer coefficient k_{s,O_2}, as shown in the last term, is equal to the intra-particle diffusion and accumulation of oxygen in the catalyst particle, and the reaction of oxygen at the platinum surface in the catalyst particle. These processes are treated as described by the catalyst particle model of Gangwal et al. [12]. The change in the oxygen concentration at the catalyst particle surface $C_{O_2,s}$ is treated in the catalyst particle model as a function of the intra-particle oxygen diffusion and the oxidation of MGP. This intra-particle diffusion and reaction in series will be treated in section 6.3.3.

Table 6.1: Dimensionless groups used in the oxygen mass balances for the riser

Dimensionless group	Symbol	Definition
Time	τ	$\frac{tU_{ss}}{H}$
Axial position	ξ	$\frac{h}{H}$
Peclet number large bubbles	Pe_{large}	$\frac{U_g H}{E_{g,large}}$
Peclet number small bubbles	Pe_{small}	$\frac{U_g H}{E_{g,small}}$
Stanton number large bubbles	St_{large}	$\frac{k_{l,O_2,large} a_{large} H}{U_g}$
Stanton number small bubbles	St_{small}	$\frac{k_{l,O_2,small} a_{small} H}{U_g}$
Stanton number catalyst particles	St_{part}	$\frac{k_{s,O_2} A_{part} H}{U_g}$

Equations 6.2 till 6.4 were made dimensionless with respect to time and the reactor coordinate with the parameters listed in Table 6.1. The resulting equations are:

$$\frac{\partial C_{O_2,large}}{\partial \tau} = \frac{1}{Pe_{large}} \frac{\partial^2 C_{O_2,large}}{\partial \xi^2} - \frac{(U_g - U_{df})}{\varepsilon_{large} U_g} \frac{\partial C_{O_2,large}}{\partial \xi} - \frac{St_{large}}{\varepsilon_{large}} \left(\frac{C_{O_2,large}}{H_{O_2}} - C_{O_2,l} \right) \tag{6.5}$$

$$\frac{\partial C_{O_2,small}}{\partial \tau} = \frac{1}{Pe_{small}} \frac{\partial^2 C_{O_2,small}}{\partial \xi^2} - \frac{U_{df}}{\varepsilon_{small} U_g} \frac{\partial C_{O_2,small}}{\partial \xi} - \frac{St_{small}}{\varepsilon_{small}} \left(\frac{C_{O_2,small}}{H_{O_2}} - C_{O_2,l} \right) \tag{6.6}$$

$$\frac{\partial C_{O_2,l}}{\partial \tau} = \frac{U_{ss}}{\varepsilon_{liquid} U_g} \left(C^0_{O_2,l} - C_{O_2,l} \right) + \frac{St_{large}}{\varepsilon_{liquid}} \left(\frac{C_{O_2,large}}{H_{O_2}} - C_{O_2,l} \right) + \frac{St_{small}}{\varepsilon_{liquid}} \left(\frac{C_{O_2,small}}{H_{O_2}} - C_{O_2,l} \right) - \frac{St_{part}}{\varepsilon_{liquid}} \left(C_{O_2,l} - \frac{C_{O_2,s}}{m_{part}} \right) \tag{6.7}$$

with the initial condition for $0 \leq \xi \leq 1$:

$$C_{O_2,large} = C_{O_2,small} = C_{O_2,l} = 0 \tag{6.8}$$

The boundary conditions for the large and small bubble phases are given by the Danckwerts boundary conditions, at ξ=0:

$$\frac{\partial C_{O_2,large}}{\partial \xi} = \frac{Pe_{large}}{\varepsilon_{large}} \left(C_{O_2,large} - C^0_{O_2,large} \right) \tag{6.9}$$

$$\frac{\partial C_{O_2,small}}{\partial \xi} = \frac{Pe_{small}}{\varepsilon_{small}} \left(C_{O_2,small} - C^0_{O_2,small} \right), \tag{6.10}$$

and at ξ=1:

$$\frac{\partial C_{O_2,large}}{\partial \xi} = 0 \tag{6.11}$$

$$\frac{\partial C_{O_2,small}}{\partial \xi} = 0 \tag{6.12}$$

Equations 6.5 to 6.12 form the differential equations, the initial, and boundary conditions to calculate the oxygen concentrations in the gas and liquid phases in the riser. These differential equations are solved simultaneously with the catalyst particle model of Gangwal et al. [12], using the ODE and PDE solvers of Matlab 6.0. Both time step and grid spacing were determined by the solver.

6.3.2 Downcomer

It is assumed that the liquid and the catalyst particles in the downcomer are in plug flow. The decrease of the oxygen concentration in the bulk liquid, is caused by the flux of oxygen to the catalyst particles. The decrease in bulk oxygen concentration is obtained by multiplying the flux of oxygen with the total catalyst surface in the downcomer. The resulting change in the liquid oxygen concentration is then expressed as:

$$\frac{\partial C_{O_2,bulk}}{\partial t} = k_{s,O_2} A_{part} \left(C_{O_2,bulk} - \frac{C_{O_2,s}}{m_{part}} \right) \tag{6.13}$$

As for the riser, the change in oxygen concentration at the catalyst surface $C_{O_2,s}$ is described by the catalyst particle model of Gangwal et al. [12] which is treated in the next section.

6.3.3 Catalyst particle model

The catalyst particle model of Gangwal et al. [12] treats the changes of the oxygen concentration at the catalyst surface $C_{O_2,s}$ due to intra-particle diffusion and reaction at the platinum surface, in the particle. This model includes the kinetic model for the oxidation of MGP to NaMG of Markusse et al. [11], which calculates both the rate of MGP oxidation and the formation of surface oxygen and surface oxide at the platinum surface. The equation governing the diffusion of oxygen into the particle is given as:

$$\frac{\partial C_{O_2}}{\partial t} = \frac{1}{r^2} \frac{\partial}{\partial r} (D_e r^2 \frac{\partial C_{o_2}}{\partial r}) - R_{v,O_2} \tag{6.14}$$

with the initial condition at t=0 for ($0 \leq r \leq R_p$):

$$C_{o_2} = 0, \tag{6.15}$$

and the boundary conditions, for t > 0 at r=0:

$$\frac{\partial C_{O_2}}{\partial r} = 0, \tag{6.16}$$

and at r = R_p:

$$k_{l,O_2,s} a_{part} (C_{O_2,l} - \frac{C_{O_2,s}}{m_{part}}) = (-a_{part} D_e \frac{\partial C_{O_2,s}}{\partial r}) \tag{6.17}$$

Equation 6.17 describes the change in the oxygen concentration at the particle interface due to diffusion of oxygen from the bulk liquid to the catalyst particle and diffusion of oxygen inside the catalyst particle. Equation 6.17 is obtained from the balance at the particle interface. The equations were solved using a second order Crank Nicholson finite difference scheme, with non-equidistant grid spacing [12].

6.3.4 Reaction kinetics

The kinetic model for the oxidation of methyl-α-D-glucopyranoside of Markusse et al. [11] is used to calculate the rate of reaction R_{v,O_2} in Equation 6.14, the change in the oxygen concentration at the particle surface $C_{O_2,s}$, and the rates of catalyst deactivation and reactivation R_{v,θ_O} and $R_{v,\theta_{ox}}$. The reaction scheme in Table 6.2

*Table 6.2: Reaction scheme of the oxidation of methyl-α-D-glucoyranoside [11, 12]. * or $*_p$ behind a species denotes that the species is respectively chemisorbed or physisorbed at the catalyst surface, whereas * or $*_p$ denotes the fraction of free surface sites at the catalyst surface for respectively chemisorption and physisorption.*

Reaction	Rate equation	
$O_2 + 2* \longrightarrow 2O*$	$R_1 = k_1 C_{o_2} \theta*^2$	(R1)
$MGP + *_p \longleftrightarrow MGP*_p$	$\theta_{MGP} = K_2 C_{MGP} \theta *_p$	(R2)
$MG + *_p \longleftrightarrow MG*_p$	$\theta_{MG} = K_3 C_{MG} \theta *_p$	(R3)
$O* + * \longrightarrow Ox*$	$R_4 = k_4 \theta_o (1 - \theta_{ox})$	(R4)
$MGP*_p + * \longrightarrow$	$R_5 = k_5 \theta_{MGP} \theta * \exp\left(\frac{EF}{RT}\right)$	(R5)
$MAGP*_p + 2H^+ + 2e^- + *$		
$MAGP*_p + H_2O + * \longrightarrow$	fast	(R6)
$MG*_p + 2H^+ + 2e^- + *$		
$Ox* + H^+ + 2e^- + * \longrightarrow OH^- + 2*$	$R_6 = k_6 C_{H^+} \theta_{ox} \theta * \exp\left(\frac{-EF}{RT}\right)$	(R7)
$O* + H^+ + 2e^- \longrightarrow OH^- + *$	$R_7 = k_7 C_{H^+} \theta_o \exp\left(\frac{-EF}{RT}\right)$	(R8)

shows the reaction steps at the catalyst surface. Oxygen is adsorbed in reaction step R1. Both the reactant MGP and the product NaMG are physisorbed at the platinum surface in reaction steps R2 and R3. It is assumed that surface sites on which species are chemisorbed are still available for physisorption of MGP and NaMG. The only

reaction leading to the oxide at the platinum surface, and thus to catalyst deactivation, is step R4. MGP is oxidized via two steps (R5 and R6) of which R6 is much faster compared to R5. In reaction steps R5 and R6 electrons are produced. These electrons are consumed in reactions R7 and R8, in which oxygen and oxide are consumed from the catalyst surface. The formation and consumption of electrons at the catalyst surface give rise to a change in the potential E of the catalyst. Markusse et al. [11] showed that this potential is of great influence on the rate of reaction and the catalyst deactivation and reactivation, because it influences reaction steps R5, R7 and R8 exponentially. The potential of the catalyst can be obtained from the electron balance in the catalyst particle. The carbon particle is assumed to be fully conductive, thus the potential is equal throughout the catalyst particle. The balance over the electrons inside the catalyst particle results in the catalyst potential given as [11]:

$$E = \frac{RT}{2F} \ln \frac{C_{H^+} < k_7\theta_O + k_6\theta_{ox}\theta_* >}{< 2k_5\theta_{MGP}\theta_* >} \tag{6.18}$$

The brackets indicate that the terms are averaged over the catalyst particle.

The rate parameters of the reaction steps in Table 6.2, were fitted from experimental data obtained in a stirred tank reactor, using an egg-shell distributed platinum catalyst on a graphite support, at a temperature of 323 K at atmospheric pressure [11]. The rate parameters of the reactions are presented in Table 6.3.

Table 6.3: List of values of kinetic parameters, obtained in a 1 liter stirred tank reactor using an egg-shell distributed platinum catalyst at T = 323K and p = 1 atm [11].

Symbol	Description	Value
k_1 $[m^3 mol^{-1} s^{-1}]$	oxygen adsorption rate constant	6.5×10^3
K_2 $[m^3 mol^{-1} s^{-1}]$	MGP adsorption constant	1.26×10^{-2}
K_3 $[m^3 mol^{-1} s^{-1}]$	MG adsorption constant	1.77×10^{-1}
k_4 $[s^{-1}]$	oxide formation rate constant	1.20×10^{-3}
k_5 $[s^{-1}]$	MGP dehydrogenation rate constant	3.93×10^{-6}
k_6 $[m^3 mol^{-1} s^{-1}]$	oxide reduction rate constant	1.61×10^{9}
k_7 $[m^3 mol^{-1} s^{-1}]$	oxygen reduction rate constant	3.53×10^{10}

Following the reaction scheme in Table 6.2, the rates of oxygen consumption (R_{v,O_2}), surface oxygen coverage formation (R_{v,θ_O}), and oxide formation ($R_{v,\theta_{ox}}$) can be determined, which are given by:

$$R_{v,O_2} = -C_{cat} L_t k_1 C_{O_2,s} \theta_*^2 \tag{6.19}$$

$$R_{v,\theta_O} = 2k_1 C_{O_2,s} \theta_O^2 - k_4 \theta_o (1 - \theta_{ox}) - k_7 \theta_o C_{H^+} \exp\left(\frac{-EF}{RT}\right) \tag{6.20}$$

$$R_{v,\theta_{ox}} = k_4\theta_o(1-\theta_{ox}) - k_6\theta_{ox}\theta_* C_{H^+} \exp\left(\frac{-EF}{RT}\right). \tag{6.21}$$

The resulting kinetic equations were solved simultaneously with the catalyst particle model equations and the hydrodynamic equations of riser and downcomer.

6.3.5 Numerical procedure

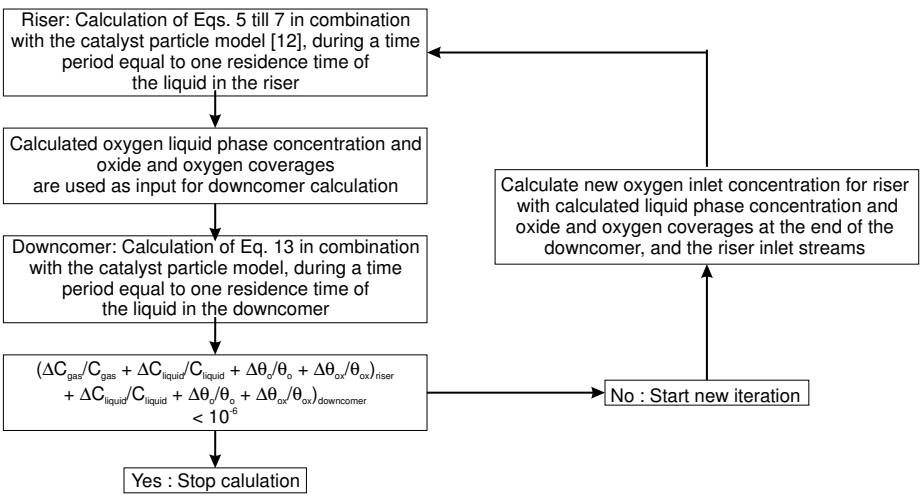

Figure 6.3: Iterative procedure for solving the hydrodynamic and kinetic equations of the riser and the downcomer coupled with the catalyst particle model of Gangwal et al. [12].

As can be seen in Figure 6.3, the solution of Equations 6.5 to 6.13 is an iterative process in which the equations are solved in series. The results are the time dependent concentrations and surface coverages in the liquid and in the catalyst particles. Because the catalyst particles and the liquid travel through the reactor in cycles, this time dependent solution will converge to the steady-state solution after a sufficient number of iterations. Therefore, after each iteration the present solution is compared with the previous solution. The calculation is stopped if the relative deviations of all concentrations and surface coverages between two iterations is smaller than 10^{-6}. This criterion assured that the change in all concentrations and surface coverages between the present and the previous iteration was less than 0.1%.

6.3.6 Verification of model assumptions

A useful interpretation of the simulations can only be performed if the model assumptions raised in section 6.2.3 are correct. The verification of the assumptions for the riser and downcomer is treated below. The corresponding assumptions are denoted by the letters as given in section 6.2.3.

Riser

Assumption a) The liquid phase in the riser is assumed to be perfectly mixed. This assumption is verified by comparing the simulation results of the simulations with a perfectly mixed liquid phase with simulations assuming an axial dispersion model for the liquid phase. Due to computational limitations, in this case, the kinetic model without intra-particle diffusion limitation was used. Figure 6.4 shows the oxygen concentration in the liquid as a function of the reactor height, when applying the axial dispersion model for the liquid phase in a 6.0 m high reactor with an inner diameter of 1.5 m. The dimensions are chosen based on the reactor volume of the stirred tank process of Markusse et al. [11]. The deviation along the reactor height in the liquid phase oxygen concentration is less then 0.4% . The assumption that the liquid phase is perfectly mixed is justified.

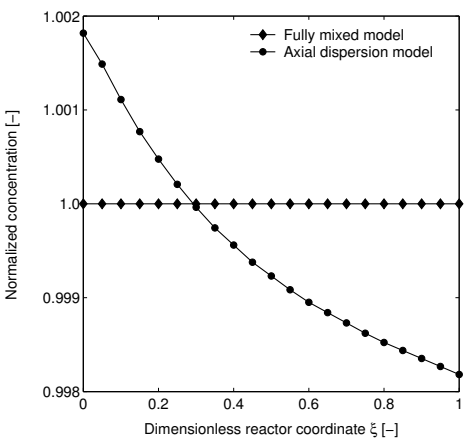

Figure 6.4: Normalized oxygen concentration profile in the liquid, calculated with the axial dispersion model compared to the oxygen concentration profile calculated with the fully mixed model, as a function of the dimensionless reactor coordinate.

Assumption b) The assumption that the catalyst particles are perfectly mixed and evenly distributed in the riser is addressed in the modelling study of De Swart and Krishna [16]. The axial dispersion of their catalyst (density 1300 kg m^{-3}, particle size 5 μm) is modelled in a reactor of 30 meters height with a diameter of 6 meters, incorporating the settling velocity of the particles in the liquid. The local fraction of the catalyst varied from the bottom to the top of the reactor with less then 1%. Although the catalyst particles used in our study are slightly larger and have a somewhat lower density (density of the dry catalyst 900 kg m^{-3}, particle size 15 μm), the settling velocity of the catalyst particles is hardly affected.

Assumption c) The assumption that the effect of the residence time distribution of the catalyst particles in the riser can be neglected, is verified by calculating the average rate of reaction. First, the rate of reaction is calculated for a single particle, for several liquid bulk oxygen concentrations, with a specific residence time. Secondly, the average rate of reaction is then calculated assuming the residence time distribution for all particles in the riser:

$$\overline{R} = \int_0^\infty E(t) R_{single}(t) dt \tag{6.22}$$

with $\overline{R}$ the average reaction rate for all particles, τ the average residence time of a particle in the riser, as given in Table 6.1, $R_{single}(t)$ the reaction rate of a single particle as a function of time, and E(t) the residence time distribution for the particles in a CSTR given by E(t) = $e^{-\frac{t}{\tau}}/\tau$. For several oxygen bulk concentrations (0 - 0.3 mol m^{-3}) and particle residence times (20 - 240 seconds), the average reaction rate for a single particle $R_{single}(\tau)$, is 3-5 % higher than the average reaction rate for all particles in the riser ($\overline{R}$). This deviation is found to be acceptable, therefore the average rate of reaction is taken as $R_{single}(\tau)$.

Assumptions d) and e) The assumptions for the flow behavior of the large and small bubbles in the riser, have been extensively verified by De Swart and Krishna [16]. They concluded that for small reactors with a height of 6 meter, and for large reactors with a height of 30 meter, the axial dispersion model was valid for the description of the large and small bubble phases with different axial dispersion coefficients for the large and small bubble phases. To express the difference in behavior of the small bubbles in the homogeneous regime (plug flow) and the heterogeneous regime (perfectly mixed), the dispersion coefficient of the small bubbles is calculated with the correlation of Deckwer and Schumpe [18] as a function of the superficial gas velocity: $E_{small} = 0.768 U_{g0}^{0.32} D_T^{1.34}$. The dispersion coefficient of the large bubbles is assumed to be constant and is equal to E_{large} = 100. De Swart and Krishna [16] showed that with these dispersion coefficients the flow behavior of the small and the large bubbles is described according to assumptions d and e.

Downcomer

Assumption f) The only assumption concerning the downcomer states that the flow of liquid and particles is in plug flow. Furthermore, the residence time of the liquid and the particles should be long enough to allow the ongoing reaction to consume all oxygen from the liquid and from the catalyst surface. A perfectly mixed downcomer is less suitable for this purpose because in that case the constant feed of oxygen entering at the top of the downcomer would be immediately mixed into the liquid in the downcomer. An oxygen free environment is in that case difficult to establish. The flow in the downcomer can be considered as plug flow when $L_{down}/D_{down} > 20$. The length and diameter of the downcomer need to be chosen as such to allow a long enough residence time for the catalyst particles to become fully reactivated. In case of an external airlift loop reactor, this can always be achieved without affecting the configuration of the riser or its performance.

6.4 Hydrodynamic parameters

As mentioned in the previous sections, the hydrodynamic parameters in the model are obtained from experiments in a 2D laboratory reactor (H = 2.0 m, D = 0.3 m, depth = 0.015 m). A recent study [14] clearly shows that this data can be applied in

the modelling of 3D bubble columns. Most of the mass transfer and gas hold-up experiments as shown in Chapter 3 and 5 are performed at lower carbon concentrations then 14 kg m^{-3} as used for the model simulations. However, additional experiments with carbon concentrations of 10 and 20 kg m^{-3}, like some of the mass transfer experiments shown in Figure 5.2, showed no deviation in the measured parameters as presented in the previous Chapters. The large and small bubble gas hold-ups and the specific gas liquid surface areas of the large and small bubbles were determined from high speed video-imaging and are shown in Figures 6.5a and b. Figure 6.5a

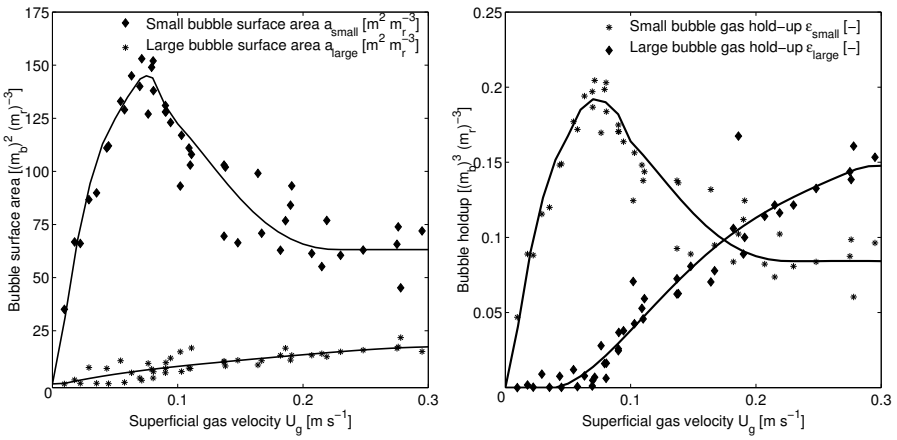

(a) Bubble gas hold-up (b) Bubble surface area

Figure 6.5: Measured data from a 2D slurry bubble column reactor of fractions of large and small bubbles (a), and the specific gas liquid surface areas (b), obtained at different superficial gas velocities. The lines are drawn to guide the eye, and are based on a polynomal fit of the data.

shows that the specific gas-liquid interfacial areas for the small and large bubbles vary with increasing superficial gas velocity. It can also be seen that the contribution of the large bubbles to the gas-liquid surface area is very small, because of the relatively low gas hold-up of the large bubbles (Figure 6.5b). It can be seen from both figures that both the large and small bubble surface areas and the small bubble gas hold-up become constant at superficial gas velocities above 0.3 m s^{-1}. The values at higher superficial gas velocities are therefore assumed to be the same as those at the superficial gas velocity of 0.3 m s^{-1}. The mass transfer coefficients $k_{l,O_2,large}$ and $k_{l,O_2,small}$ are obtained from previous work in the 2D bubble column [17] and are equal to respectively 8.0 10^{-3} m s^{-1} and 5.3 10^{-4} m s^{-1}. The liquid-to-solid mass transfer coefficient is taken from Gangwal et al. [12] and equals to k_{s,O_2} = 4.0 10^{-4} m s^{-1} for catalyst particles with a diameter of 15 μm.

6.5 3D pilot ALRC reactor

6.5.1 Optimal superficial gas velocity U_g

A 3D pilot ALRC reactor is modelled to determine at which superficial gas velocity the highest rate of reaction is reached. The rates of the MGP oxidation obtained from these simulations are shown in Figure 6.6. Figure 6.6 shows that a large difference exists between the rates of reaction in the homogeneous regime, at gas velocities below 0.06 m s^{-1}, and in the heterogeneous regime, at superficial gas velocities above 0.1 m s^{-1}. The rate of reaction hardly changes with increasing superficial gas velocity in the heterogeneous regime. The large difference in simulated reaction rates between the homogeneous and heterogeneous regimes is because of the difference in the bubble size distributions in both regimes. Although the specific gas-liquid surface area in the homogeneous regime is large, the transfer of oxygen towards the liquid is low, because of the low mass transfer coefficient of the small bubbles. At higher superficial gas velocities, large bubbles start to develop, which have a much lower specific gas-liquid surface area, but a much higher mass transfer coefficient. Therefore, the total supply of oxygen from the gas phase towards the liquid phase is much higher in the heterogeneous regime, and thus favors the oxidation of MGP. At superficial gas velocities above 0.2 m s^{-1}, both the bubble gas hold-up and the specific gas-liquid interfacial area do not change significantly as shown in Figures 6.5a and b. This results in only a minor increase in the rate of reaction with increasing superficial gas velocity. From these simulations it is concluded that the ALRC reactor is best operated at superficial gas velocities above 0.1 m s^{-1}.

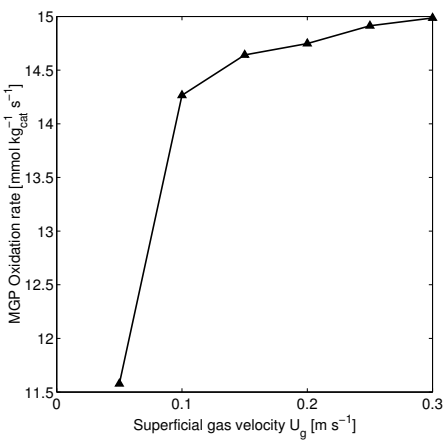

Figure 6.6: Simulated rate of MGP oxidation as a function of the superficial gas velocity for a 3D pilot scale ALRC reactor (H = 1.5 m, D_{riser} = 0.3 m, $D_{downcomer}$ = 0.1 m).

6.5.2 Model sensitivity analysis

To explore the sensitivity of the simulation results with respect to the model parameters, simulations are performed with the model parameters in the ranges listed in Table 6.4. The default value of each model parameter denotes the value of each parameter as used in the simulations, in which one of the other parameters is changed. The gas hold-up of the large bubbles does not affect the rate of reaction significantly

Table 6.4: Parameters used for the model sensitivity analysis. The default value of each model parameter denotes the value as used in the simulations in which one of the other parameters was changed. All simulations were carried out for the 3D pilot scale ALRC reactor.

Parameter	Range	Default
Oxygen inlet partial pressure $P^*_{O_2,g}$ [bar]	0.1 - 1.0	0.2
Superficial gas velocity U_g [m s^{-1}]	0.07 - 0.15	0.1
Large bubble hold-up ε_{large} [-]	0.1 - 0.2	0.15
Small bubble hold-up $\varepsilon_{small}[-]$	0.01 - 0.14	0.09
Stanton number large bubbles St_{large} [-]	0.3 - 3	1.5
Stanton number small bubbles St_{small} [-]	0.045 - 0.45	0.225
Superficial liquid velocity U_{ss} [m s^{-1}]	0.01 - 0.2	0.1

and is therefore not shown. The results of the sensitivity analysis are shown in Figures 6.7a-f. It is found that the influence of the model parameters on the rate of reaction is, except for the inlet gas phase oxygen concentration and the slurry velocity, limited. Changes in the Stanton numbers and the hold-ups of the small and large bubbles result only in slight changes of the oxygen liquid bulk concentration and in the rate of reaction. Based on these considerations, the oxygen inlet partial pressure and the velocity of the liquid in the riser are the main parameters which determine the reactor performance, when the ALRC reactor is operated at a superficial gas velocity above 0.1 m s^{-1} as determined in the previous paragraph.

6.6 Industrial size ALRC reactor design

6.6.1 Design considerations

Starting points for the design of the industrial size ALRC reactor are:

- The production capacity is 1.27 10^7 mole of NaMG per year.
- In view of economic considerations the reactor design is made using air as oxygen supply in the gas phase.
- The gas velocity is chosen in the heterogeneous regime above superficial gas velocities of 0.1 m s^{-1}.

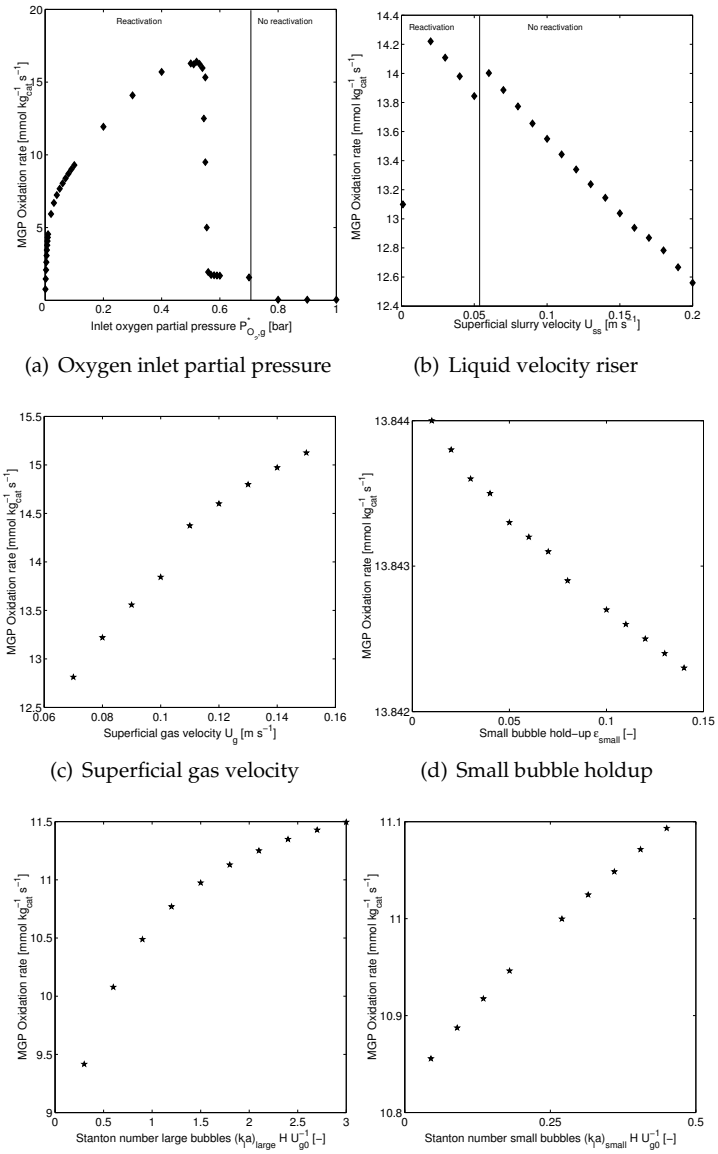

(a) Oxygen inlet partial pressure (b) Liquid velocity riser

(c) Superficial gas velocity (d) Small bubble holdup

(e) Stanton number large bubbles (f) Stanton number small bubbles

Figure 6.7: Sensitivity of the rate of MGP oxidation, with respect to several model parameters. Simulations are based on the 3D pilot scale ALRC reactor (H = 1.5 m, D_{riser} = 0.3 m, $D_{downcomer}$ = 0.1 m). The lines in Figures a and b are drawn to indicate at which point the catalyst surface is not fully reactivated in the downcomer. In all other cases the catalyst is completely reactivated. Note the different scales on the y-axis in all figures. For the model simulation in Figures (e) and (f) the values of small and large bubble hold-up according to Figures 6.5a and b are used, different from their default values.

- The superficial gas velocity and the superficial slurry velocity in the riser are chosen as such in order to reach the highest reaction rate with air as feed gas.
- The downcomer needs to be long enough to assure full catalyst reactivation.
- The catalyst concentration is 14 kg m^{-3}. Section 6.2.1

6.6.2 Reactor design

Taking into account the design considerations of the previous paragraph, simulations were performed to determine the size of the industrial scale reactor for the oxidation of MGP. The volume of the reactor is calculated based on the average reaction rate of 8.14 mmol MGP kg_{cat}^{-1} s^{-1}, and the production rate of 1.27 10^7 mol NaMG per year. The riser height-to-diameter ratio is estimated from the correlation of Hwang et al. [19], based on the values for the slurry velocity (U_{ss}) and superficial gas velocity (U_g) which resulted in the highest reaction rate. The oxide and oxygen surface coverages at the catalyst surface in the riser and downcomer as a function of the residence time of a catalyst particle are shown in Figure 6.8. These figures show the concentration-time profiles of two successive passages through the riser and downcomer at steady state conditions. The oxygen liquid concentration and the oxygen coverage in the riser reach a steady state quite fast, while the oxide coverage at the platinum surface (the catalyst deactivation) shown in Figure 6.8d increases steadily. While entering the downcomer, the oxygen from the liquid and the platinum surface is consumed fast whereafter the oxide from the catalyst is consumed, resulting in a fully reactivated catalyst. The rate of reaction in the downcomer (Figure 6.8b) drops because of the oxygen depletion in the downcomer. However, it increases again when the catalyst particles enter the riser.

The simulated average reaction rate of 8.14 mmol kg_{cat}^{-1} s^{-1}, is much higher than the

Table 6.5: Design parameters of the industrial size ALRC reactor for the oxidation of MGP to NaMG

Reactor height H [m]	7.0
Diameter riser D_{riser} [m]	1.25
Diameter downcomer D_{down} [m]	0.25
Superficial gas velocity U_g [m s^{-1}]	0.5
Superficial slurry velocity U_{ss} [m s^{-1}]	0.3
Gas hold-up large bubbles ε_{large} [-]	0.15
Gas hold-up small bubbles ε_{small} [-]	0.09
Liquid hold-up ε_{liquid} [-]	0.76
Stanton number large bubbles St_{large} [-]	2.28
Stanton number small bubbles St_{small} [-]	0.384

simulated reaction rate in the process design of Markusse et al. [11], which is equal to 3.52 mmol kg_{cat}^{-1} s^{-1}. This shows that a higher catalyst activity is maintained in both the downcomer and the riser in this industrial size ALRC reactor design. The higher activity of the catalyst is accomplished by maintaining a much lower oxygen concentration in the liquid, which is favorable for the activity of the catalyst. Moreover, a low liquid bulk oxygen concentration favors fast reactivation of the catalyst. The redox cycle of Markusse et al. [11] consists of an oxidation period of 100 seconds and a reduction period of 54 seconds. In our case, fast recycling of the liquid phase results in an oxidation period of 25 seconds and a reduction period of only 4-8 seconds. The fast reactivation of the catalyst in the downcomer might get disturbed when gas is entrained in the liquid in the downcomer. In this case, the length of the downcomer should be increased to allow more time for the reaction to consume all oxygen, before regenerating the catalyst surface. However, when a complete gas free downcomer is used, the reactor volume in the industrial size ALRC reactor ($V_r \sim 9$ m^3) is considerably smaller compared to the reactor volume of the stirred tank reactor of Markusse et al. [11] ($V_r \sim 20$ m^3). This is favorable in view of the investment costs.

6.6.3 Cost comparison

The simulations of the industrial size ALRC reactor clearly show that the concept of a redox cycle reactor is capable of maintaining a high catalyst activity during alcohol oxidation reactions with a much smaller reactor volume compared to the stirred tank process of Markusse et al. [11]. The feasibility of the ALRC reactor compared to the stirred tank reactor process can only properly be demonstrated when the operating costs and capital investment costs of both processes are compared. Some of the capital investment costs are assumed to be equal, because both processes are simulated with the same MGP conversion of 10%, the same yearly production rate of 1.27 10^7 mole per year, and at the same reactor temperature and operating pressure. Furthermore, it is assumed that the complexity and the construction costs are equal for both processes. Therefore, these costs are not included in the cost comparison and only components which are clearly different in size or capacity are included in the cost comparison. This results in a cost comparison that includes the reactor vessels, a gas feed compressor (capacity for the airlift loop reactor is much larger because of pressure drop over the riser and the large volumetric gas feed), and a liquid circulation pump for the recycling of the liquid in the stirred tank process. Because the same amounts of catalyst and reactants are used, only the gas feed streams are included in the comparison of the operating costs.

A cost comparison was made including the above mentioned components based on the 2002 investment prices of the Dutch Association of Cost Engineers. Operating costs were estimated based on the prices for industrial supply of air, oxygen and nitrogen as mentioned on the website of the IChemE Education subject group,

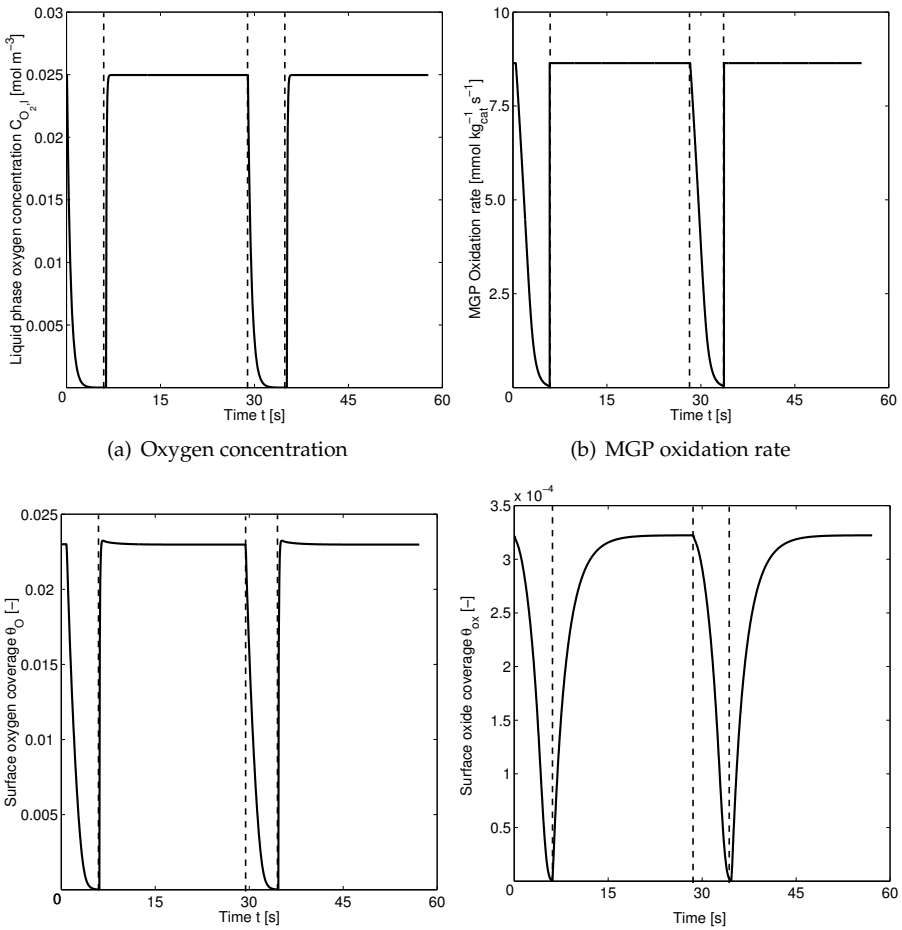

(a) Oxygen concentration

(b) MGP oxidation rate

(c) Oxygen coverage

(d) Oxide coverage

Figure 6.8: Simulation results of the industrial size ALRC reactor (see Table 6.5): a) Oxygen concentration in the liquid phase, b) MGP oxidation rate, c) Oxygen coverage of the Pt surface, d) Oxide coverage. Each figure shows two cycles, starting with the downcomer.

Sheffield University, UK[1]. The cost comparison is given in Table 6.6.

Table 6.6: Comparison of the investment and yearly operating costs for the industrial scale airlift loop process and the stirred tank process of Markusse et al. [11]. Prices are based on the separate components according to the capacity and size of the equipment. All prices in kEuro, excluding VAT.

Item	Airlift process	Stirred tank process
Investment costs		
Reactor	49	87
Downcomer	25	-
Gas feed compressor	68	25
Agitator	-	Included in reactor
Liquid recirculation pump	-	6
Operating costs per year (quantities in m^3 per year)		
Compressed Air	101 ($13.6.10^6$)	-
Oxygen	-	115 ($0.74.10^6$)
Nitrogen	-	62 ($0.40.10^6$)

It shows that the investment costs for the stirred tank reactor process are 25.000 Euros less compared with the ALRC reactor. The main difference is the investment in the gas compressor, which needs to be of higher capacity for the ALRC reactor, to overcome the static pressure of the slurry in the reactor.

The operating costs for the ALRC reactor per year are 76.000 Euros less, compared with the stirred tank process, which uses air and nitrogen. The usage of feed streams with a higher oxygen partial pressure in the airlift loop process might increase the rate of reaction as shown in Figure 6.7a up to 16.0 mmol kg_{cat}^{-1} s^{-1}. This will lead to a reduction of the riser volume of 50%. Higher oxygen partial pressures can be achieved by mixing pure oxygen into the air feed stream. However, as shown in Table 6.7, this would lead to only a minor reduction of the reactor volume and capital costs, while considerably increasing the costs for reactor operation.

[1]http://ed.icheme.org/costs.html

Table 6.7: Comparison of the investment and yearly operating costs for the industrial ALRC reactor operated at an average rate of reaction of 8.14 mmol kg_{cat}^{-1} s^{-1} (Air process) and 16.0 mmol kg_{cat}^{-1} s^{-1} (Oxygen process); prices in kEuro, excluding VAT.

	Air process	Oxygen process
Investment costs reactor	74	55
Operating costs gases	101	584

6.7 Concluding remarks

An industrial size airlift loop redox cycle reactor (ALRC) reactor has been designed based on kinetic, hydrodynamic, and economic considerations. This evaluation has lead to the following conclusions:

- A sensitivity study demonstrated that the oxygen liquid bulk concentration is one of the main parameters affecting the reactor performance. The oxygen liquid bulk concentration is most affected by the superficial gas velocity and the superficial slurry velocity. Other parameters, like the large bubble and small bubble hold-up and the Stanton numbers of the large and small bubbles only affect the oxygen liquid bulk concentration and the rate of reaction to a limited extent. This means that in the ALRC reactor design, the main attention is to keep the oxygen bulk concentration low, while keeping the supply of oxygen from the gas phase to the liquid high enough to prevent total oxygen depletion in the bulk liquid.

- A low oxygen bulk concentration is beneficial for a high activity of the catalyst as well as for the fast reactivation of the catalyst. Markusse et al. [11] showed that most of the time needed for reactivation of the catalyst is used for the consumption of oxygen from the liquid. A low oxygen concentration in the bulk liquid is therefore favorable, allowing a shorter residence time in the downcomer.

- The main difference between the redox cycle airlift loop reactor design and the stirred tank reactor design is the fact that Markusse et al. [11] do not consider reactivation of the catalyst in the product separation recycle stream. Further-

more, Markusse et al. [11] did not include the intra-particle diffusion limitation of oxygen. If this is included, this will probably lead to a similar rate of reaction as obtained for the airlift loop reactor design. The stirred tank reactor could then be operated with air, without the necessity of switching of the gas feed streams. In this case, it is expected that the stirred tank reactor and the airlift loop reactor will not differ significantly in both investment and operating costs.

Table 6.8: List of symbols

Greek and Roman symbols				
ε_{large}	Gas hold-up large bubble phase	[-]	-	
ε_{small}	Gas hold-up small bubble phase	[-]	-	
ε_{liquid}	Gas hold-up liquid phase	[-]	-	
θ_*	Fraction of uncovered platinum sites	[-]		
θ_O	Fraction of platinum sites covered with oxygen	[-]		
θ_{ox}	Fraction of platinum sites covered with oxide	[-]		
θ_{MGP}	Fraction of platinum sites covered with physisorbed MGP	[-]		
Other symbols				
$C_{O_2,large}$	Oxygen concentration large bubbles	[mol m_l^{-3}]	-	
$C_{O_2,small}$	Oxygen concentration small bubbles	[mol m_l^{-3}]	-	
$C_{O_2,l}$	Oxygen concentration liquid	[mol m_l^{-3}]	-	
$C_{O_2,s}$	Oxygen concentration at catalyst surface	[mol m_l^{-3}]	-	
$C_{O_2,f}$	Oxygen concentration in film around catalyst	[mol m_l^{-3}]	-	
$C^0_{O_2,l}$	Inlet oxygen concentration in the slurry	[mol m_l^{-3}]	-	
C_{cat}	Catalyst concentration	[kg m_l^{-3}]	-	
h	Reactor space coordinate	[m]	-	
t	Time	[s]	-	
E_{large}	Axial dispersion coefficient large bubbles Pe_{large}=100	[m_r^2 s^{-1}]	-	[16]

E_{small}	Axial dispersion coefficient small bubbles $0.768 U_g^{-0.32} D_T^{1.34}$	[m_r^2 s^{-1}]	-	[16]
U_g	Superficial gas velocity	[m s^{-1}]	-	
U_{df}	Superficial gas velocity small bubbles	[m s^{-1}]	-	
U_{ss}	Superficial slurry velocity	[m s^{-1}]	-	
$k_{l,O_2,large}$	Mass transfer coefficient large bubble phase at 323 K	[m s^{-1}]	$8.0 \cdot 10^{-3}$	[17]
$k_{l,O_2,small}$	Mass transfer coefficient small bubble phase at 323 K	[m s^{-1}]	$5.4 \cdot 10^{-4}$	[17]
k_{s,O_2}	Mass transfer coefficient liquid to particle at 323 K	[m s^{-1}]	$4.0 \cdot 10^{-4}$	[12]
a_{large}	Specific surface area large bubbles per m^3 expanded bed volume	[m^2 m_r^{-3}]	-	
a_{small}	Specific surface area small bubbles per m^3 expanded bed volume	[m^2 m_r^{-3}]	-	
a_{part}	Specific surface area of one particle	[m^2]	-	
A_{part}	Specific surface area of all particles er m^3 expanded bed volume	[m^2 m_r^{-3}]	-	
H_{O_2}	Henry coefficient of oxygen in water (323K, 1atm)	[m^3 mol^{-1}]	41.09	
m_{part}	Partition coefficient particle	[-]	1	[12]
Pe_{large}	Peclet number large bubbles $\frac{U_g H}{E_{g,large}}$	[-]	100	[16]
Pe_{small}	Peclet number small bubbles $\frac{U_g H}{E_{g,small}}$	[-]	-	[16]
St_{large}	Stanton number large bubbles $\frac{k_{l,O_2,large} a_{large} H}{U_g}$	[-]	-	
St_{small}	Stanton number small bubbles $\frac{k_{l,O_2,small} a_{small} H}{U_g}$	[-]	-	
St_{part}	Stanton number particles	[-] $\frac{k_{s,O_2} A_{part} H}{U_g}$	-	
D_e	Oxygen diffusivity in water (293K, 1atm)	[m^2 s^{-1}]	$3 \cdot 10^{-9}$	[20]
r	Spatial particle coordinate	[m]	-	-
R_{v,O_2}	Volumetric reaction rate of oxygen	[mol m^{-3} s^{-1}]	-	-
R_{v,θ_O}	Volumetric reaction rate of surface oxygen	[s^{-1}]	-	-
$R_{v,\theta_{ox}}$	Volumetric reaction rate of subsurface oxygen	[s^{-1}]	-	-

V_f	Volume of the liquid film around a particle	[m_l^3]	-	
L_t	Weight specific catalyst surface	[mol kg_{cat}^{-1}]	0.073	[11]
k_i	Reaction rate coeffiecient	[various]		[11]
E	Catalyst potential	[V]	-	[11]
F	Faraday's constant	[C mol^{-1}]	-	[20]
R	Gas constant	[J mol^{-1} K^{-1}]	8.314	[20]
T	Temperature	[K]	323	
R_i	Reaction rate of species i	[various]	-	
C_{H^+}	Proton concentration	[mol m^{-3}]	$1{\cdot}10^{-5}$	

Bibliography

[1] Al Masry, W.A., and Abasaeed, A.E., On the scale-up of external loop airlift reactors: Newtonian systems. *Chem. Eng. Sci.*, 53(24) 4085-4094, 1998.

[2] Heijnen, J.J., Hols, J., Lans, R.G.J.M. van der, Leeuwen, H.L.J.M. van, Mulder, A., and Weltevrede, R., A simple hydrodynamic model for the liquid circulation velocity in a full-scale 2-phase and 3-phase internal airlift reactor operating in the gas recirculation regime. *Chem. Eng Sci.*, 52(15), 2527-2540, 1997.

[3] Chisti, Y., and Jauregui-Haza, U.J., Oxygen transfer and mixing in mechanically agitated airlift bioreactors. *Biochem. Eng. J.*, 10(2), 143-153, 2002.

[4] Benthum, W.A.J. van, Hoogen, J.H.A. van den, Lans, R.G.J.M. van der, Loosdrecht, M.C. M. van, and Heijnen, J.J., The biofilm airlift suspension extension reactor. Part I: Design and two-phase hydrodynamics. *Chem. Eng. Sci.*, 54(12), 1909-1924, 1999.

[5] Oey, R.S., Mudde, R.F., Portela, L.M., and Akker, H.E.A. van den, Simulation of a slurry airlift using a two-fluid model. *Chem. Eng. Sci.*, 56(2), 673-681, 2001.

[6] Abashar, M.E., Narsingh, U., Rouillard, A.E., and Judd, R., Hydrodynamic flow regimes, gas holdup, and liquid circulation in airlift reactors. *Ind. Eng Chem. Res.*, 37(4), 1251-1259, 1998.

[7] Camarasa, E., Meleiro, L.A.C., Carvalho, E., Domingues, A., Maciel Filho, R., Wild, G., Poncin, S., Midoux, N., and Bouillard, J., A complete model for oxidation air-lift reactors. *Comput. Chem. Eng.*, 25(4-6), 577-584, 2001.

[8] Vial, C., Poncin, S., Wild, G., and Midoux, N., A simple method for regime identification and flow characterisation in bubble columns and airlift reactors. *Chem. Eng. Process.*, 40(2), 135-151, 2001.

[9] Rubio, F.C., Garcia, J.L., Molina, E. and Chisti, Y., Steady-state axial profiles of dissolved-oxygen in tall bubble- column bioreactors. *Chem. Eng. Sci.*, 54(11), 1711-1723, 1999.

[10] Markusse, A.P., Kuster, B.F.M., and Schouten, J.C., Platinum catalysed aqueous alcohol oxidation: experimental studies and reaction model discrimination. *J. Mol. Cat. A*, 158(1), 215-222, 2000.

[11] Markusse, A.P., Kuster, B.F.M., and Schouten, J.C., Platinum catalyzed aqueous methyl-α-D-glucopyranoside oxidation in a multi-phase redox-cycle reactor. *Cat. Today*, 66(2-4), 191-197, 2001.

[12] Gangwal, V.R., Wachem, B.G.M. van, Kuster, B.F.M., and Schouten, J.C., Platinum catalysed aqueous alcohol oxidation: model-based investigation of reaction conditions and catalyst design. *Chem. Eng. Sci.*, in press, 2002.

[13] Schuurman, Y., Kuster, B.F.M., Wiele, K. van der, and Marin, G.B., The selective oxidation of methyl-α-D-glucoside on a carbon supported platinum catalyst. *Stud. Surf. Sci. Catal.*, 72, 43-55, 1992.

[14] Kluytmans, J.H.J., Wachem, B.G.M. van, Kuster, B.F.M., Krishna, R. and Schouten, J.C., 2D slurry bubble column hydrodynamic phenomena clarified with a 3D gas-liquid model. *Accepted for presentation at the GLS 6 conference, Vancouver, Canada, to be published in Can. J. Chem. Eng.*, 2003.

[15] Vleeming, J.H., Bruijn, F.A., Kuster, B.F.M., and Marin, G.B., Deactivation of carbon-supported platinum catalysts during oxidations in aqueous media. *Stud. Surf. Sci. Catal.*, 88, 467-474, 1994.

[16] Swart, J.W.A. de, and Krishna, R., Simulation of the transient and steady state behaviour of a bubble column slurry reactor for Fischer-Tropsch synthesis. *Chem. Eng. and Process.*, 41(1), 35-47, 2001.

[17] Kluytmans, J.H.J., Wachem, B.G.M. van, Kuster, B.F.M., and Schouten, J.C., Mass transfer in stirred and sparged reactors: Influence of carbon particles and electrolyte. *Chem. Eng. Sci.*, Sumbitted for publication.

[18] Deckwer, W.-D. and Schumpe, A., Improved tools for bubble column reactor design and scale-up. *Chem. Eng. Sci.*, 48(5), 889-911, 1993.

[19] Hwang, S.J., and Cheng, Y.L., Gas holdup and liquid velocity in 3-phase internal-loop airlift reactors. *Chem. Eng. Sci.*, 52(21-22), 3949-3960, 1997.

[20] Perry, R.H., Green, D., and Maloney, J.O., *Perry's Chemical Engineers' Handbook*. McGraw-Hill, New York, 87^{th} edition, 1997.

7

Conclusions and outlook

The selective oxidation of alcohols provides valuable intermediates for fine chemistry and pharmaceutical applications. The kinetics and reaction pathways of many catalytic alcohol oxidation reactions, have been studied at our laboratory. Although most of these reactions seem economically feasible to be applied on industrial scale, some major problems still have to be overcome. One of the most challenging problems to overcome is the fast deactivation of the platinum catalyst, due to over-oxidation of the noble metal. This loss of catalyst activity can be minimized by contacting the catalyst alternatingly with a reducing and oxidizing environment, the so called redox-cycle. One of the possibilities to achieve this redox cycle inside one reactor, is in an airlift loop reactor. This thesis describes the investigations of the hydrodynamic and mass transfer properties of such an airlift loop reactor, and the design of industrial size airlift loop redox cycle (ALRC) reactor, for the selective oxidation of alcohols, while maintaining a high catalyst activity.

The feasibility of an ALRC reactor for this oxidation process, is shown based on experimental and mechanistic insight in the hydrodynamic and mass transfer properties of a slurry bubble column, together with a kinetic model describing the alcohol oxidation and the catalyst deactivation and reactivation. The experimental investi-

gations on the hydrodynamics and mass transfer of a slurry bubble column, has led to the following conclusions:

The imaging technique is a powerful method to obtain quantitative data on the bubble size distribution, specific gas-liquid surface area, bubble rise velocity, and on the process of bubble coalescence. This data is used for mass transfer, gas hold-up, and modelling studies to increase the insight in the hydrodynamic and mass transfer properties of the system. For example, while studying the process of bubble coalescence with the imaging technique, it is shown that the experimental conditions should be adapted, to obtain statistically correct coalescence probabilities and coalescence times.
The gas hold-up in a bubble column is increased with increasing concentration of both carbon particles and electrolyte. However, increasing these concentrations above a carbon particle concentration of 0.1 g l^{-1} and an electrolyte concentration of 0.1 M, does not increase the gas hold-up any further. Multiple mechanisms are responsible for the increase in gas hold-up upon addition of carbon particles and electrolyte. Experiments with two different gas spargers show that the increase in gas hold-up caused by the presence of carbon particles proceeds via different mechanisms than the increase in gas hold-up caused by the presence of electrolyte. For carbon particle slurries it is concluded that the increase in the gas hold-up is due to a decreased rate of bubble coalescence and because of a slightly lower rise velocity of the gas bubbles. For electrolyte solutions it is concluded that the rate of bubble coalescence was decreased, while also the average bubble size was smaller compared to distilled water and carbon slurries, due to a change in the surface tension of the liquid.

The influence of the width and the depth of a 2D bubble column on the hydrodynamics, is investigated by modelling the 2D gas hold-up data with an existing 3D gas hold-up model. In this way insight is obtained on the influence of the scale of the 2D column on different parameters determining the gas hold-up. It is shown that the gas hold-up in a 2D bubble column, can be modelled with a 3D gas hold-up model if the rise velocity of the large bubbles is adapted for 2D columns, and the proper transition points between the homogeneous and heterogeneous regime are chosen. The rise velocity of the large bubbles is corrected according to the correlation of Pyle and Harrision, which is explicitly derived for 2D columns with a depth larger than 1 cm. It is found that while using this correlation, the scale factor derived for 3D columns still applies for 2D columns. Further, it is found that the transition point between the homogeneous regime and the heterogeneous regime is most affected by the depth of the 2D column. Estimation of the location of the transition point thus needs to be performed based on the smallest dimension, viz. the depth, of the 2D column. The derived 2D gas hold-up model is verified with gas hold-up data obtained in distilled water, carbon slurries and electrolyte solutions. The gas hold-up in all three systems is described satisfactorily with the 2D gas hold-up model. Furthermore, it is shown that the 2D gas hold-up prediction is almost equal to the gas hold-up prediction of

the 3D model at higher superficial gas velocities. This opens opportunities to use 2D gas hold-up data in scale up studies.

One of the most important parameters in the design of the ALRC reactor is the rate of gas-liquid mass transfer in the reactor. The mechanisms for the increased rate of mass transfer upon addition of carbon particles and electrolyte are investigated in three different sparged and stirred reactors. Three possible mechanisms are evaluated that might account for the increased rate of gas-liquid mass transfer, the shuttle effect, an increased specific gas-liquid surface area and changes in the hydrodynamics of the system, due to interactions of electrolyte species or particles with the gas-liquid diffusion layer. For the carbon particles and electrolyte used in this study, the rate of gas-liquid mass transfer in the bubble column and in the stirred reactor with gas inducing impeller, is increased because of an increased specific gas-liquid interfacial area. The rate of mass transfer in the stirred tank reactor with flat gas-liquid interface is increased due to collisions of the carbon particles with the gas-liquid diffusion layer, viz. a hydrodynamic effect. No evidence was found for the well known shuttle effect.

A design study is performed to show the feasibility of the ALRC reactor for the selective oxidation of alcohols. The specific slurry velocity and the partial pressure of oxygen in the inlet are the most critical design parameters. An industrial scale airlift loop redox cycle reactor is designed and compared with a stirred tank reactor process with alternating gas feed streams containing oxygen or nitrogen. The ALRC reactor is economically more attractive compared to the stirred tank process. This is because the ALRC reactor is operated with air, the gas feed is constant, the catalyst activity is almost twice the value of the stirred tank process, and the reactor volume of the ALRC is half of the volume of the stirred tank reactor.

Outlook

The results of the gas hold-up and mass transfer studies show a large effect of carbon particles and electrolyte on the behavior of the gas-liquid bubble column. It is shown that several mechanisms play a role in the change in gas hold-up, and in the increase of the rate of gas-liquid mass transfer, upon addition of the substances. However, it is difficult to reveal the exact mechanisms based on overall gas hold-up and mass transfer measurements. It is known that the surface properties of the particles, the type of electrolyte used and the medium in which the reaction is performed, can have a drastic influence on the behavior of a bubble column reactor. Therefore, a detailed analysis, of the effect of the particle and electrolyte properties, on changes in the hydrodynamics and mass transfer, is needed to elucidate the fundamentals of these mechanisms. At the moment, these effects are studied in our laboratory for

both aqueous systems and systems containing organic solvents, in corporation with the University of Amsterdam, the Netherlands (particle characterization and particle modification) and the University of Delft, the Netherlands (reactor scale-up and pressure effects). The agglomeration of particles and the effect of the surface properties of particles on the gas hold-up and the mass transfer, attracts special interest in these investigations.

List of publications

Kluytmans, J.H.J., Markusse, A.P., Kuster, B.F.M., Marin, G.B., Schouten, J.C., Engineering aspects of the aqueous noble metal catalysed alcohol oxidation, *Catal. Today*, 57, p. 143, 2000.

Kluytmans, J.H.J., Wachem, B.G.M. van, Kuster, B.F.M., Schouten, J.C., Image analysis to quantify sizes, velocities, interfacial areas, and coalescence behavior of gas bubbles in a 2D bubble column, *Meas. Sci. Tech.*, submitted for publication, 2002.

Kluytmans, J.H.J., Wachem, B.G.M. van, Kuster, B.F.M., Schouten, J.C., Gas holdup in a slurry bubble column: Influence of carbon particles and electrolyte, *Ind. Eng. Chem. Res.*, 40(23), p. 5326, 2001.

Kluytmans, J.H.J., Wachem, B.G.M. van, Kuster, B.F.M., Schouten, J.C., Mass transfer in sparged and stirred reactors: Influence of carbon particles and electrolyte, *Chem. Eng. Sci.*, submitted for publication, 2002.

Kluytmans, J.H.J., Wachem, B.G.M. van, Kuster, B.F.M., Krishna, R., Schouten, J.C., 2D bubble column hydrodynamic phenomena clarified with a 3D gas-liquid model, *Can. J. Chem. Eng.*, in conjunction with the Gas-Liquid-Solid (GLS) 6 conference, August 2003, Vancouver, Canada, submitted for publication, 2002.

Kluytmans, J.H.J., Wachem, B.G.M. van, Kuster, B.F.M., Schouten, J.C., Design of an industrial size airlift loop redox cycle (ALRC) reactor for catalytic alcohol oxidation and catalyst reactivation, *Ind. Eng. Chem. Res.*, submitted for publication, 2002.

Dankwoord

Na het schrijven van de inhoud van mijn proefschrift dacht ik klaar te zijn. "Alleen nog even een dankwoord". Echter, zoals door vele mensen reeds was voorspeld, het schrijven van een dankwoord is verschrikkelijk moeilijk. Veel mensen zijn bewust en onbewust betrokken geweest bij de totstandkoming van dit proefschrift. Ik realiseer me dat ik op deze plek deze mensen kan bedanken. Die kans wil ik niet aan me voorbij laten gaan en ik hoop dat ik hierbij niemand vergeet.

Ten eerste wil ik Prof.dr.ir. Jaap Schouten en Dr.ir. Ben Kuster bedanken voor de mogelijkheid die ze me hebben geboden om mijn promotie uit te voeren binnen de groep Chemische Reactortechnologie, en voor de vier jaar die ze me daarin hebben begeleid. Jaap, bedankt voor je niet aflatende inspanning om mij de kunst van het schrijven van wetenschappelijke publicaties bij te brengen. Verder wil ik je bedanken voor de kans die je me gaf om naar congressen in Italië en vooral in Hong Kong te gaan. Deze reizen waren leerzaam, maar ook erg gezellig.

Een bijzonder woord van dank wil ik richten aan Berend van Wachem. Berend, je raakte betrokken bij het project toen ik ongeveer een jaar bezig was. Je enthousiasme, je kritische kijk op zaken en je betrokkenheid bij het werk hebben me altijd erg gestimuleerd. Jouw bijdrage is van onschatbare waarde geweest voor het werk dat in dit proefschrift is beschreven. Ook vanuit Zweden ben je enthousiast betrokken gebleven bij het afronden van het project, ondanks je drukke werkzaamheden daar. Naast de inhoudelijk kant, heb ik ook onze discussies over "van alles en nog wat" en onze fietstochten erg gewaardeerd.

Een experimentele opstelling bouwen is leuk, maar het is nog veel leuker als deze uiteindelijk helemaal af is. De mensen, die er voor hebben gezorgd, dat de 2D bellenkolom uiteindelijk werkend op het lab werd afgeleverd, ben ik dan ook zeer erkentelijk. Zonder het vakmanschap van de mensen van de GTD was dit niet gelukt: Hans, Jan, Hans, Evert, Toon, Theo, Mijndert, bedankt voor jullie bijzonder belangrijke bijdrage aan dit project. Vanuit onze vakgroep werd de bouw gecoördineerd door Dick François. Dick, je praktische ideeën, je adviezen en je uithoudingsvermogen om de opstelling te realiseren heb ik bewonderd en gewaardeerd. Anton Bombeeck en Chris Luijk wil ik bedanken voor hun niet aflatende inzet om de opstelling in goede conditie te houden. Bijzonder veel dank ben ik verschuldigd aan Jovita Moerel. Jovita, je betrokkenheid bij het hele project, van het elektronische gedeelte tot de uiteindelijke bouw en oplevering van de opstelling zijn van onschatbare waarde geweest. Verder bewaar ik goede herinneringen aan onze zakelijke en niet zakelijke besprekingen over het reilen en zeilen op de universiteit en alles wat daar mee samen hangt.

Het werken op de vakgroep heb ik altijd zeer prettig gevonden. De prettige werksfeer waarbij iedereen voor elkaar klaar stond heeft zeker bijgedragen aan vier jaar

werkplezier. Daarnaast waren de vele uitstapjes, weekenden, pizza en filmavonden, borrels, koffiepauzes etc., altijd heel gezellig. Arjen, Patrick, Attasak, Yogi, Ton, Krzysztof, Andre, Evgeny, Jan, Jozef, Peter, Vikrant, Martijn, Erik, Poul, Karen, Peter, Marlies en vele afstudeerders en researchstudenten, bedankt! Wim Groenland ben ik zeer erkentelijk voor de vele experimenten die hij heeft uitgevoerd en voor de ondersteuning bij de experimenten, die ik zelf of één van de afstudeerstudenten hebben uitgevoerd. Anton, als "vroege vogels" dronken we elke ochtend koffie om de dag goed te beginnen en dat is zonder uitzondering elke dag gelukt. Gelukkig is deze groep steeds groter geworden, zodat ik erop vertrouw dat deze traditie nog lang in ere wordt gehouden.

In het bijzonder wil ik de collega's Carlo de Smet, Eric van Dijk, Mart de Croon en John van der Schaaf noemen, die naast vele gezellige gesprekken onder het genot van de nodige koppen koffie, op belangrijke momenten me ook terzijde hebben gestaan met het beantwoorden van vragen over programmeren, het oplossen van ingewikkelde wiskundige problemen, of me op de juiste momenten een zetje in de goede richting gaven. Keshav, als kamergenoot en bellenkolom collega hebben we veel plezier gehad in de afgelopen twee jaar. Ik heb veel van je geleerd over bellenkolommen, cricket en hoe mensen uit India tegen Nederlanders aankijken. Hopelijk heb ik je genoeg kennis van de Nederlandse taal bijgebracht zodat je dit stukje van het dankwoord kan ontcijferen. Als dat niet het geval is: "Thanks for two nice years as my bubble-column colleague and roommate, I have learned a lot from you and I wish you success in continuing the bubble column research at our department."

Denise, ik vroeg me altijd af wat het verschil was tussen een secretaresse en "Management Assistent". Toen jij in onze groep kwam is me dat helemaal duidelijk geworden. Met recht ben je een "Management Assistent", waarop ik altijd kon vertrouwen voor het regelen van veel zaken, voor de nodige pepermuntjes, maar nog belangrijker, om me aan te sporen dingen te doen die ik zelf al lang was vergeten. Bedankt voor deze geweldige ondersteuning.

Veel mensen ben ik dank verschuldigd die me hebben gesteund door het tonen van interesse, het proberen te begrijpen waar ik mee bezig was en door de broodnodige afleiding. De gezellige weekenden en avonden zijn zeer waardevol geweest en zullen dit in de toekomst ook blijven. Bedankt, bestuursgenoten van Japie, Martine, Jan en Hester, Mayk, Yvonne en Bastiaan, Jarl, mijn ex-huisgenoot en consorten, Björn, Frank, Erik en Jok, familie en kennissen, Roel en Yvonne, Alie en Dirk, Vivian en Hans, Milo, en de heren van het herendispuut I.G. Bibimus en de bijbehorende Bibi+, Wouter en Veele, Sebas en Anne, Stan, Pjotr en Claudine, Frank en Karin, Teus en Regina, Jean-Paul en Cindy, Armand en Nathalie, Mark en Anita, Stefan en Suzanne.

Mijn paranimfen Jan van Leur en Carlo de Smet zullen niet alleen achter me staan

tijdens de verdediging van mijn proefschrift. Zij hebben altijd achter me gestaan tijdens mijn studie en promotie. Jan, onze uren op de practicumzaal, nog meer uren achter de computer om verslagen te typen en onze vele uren buiten de studie die we hebben besteed aan zinnige en onzinnige dingen zijn me zeer dierbaar. Carlo, gesteund door hoe ik zag hoe jij met je promotieonderzoek bezig was, ben ik aan mijn promotieonderzoek begonnen. Onze eerste fietstocht was onvergetelijk, "tot op de draad nat" met een zonnetje in de verte, militairen in de sloot en twee lekke banden hebben onze band definitief gesmeed. Je interesse tijdens mijn promotie en de bijzonder gezellige wederzijdse bezoeken waren zeer bijzonder. Ik spreek vanaf deze plek de hoop uit dat deze vriendschappen tot in lengte van dagen zo blijven zo als ze op dit moment zijn.

Ook al staat alleen mijn naam op de kaft van dit proefschrift, de bijdrage van een aantal mensen is van onschatbare waarde geweest. Ik wil dan ook de afstudeerders Mercedes Viñas, Bas Tilborghs, Mynco Fliermans en Tjalling van Elst en de researchstudenten Duy Nuygen en Ralf Knibbeler bedanken voor hun bijdrage aan dit werk.

Veel woorden voor vele mensen die me terzijde hebben gestaan. Echter, de laatste woorden zijn gericht aan de mensen, waar ik altijd onvoorwaardelijk op terug kan vallen. De mensen die me hebben gesteund in alle keuzes die ik gemaakt heb, die ik vele uren heb mogen lastig vallen met de verhalen over het wel en wee van het promoveren en die me met gepaste trots op de voet blijven volgen. Susan en John, bedankt voor jullie steun, de etentjes in Bladel, de interesse en de steun. Pap en mam, de avonden die we in vele weekenden hebben doorgebracht met gezellige gesprekken en boeiende discussies samen met de uren die jullie me hebben aangemoedigd via de telefoon hebben er voor gezorgd dat dit proefschrift uiteindelijk klaar is. Zonder deze steun had ik het zeker niet kunnen bolwerken.

Mijn vader droeg zijn proefschrift op aan mijn moeder omdat ze "...zelfs mijn zwijgen verstaat...". Iedereen die me een beetje kent weet dat ik zou liegen als ik deze zin zou kopiëren om Tanja te bedanken. Toch zijn er momenten geweest waarop ik stil viel, en waarop ik het even niet meer zag zitten. Op deze momenten is het heel belangrijk iemand naast je te hebben die precies weet wat te doen of juist niet te doen. Tanja, bedankt voor het geduld om mijn grillen te begrijpen, bedankt voor je onvoorwaardelijke steun, bedankt voor alles tot nu toe, en voor alles wat we samen nog in het verschiet hebben.

14 Januari 2002,
Jeroen Kluytmans

About the Author

Jeroen Kluytmans was born on September 22^{nd}, 1975 in Berkel-Enschot. In 1993 he obtained his "VWO" highschool certificate at the Grotius College in Heerlen. He then started his university studies in Chemical Engineering at the Eindhoven University of Technology. In 1998 he obtained his M.Sc. degree, with distinction, in Chemical Engineering on the topic of "Transient oxidation of ethylene oxidation over a $Pt/Rh/CeO_2/\gamma$-Al_2O_3 automotive exhaust catalyst", under supervision of Prof.dr.ir. J.C. Schouten. In the same year he started his Ph.D. research at the laboratory of chemical reactor engineering at the Eindhoven University of Technology, under supervision of Prof.dr.ir. J.C. Schouten and Dr.ir. B.F.M. Kuster. Since January 1^{st}, 2003 he works as Process Development Engineer in the group Performance Materials, Chemistry and Technology at DSM Research, Geleen.